UNDERSTANDING THE MEMBRANE PENETRATION OF ANTIMICROBIAL PEPTIDES

by

Begüm Alaybeyoğlu

B.S., Chemical Engineering, Middle East Technical University, 2010

Submitted to the Institute for Graduate Studies in
Science and Engineering in partial fulfillment of
the requirements for the degree of
Master of Science

Graduate Program in Chemical Engineering

Boğaziçi University

2012

UNDERSTANDING THE MEMBRANE PENETRATION OF ANTIMICROBIAL PEPTIDES

APPROVED BY:

Assist. Prof. Elif Özkırımlı Ölmez (Thesis Supervisor)	…….
Assoc. Prof. Berna Sarıyar Akbulut (Thesis Co-Supervisor)	…….
Assist. Prof. Burak Alakent	…….
Assoc. Prof. Arzu Çelik	…….
Assist. Prof. Hamdi Torun	…….

DATE OF APPROVAL: 07/06/2012

to my mother

ACKNOWLEDGEMENTS

I would like to express my sincere thanks to my thesis supervisor Prof. Elif Özkırımlı Ölmez and co-supervisor Assoc. Prof. Berna Sarıyar Akbulut. Their motivation and understanding helped me throughout my studies and improved my work.

I am very grateful to my thesis committee members; Assist. Prof. Burak Alakent, Assoc. Prof. Arzu Çelik and Assist. Prof. Hamdi Torun for spending time on my thesis and their valuable recommendations.

I wish to express my gratitude to Assist. Prof. Amitav Sanyal and Sadık Kağa, who deserve special thanks for their guidance and help throughout my experimental studies.

I would like to thank Deniz Menekşedağ who was not only a great lab partner but also a journey fellow. The memories of our miserable all-nighters at the U.S airports and our tiny but the most comfortable double bed in San Diego will always remain. I would also like to express my gratitude to the other members of KB407; Gizem Özbüyükkaya, Seval Aladağ, Oya Gürsoy Yılmaz and Simay Yalaz for their kind support and help.

I would like to express my very great appreciation to my family and especially to my mother and father for their financial support for life time. They were always proud of me and respected my choices even at times when I was in doubt. I would have been exhausted without those meals my grandmother cooked in my imperfect kitchen.

I should express my very special thanks to my patient flat mate Sinemis Süzer for always keeping the volume down, washing the dishes when I was busy and for letting me mess the flat during the preparation of this thesis.

Finally, I cannot thank enough to Aziz Aslan, who was always there for me. Being an artist, most of the time he thought I was talking gibberish when I mentioned my studies,

yet he never gave up on me and pretended not to get bored. He not only fixed my car, but fixed my life.

TUBITAK Project No. 108M644, Project No. 109M229 and BAP Project No. 09HA504P are gratefully acknowledged for the funding.

ABSTRACT

UNDERSTANDING THE MEMBRANE PENETRATION OF ANTIMICROBIAL PEPTIDES

The studies on β-lactam antibiotics have found great interest since the use of antimicrobial therapy became widespread and as a result, bacteria started to develop resistance against β-lactam antibiotics. The most effective resistance mechanism is the production of β-lactamases. The need of successful inhibitors against β-lactamase led to the studies that revealed the structure of β-lactamase inhibitory protein (BLIP) and its interactions with β-lactamase. The structure of TEM-1-BLIP complex indicated that a type II β turn (residues 46-51) of BLIP made critical interactions with the active site of the TEM-1 β-lactamase, suggesting that a peptide including this loop would be a good lead toward the development of a peptide based inhibitor. In peptide based drug design, one of the most common challenges is penetration through the membrane. It was aimed to investigate the translocation mechanism of the cell-penetrating peptide pVEC (LLIILRRRIRKQAHAHSK) and to analyze it on a residue basis in order to identify mechanism by which bacterial uptake occurs. The wild-type pVEC, eight mutants, retro- and scramble pVEC were chosen to be studied using molecular dynamics (MD) and steered molecular dynamics (SMD) simulations. The peptide transport was observed to occur in three main stages and it was distinguished that for peptides with increased uptake potential, the work performed was higher. Residues L1, R6, R7, R8, R10, K11 and K18 was shown to contribute to the interaction of pVEC with the lipid bilayer. In the experimental part of the study, effect of Peptide 1 (5-Fluorescein-NH-HA AGDYYAY-$CONH_2$), Peptide 2 (5/6-Fluorescein-NH-RRGHYY-COOH) and Peptide 3 (5/6-Fluorescein-NH-LLIILHAAGDYYAY- $CONH_2$) on growth of antibiotic resistant *E. coli* K12 pUC18 cells expressing β-lactamase was examined. Peptide 1 did not have an inhibitory effect on the cell growth. On the other hand, Peptide 3 was taken into the cells, as revealed by microscopy and incubation with this peptide led to cell death. Our studies showed that inclusion of the five hyrophobic residues at the N-terminus enhanced the uptake potential of the inhibitory peptide.

ÖZET

ANTİMİKROBİYAL PEPTİTLERİN HÜCRE ZARINA GİRİŞ MEKANİZMASININ İNCELENMESİ

β-laktam antibiyotikleri üzerindeki çalışmalar antimikrobiyal terapinin kullanımının yaygınlaşmasıyla ve bunun sonucu olarak bakterilerin β-laktam antibiyotiklerine karşı direnç geliştirme başlamasından itibaren büyük ilgi gördü. Direnç mekanizmaları içinde en etkili antibiyotik direnç mekanizması β-laktamaz üretimidir. Bu direnci yok edebilecek mekanizmalara olan ihtiyaç β-laktamaz inhibitör proteininin (BLIP) ve β-laktamaz ile oluşturduğu kompleksin yapısının keşfedilmesine öncülük etmiştir. BLIP ve TEM-1-BLIP kompleks yapılarında, BLIP üzerinde bulunan tip II β yapısının (46-51 kalıntıları) TEM-1 β-laktamaz aktif kısmı ile kritik bir etkileşim içerisinde olduğunu göstermektedir. Bu kalıntıları içeren bir peptidin peptid bazlı bir inhibitor tasarımı için bir başlangıç noktası olduğu düşünülmüştür. Peptid bazlı ilaç tasarımında en yaygın sorunlardan biri peptidin hücre zarına girişidir. Bu çalışmada, hücre-delici bir peptid olan pVEC'in (LLIILRRRIRKQAHAHSK) translokasyon mekanizmasının ve bakteri hücrelerine alımında rol oynayan kalıntıların araştırılması amaçlanmıştır. Yabani tür pVEC, sekiz mutant, retro- ve scramble pVEC dizileri moleküler dinamik (MD) ve yönlendirilmiş moleküler dinamik (SMD) simülasyonları kullanılarak incelenmiştir. Peptidin hücre zarından üç ana aşamada geçtiği gözlenmiş ve artan hücre içine alım potansiyeline sahip peptidler için, yapılan işin daha yüksek olduğu tespit edilmiştir. L1, R6, R7, R8, R10, K11 ve K18 kalıntılarının pVEC ve hücre zarın etkileşimlerinde katkıda bulundukları gösterilmiştir. Deneysel çalışmalarda, Peptid 1 (5-Fluoresein-NH-HA AGDYYAY-CONH2), Peptid 2 (5/6-Fluorescein-NH-RRGHYY-COOH) ve Peptid 3'ün (5/6-Fluorescein-NH-LLIILHAAGDYYAY-CONH2) antibiyotiğe dirençli *E. coli* K12 pUC18 hücrelerinin büyümesi üzerinde etkisi incelenmiştir. Peptid 1'in hücre büyümesi üzerinde inhibe edici bir etkisinin olmadığı ve floresans mikroskobu görüntülerinde ise ortamda hücre örneklerinde bulunandan daha yüksek miktarda peptid olduğu tespit edilmiştir. Peptid 3'ün ise mikroskop görüntülerine dayanarak hücre içine alındığı ve eklendiği ortamda hücre ölümlerine yol açtığı gözlenmiştir. Yapılan çalışmalar N-terminaline eklenen 5 kalıntının inhibitor peptidin hücre içine alımını arttırdığını göstermiştir.

TABLE OF CONTENTS

LIST OF FIGURES

LIST OF TABLES

LIST OF SYMBOLS

R_{min}	Lennard-Jones radius
q	Partial atomic charge
$\vec{F}$	Force applied
U	Potential energy
v	Pulling velocity
$\vec{r}$	Actual position of the SMD atom
$\vec{r}_0$	Initial position of the SMD atom
$\vec{n}$	Direction of pulling
$b - b_o$	Distance from equilibrium that the atom has moved
K_b	Bond force constant
n	Multiplicity
$r_{1,3} - r_{1,3,o}$	Distance between the 1, 3 atoms in the harmonic potential
K_{UB}	Force constant
F_i	Force exerted on the particle I
m_i	Mass of the particle i and
a_i	Acceleration of the particle I
V	Potential energy
r_i	Atomic coordinates of the particle i
t	Time
Å	Angstrom
ΔPMF	Potential of mean force
dt	Timestep
mg	Milligram
µM	Micromolar
M	Molar
kcal	Kilocalorie
k	Spring constant
vel	Velocity
kDa	Kilodalton

fs	Femtosecond
pN	Piconewton
ns	Nanosecond
ps	Picoseconds

α	Alpha
ε	Lennard-Jones well-depth
$K\phi$	Dihedral force constant
K_{φ}	Impropers force constant
K_{θ}	Angle force constant
ϕ	Dihedral angle
$\varphi - \varphi_o$	Out of plane angle
δ	Phase shift
$\theta - \theta_o$	Angle from equilibrium between 3 bonded atoms

LIST OF ACRONYMS/ABBREVIATIONS

1PB	1, 4-diphenyl-2-butene
A	Alanine
Ala	Alanine
AMP	Antimicrobial peptide
Arg	Arginine
Arg_9	Polyarginine
Asp	Aspartic acid
BLIP	Beta-Lactamase Inhibitory Protein
C	Carbon
C17	7-[(3-chlorobenzyl) oxy]-2-oxo-2H-chromene-4-carbaldehyde
C18	7-[(3-chlorobenzyl) oxy]-4-[(methylamino) methyl]-2H-chromen-2-one
CbnB2	Carnobacteriocin B2
CD	Circular dichroism
Chol	Cholesterol
CL	Cardiolipin
CPP	Cell-penetrating peptide
D-pVEC	D-enantiomer of pVEC
DMPC	1, 2-Dimyristoyl-*sn*-Glycero-3-Phosphocholine
DMPG	1, 2-Dimyristoyl-*sn*-Glycero-3-[Phospho-*rac*-(1-glycerol)]
DOPC	1, 2-dioleoyl-sn-glycro-3-phosphocholine
DOPG	Dioleoylphosphatidylglycerol
DOPS	Dioleoylphosphatidylserine
DPPC	1, 2-dipalmitoyl-sn-glycro-3-phosphocholine
DPPE	Dipalmitoylphosphatidylethanolamine
DPPG	Dipalmitoyl phosphatidyl glycerol
DSC	Differential scanning calorimetry
DSPC	1, 2-Distearoyl-*sn*-Glycero-3-Phosphocholine
DSPG	1, 2-Distearoyl-*sn*-Glycero-3-[Phospho-*rac*-(1-glycerol)]

ESBL	Extended-spectrum beta-lactamase
EDTA	Ethylenediaminetetraacetic acid
FOH	Farnesol
G	Glycine
h	Hour(s)
H	Hydrogen
H	Histidine
His	Histidine
I	Isoleucine
IL	Indolicidin
Ile	Isoleucine
ISN	1H-indole-2, 3-dione (isatin)
K	Lysine
K	Potassium
L	Leucine
LJ	Lennard-Jones
Lys	Lysine
MAO B	monoamine oxidase B
MAP	Multiple antigenic peptide
MD	Molecular dynamics
MLV	Multilamellar vesicles
N	Nitrogen
OAK	Oligomer of acyllysine
P	Phosphorus
pAntp	*Drosophila* antennapedia transcription protein
PE	Phosphodylethanolamine
Peptide 1	5-Fluorescein-NH-HAAGDYYAY- $CONH_2$
Peptide 2	5/6-Fluorescein-NH-RRGHYY-COOH
Peptide 3	5/6-Fluorescein-NH-LLIILHAAGDYYAY- $CONH_2$
PG	Phosphatidyglycerol
PME	Particle mesh Ewald
POPC	1-palmitoyl-2-oleoyl-sn-glycero-3-phosphocholine
POPE	1-Palmitoyl-2-oleoyl-*sn*-glycero-3-phosphoethanolamine

POPG	1-Palmitoyl-2-Oleoyl-*sn*-Glycero-3-Phosphocholine
PTD	Protein transduction domain
pVEC	Vascular endothelial-cadherin protein
Q	Glutamine
R	Arginine
RM1	N-methyl-1(R)-aminoindan
Rt	Retention time
S	Serine
SAG	(S)-(+)-2-[4-(fluorobenzyloxybenzylamino) propionamide]
S.A.R	Structure-activity relationship
Ser	Serine
SM	Sphingomyelin
SMD	Steered molecular dynamics
Tat	Trans-activating transcriptional activator
TM	transmembrane
TOCL	Tetraoleoylcardiolipin
vdW	van der Waals
VMD	Visual molecular dynamics

1. INTRODUCTION

1.1. β- Lactam Antibiotics and β-Lactamase Mediated Resistance

1.1.1. β-Lactam antibiotics

The history of the discovery of β-lactam antibiotics began with the study of Alexander Fleming, when he inoculated agar plates with his own nasal secretion to determine the change in his nasal bacterial flora in 1921. The substance, a protein Fleming named lysozyme, was found to be an enzyme capable of dissolving the cell wall and causing lysis in many Gram-positive bacteria. The discovery of lysozyme led to the discovery of penicillin [1]. Later, the work at the Northern Regional Research Laboratory revealed that different strains, culture conditions and media resulted in the production of different penicillin compounds. In the English clinical trials 2-pentenylpenicillin (Penicillin F or I) was used while in the United States penicillin (Penicillin G or Penicillin II) which was tested. It was later shown that both forms of penicillin contained β-lactam rings [1].

Penicillin G (benzylpenicillin) was the first β-lactam antibiotic introduced into clinical practice. Today, β-lactam antibiotics include: penicillinase-resistant, amino-, carboxy-, indanyl- and ureido-penicillins; cephalosporins; monobactams and carbapenems. The structures of penicillin G, carbapenem, cephalosporin and monobactam are shown in Figure 1.1 with the β-lactam rings encircled. The structural feature of a β-lactam is the highly reactive four-member ring. All β-lactam antibiotics are bactericidal agents that are capable of inhibiting cell wall synthesis [2].

As antimicrobial therapy provided prevention of some infections, the availability and success of antibiotics resulted in overconfidence. At the very beginning, resistance to antibacterial agents was recognized as a potential problem. Specifically, resistance to penicillin was the focus of Alexander Fleming's study where he exploited the substance's ability to eliminate Staphylococcus and Streptococcus contamination in 1929, but the therapeutic agent feature of penicillin overshadowed the resistance issue. Thus, it was

known from the beginning that bacteria have the ability to cancel out antibiotics. Over the years, antibiotic resistance issues have drawn increased attention [1].

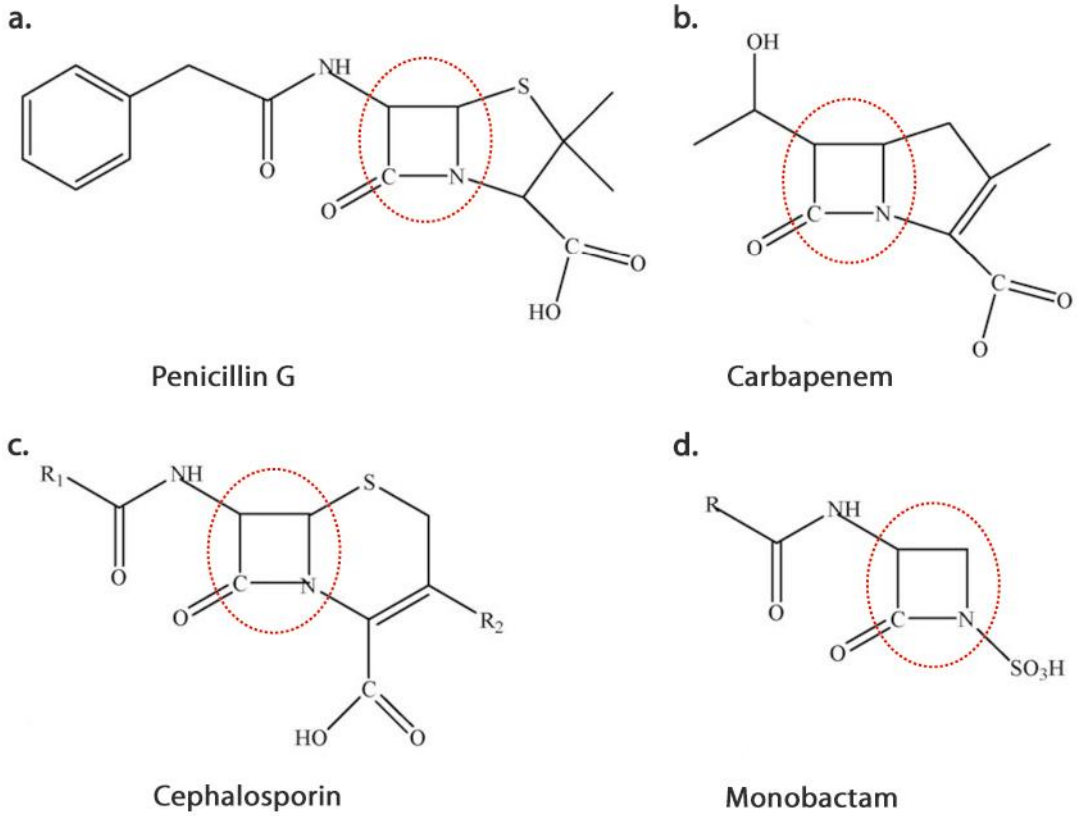

Figure 1.1. The chemical structure of the Penicillin G, Carbapenem, Cephalosporin and Monobactam β-lactam antibiotics [2]. The β-lactam rings are encircled.

β-lactam antibiotics are rendered inactive against bacteria by three primary mechanisms of resistance. The most common mechanism is the production of enzymes that degrade or modify the antibiotic before it can reach the target. In this case, the β-lactamase enzymes degrade β-lactam antibiotics and are found widely disseminated amongst Gram-positive and Gram-negative bacteria. The second mechanism is the alteration of the antibiotic target site. In this case, the β-lactam-resistant cell-wall transpeptidases perform this role. The third mechanism is the prevention of access of the antibiotic to the target by way of altered permeability or forced efflux [3].

β-Lactam was the first antibiotic that was described, and resistance to β-lactam

antibiotics was the first to be studied. The most effective way that bacteria eliminate the effectiveness the antibiotics is by producing β-lactamases, which are enzymes that inactivate the antibiotics by hydrolyzing the β-lactam ring [1].

1.1.2. β-Lactamases

The production of β-lactamase enzymes is the most common mechanism of bacterial resistance to β-lactam antibiotics such as penicillins and cephalosporins. These enzymes catalyze the hydrolysis of the β-lactam ring rendering antimicrobials ineffective. Beta-lactamases (EC 3.5.2.6) were first identified in *Staphylococcus aureus* strains in the late 1940s, prior to the introduction of penicillin into the clinical setting [4]. β-lactamases confer significant antibiotic resistance to their bacterial hosts by hydrolysis of the amide bond of the β-lactam ring. These enzymes are especially important in Gram-negative bacteria as they constitute the major defense mechanism against β-lactam based drugs. The spread of β-lactamase genes has been greatly exacerbated by their integration within mobile genetic elements, such as plasmids or transposons, which facilitate the rapid transfer of genetic material between microbes. Once expressed, β-lactamases are secreted into the periplasmic space (in Gram-negative bacteria), bound to the cytoplasmic membrane or excreted [3].

β-lactamases were catagorized based on similarity in amino acid sequence (Ambler classes A through D [5]) or on substrate and inhibitor profile (Bush-Jacoby-Medeiros Groups 1 through 4 [6]). The molecular classification of β-lactamases that is based on the nucleotide and amino acid sequences of these enzymes includes four classes (Ambler A–D), correlating with the functional classification. Classes A, C and D act by a serine-based mechanism, whereas class B or metallo β-lactamases that need zinc for their action [1].

The first beta-lactamase crystal structure determined was the class A β-lactamase (Group 2 in Bush et al. Scheme) from *Staphylococcus aureus* PC1. Since then, up to 80 structures of wild-type β-lactamases, mutant β-lactamases and co-crystal structures of β-lactamase with substrate or inhibitor have been revealed. As most of the revealed structures belong to class A β-lactamases, this class is the most studied β-lactamase enzymes [4].

The TEM-1 and SHV-1 β-lactamases, which belong to Ambler class A and Bush-Jacoby-Medeiros Group 2b, are the β-lactamases usually found in *E. coli* and *K. pneumoniae* that confer resistance to penicillins (ampicillin and piperacillin) [2].

Table 1.1. Beta-lactamase classification schemes [2].

Ambler classification system		
class A	penicillinases	TEMs, SHVs, PC1, CTX-Ms, SME-1, KPC-1
class B	metallo-beta-lactamases (zinc)	IMP-1, VIM-1, Ccr A
class C	cephalosporinases	AmpCs, CMY-2, ACT-1
class D	oxacillinases	OXA-1
Bush-Jacoby-Medeiros classification		
Group 1	cephalosporinases	AmpCs, CMY-2, ACT-1, MIR-1
	hydrolyze extended-spectrum cephalosporins; clavulanate resistant	
Group 2	all clavulanic acid susceptible	
2a	penicillinase	PC1 from S. aureus
2b	broad-spectrum penicillinase	TEM-1, SHV-1, TEM-2
2be	ESBLs	SHV-2, TEM-10, CTX-Ms
2br	inhibitor resistant	TEMs, IRTs TEM-30, TEM-31
2c	carbenecillin hydrolyzing	PSE-1
2d	oxacillin hydrolyzing	OXA-10, OXA-1
2e	cephalosporinases inhibited by clavulanate	FEC-1
2f	carbapenemases	KPC-1, SME-1
Group 3	metallo-beta-lactamases	IMP-1, VIM-1, Ccr A
	hydrolyze imipenem, inhibited by EDTA, resistant to clavulanate	
Group 4	Miscellaneous	

1.1.3. β-Lactamase Inhibitory Protein (BLIP)

β-Lactamase inhibitors are proved to be effective for overcoming the mechanism of resistance when combined with a susceptible antibiotic to restore its activity against β-lactamase-producing organisms [7].

Two approaches have been suggested to overcome TEM-1 and SHV-1 β-lactamase-mediated resistance. As the first approach, extended-spectrum cephalosporins such as cefotaxime and ceftazidime which TEM-1 and SHV-1 β-lactamases are not able to hydrolyze were developed. Second, the coadministration of an inhibitor of β-lactamase, such as clavulanic acid or sulbactam, with a β-lactam antibiotic, such as ampicillin or amoxicillin, has been shown to overcome β-lactamase-mediated resistance. The disadvantage of both approaches are that they apply selective pressure for mutations that result in a β-lactamase that either cleaves extended-spectrum cephalosporins or is no longer sensitive to β-lactamase inhibitors [8].

The evolution of bacterial resistance necessitates a thorough understanding of the resistance mechanisms of bacteria and the production of β-lactamase. The discovery of β-lactamase inhibitor protein (BLIP) a 165-amino-acid protein produced by the gram-positive soil bacterium *Streptomyces clavuligerus* has led to intense research toward elucidation of the β-lactamase-BLIP interaction mechanism [9-12]. *S. clavuligerus* also produces β-lactam antibiotics such as cephamycins as well as a β-lactamase inhibitor, clavulanic acid. BLIP is able to bind to and inhibit the class A β-lactamases from *Staphylococcus aureus, Bacillus cereus,* and *Bacillus licheniformis* with K_i values of 1 to 3 μM. BLIP does not efficiently bind to class B, C or D β-lactamases [8].

BLIP inhibits class A β-lactamases with a wide range of affinities. It inhibits TEM-1 β-lactamase with a K_i of 0.5 nM, but inhibits SHV-1 β-lactamase, which is 68% identical in amino acid sequence to TEM-1, with a K_i of 1.1 μM. The structures of TEM-1-BLIP and SHV-1-BLIP complexes suggest that the small difference between TEM-1 and SHV-1 structures (Glu104 residue of TEM-1 and Asp104 residue of SHV-1) leads to a large difference in affinity [10].

Figure 1.2 shows the structure of TEM-1-BLIP interface. The coordinates of the complex are found in the Protein Data Bank with the accession code 1JTG. BLIP consists of a tandem repeat of a 76-residue α/β domain. The two domains form a large concave eight-stranded β-sheet upon which aromatic side chains make extensive hydrophobic contacts with the loop-helix region of TEM-1. A circular arrangement of nonpolar atoms at the TEM-1–BLIP interface surrounds a central hydrogen bonding interaction between Glu 73 of BLIP and the peptide nitrogens of Tyr 105 and Ser 106 on TEM-1. Two protruding β-hairpin loops on BLIP structurally mimic penicillin and are inserted into the TEM-1 active site The large concave eight-stranded β-sheet of BLIP wraps around the TEM-1 loop-helix region highlighted in green. Asp 49 and Phe 142 on the β-hairpin turns of BLIP insert into the TEM-1 active site cavity and structurally mimic the carboxylate and benzyl side chain of a penicillin substrate. To illustrate the competitive mode of inhibition, the penicilloyl moiety (thin stick rendering) of the TEM-1–penicillin G acyl-enzyme intermediate is superimposed on the active site region of the complex [9].

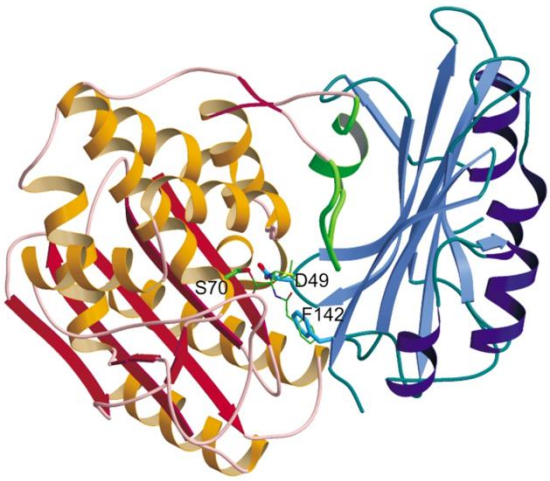

Figure 1.2. TEM-1 (orange) and BLIP (blue) complex interface [9].

The three-dimensional structures of BLIP and TEM-1-BLIP complex indicates that a type II β turn encompassing residues 46 to 51 of BLIP makes critical interactions with the active site of the TEM-1 β-lactamase. Because of these interactions, it was hypothesized that a peptide that includes turn residues 47 to 50 would retain sufficient binding energy to interact with β-lactamase in the absence of the remaining portion of BLIP [13]. As it was

proved that this peptide could inhibit β-lactamase alone, this was the starting point of the BLIP-based peptides as β-lactamase inhibitors [8].

1.2. Cell-penetrating peptides (CPPs)

In drug design, one of the most common challenges is penetration through the membrane. So far different strategies such as microinjection, electroporation, liposomes and viral vectors have been tried. However, all of these strategies have serious drawbacks such as toxicity and low efficiency. An efficient strategy was developed based on the observation that two intracellular proteins Tat (HIV-1 transcriptional activator protein) and pAntp (*Drosophila* antennapedia transcription protein) were able to pass through the membrane when added to the extracellular medium. Also it was observed that these molecules made delivery of conjugated molecules such as peptides or proteins possible. Protein transduction domains (PTDs), now mostly known as cell-penetrating peptides (CPPs) include all the peptides with the ability to translocate across membranes, regardless of the characteristics of the peptides [14].

Cell-penetrating peptides (CPPs) are generally peptides of fewer than 30 residues derived from natural or unnatural proteins or chimeric sequences. The CPPs can be divided into two main classes. The first class of CPPs requires chemical linkage with the cargo and the second class of CPPs involves formation of stable, non-covalent complexes with the cargo. Some representative CPPs can be seen in Table 1.2 [15].

Eiriksdottir et al. proposes a new classification of CPPs based on their structural properties, affinity for phospholipids and internalization pathways. For this aim, the alteration in structural state and the interaction of 10 CPPs were compared. Both the structural state and the conformational plasticity of peptides were investigated. To evaluate the structural flexibility circular dichroism (CD) spectroscopy method and to determine the affinity surface physic methods were used. Using the results of these methods CPPs were divided into three subgroups based on their secondary structures in the presence of phospholipids. The first subgroup of peptides displayed no change in structure (random

coil) in different phospholipids, lipid/peptide ratios used. The second subgroup adopted β-structure and the third subgroup adopted a helical conformational state [16].

Table 1.2. Some representative CPPs: their origins and sequences [15].

Peptides	**Origin**	**Sequences**	**Cargo Types**
Peptides derived from protein transduction domains			
Tat	HIV-Tat protein	PGRKKRRQRRPPQ	Protein/peptide/siRNA/ liposome/nanoparticle
Penetratin	Homeodomain	RQIKIWFQNRRMKWKK	peptide/siRNA/liposome
Transportan	Galanin-mastoparan	GWTLNSAGYLLGKINLKALAALAKKIL	Protein/PNA/siRNA
VP-22	HSV-1 structural protein	DAATATRGRSAASRPTERPRAPAR-SASRPRRPVD	Protein
Amphipathic peptides			
MPG	HIV Gp41-SV40 NLS	GALFLGFLGAAGSTMGAWSQPKKKRKV	siRNA/ODN/plasmid
Pep-1	Trp-rich motif-SV40 NLS	KETWWETWWTEWSQPKKKRKV	Protein/peptide
MAP	Chimeric	KALAKALAKALA	Small molecule/plasmid
SAP	Proline-rich motif	VRLPPPVRLPPPVRLPPP	Protein/peptide
PPTG1	Chimeric	GLFRALLRLLRSLWRLLLRA	plasmid
Other cell-penetrating peptides: cationic peptides			
Oligoarginine	Chimeric	Agr8 or Arg9	Protein/peptide/siRNA/ODN
hCT (9-32)	Human calcitonin	LGTYTQDFNKTFPQTAJGVGAP	Protein/plasmid DNA
SynB	Protegrin	RGGRLSYSRRRFSTSTGR	Doxorubicin
Pvec	Murine VE-cadherin	LLIILRRRIRKQAHAHSK	Protein/peptide

1.2.1. pVEC

The 18 amino acid long cell-penetrating peptide pVEC is derived from murine vascular endothelial cadherin (VE-cadherin) protein. This protein mainly functions as the contact between adjacent cells by hemophilic dimerization. Moreover, VE-cadherin serves as an intercellular glue and it also plays an active role in information transfer into the cells [17].

Cadherins are single transmembrane-spanning glycoproteins of about 700 residues. They are classified according to the tissue where they are expressed. Vascular endothelium cadherin (VE-cadherin), neuronal cadherin (N-cadherin) and epithelial cadherin (E-cadherin) are some example cadherin proteins. The cadherin protein consists of five extracellular loops and a short cytoplasmic tail [18].

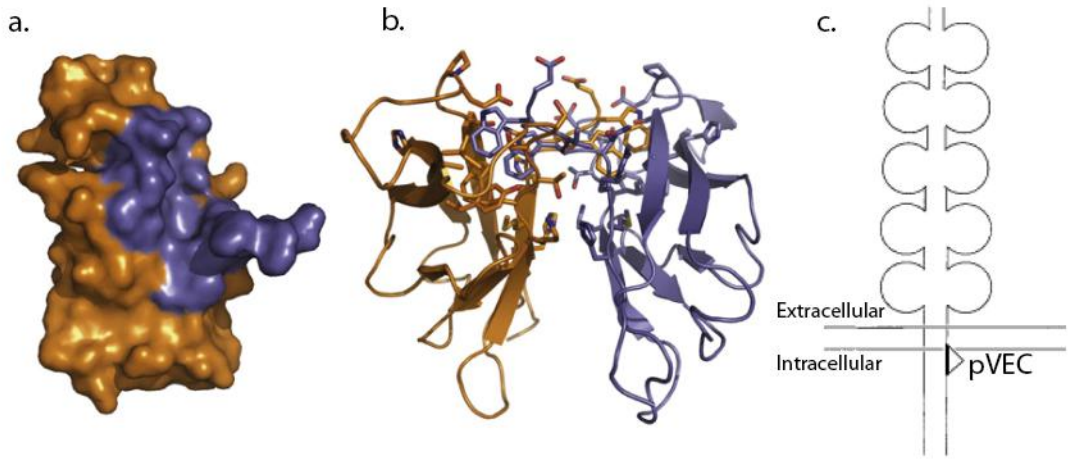

Figure 1.3. (a) Surface and (b) ribbon representations of VE-cadherin protein. The dimers of the protein are shown in orange and blue [19]. (c) Illustration of VE-cadherin homodimer and pVEC that originates from amino acids 615-632 [18].

The biophysical characterization of the complete VE-cadherin ectodomain produced in mammalian cells revealed dimers in solution, but not higher-order oligomers. Crystallographic analysis of the adhesive EC1–2 domain fragment of chicken VE-cadherin revealed strand-swap binding involving two tryptophan anchor residues, which is a characteristic of type II cadherins. However, the adhesive interface also resembles type I cadherins in that it lacks a large hydrophobic surface. The representative structure of VE-

cadherin can be seen in Figure 1.3. These findings show that VE-cadherin forms dimers like other classical cadherins via an adhesive interface with characteristics of both type I and type II subfamilies [19].

The peptide sequence, LLIILRRRIRKQAHAHSK, contains 13 cytosolic amino acids closest to the membrane and 5 amino acids from the C terminus of the transmembrane region (amino acids 615-632) of the VE-cadherin protein [18]. Four Arg and two Lys residues in the sequence of pVEC make the peptide highly positively charged when diluted in buffer solution. In general, the N terminus of the pVEC is hydrophobic, the middle part is charged and the C terminus is hydrophilic. It has been shown that pVEC uptake into gram-negative and gram-positive bacteria and fungi is possible [17]. Elmquist et al. showed that pVEC is able to internalize into several cell lines *in vivo* [18].

pVEC was shown to assume a random coil conformation in pure water, whereas it adopts a β-structure in the presence of negatively charged phospholipids DOPG (dioleoylphosphatidylglycerol). However, it conserves its random coil conformation in the presence of neutral phospholipids DOPC (dioleoylphosphatidylcholine), 80/20 mixture of DOPC/DOPG as well as in the presence of LUV (Large Unilamellar Vesicles) composed of a 40/40/20 mixture of DOPC/SM/Chol (SM: sphingomyelin, Chol: cholesterol) [16].

1.3. Peptide Uptake Studies Using Molecular Dynamics and Steered Molecular Dynamics Simulations

Molecular dynamics (MD) simulations are commonly used to observe the behavior of the peptide and the system upon the penetration of the peptide into the membrane. Protein insertion and positioning in a membrane host are of particular interest in transmembrane peptides. As experimental approaches continue to expand in this area, computational approaches are also being used. Observation of an action at microseconds to milliseconds is not currently possible by all-atom MD simulations [20]. Steered molecular dynamics simulations recently gathered attention and can be used for the analysis of peptide uptake through bacterial membranes, unfolding of proteins/peptides and protein-protein or protein-membrane interaction energy determination.

Transportan 10 (tp10) binds to the zwitterionic POPC in a parallel orientation facing its hydrophobic side to the bilayer core. Within 200ns of simulation time, the hydrophobic side of the peptide is inserted in the membrane. The simulations suggested that Lys-phosphate salt bridge determines the orientation of the peptide and stabilizes the peptide. Some snapshots of the system can be seen in Figure 1.4. Although complete insertion was not observed in the simulations due to the simulation length, complete insertion is expected to be similar to other lysine rich peptides [21].

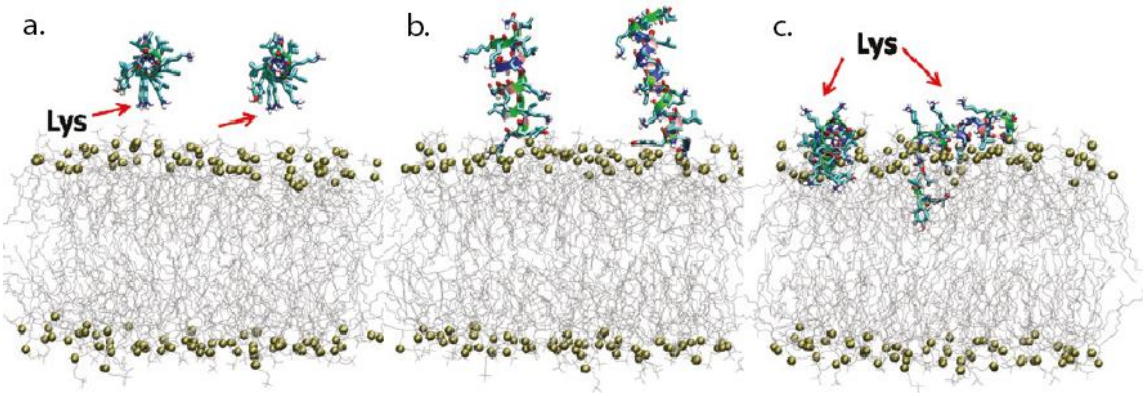

Figure 1.4. Snapshots representing the initial association of tp10 molecules with the POPC bilayer surface. (a) initial conformation of the system, (b) first contact of tp10 with the bilayer interface, and (c) snapshot after 21 ns [21].

Tat peptide (^{47}YGRKKRRQRR^{57}R) is segment responsible for cellular uptake of the HIV-1 Tat complex. Extensive molecular dynamics simulations on lipid bilayer (DOPC)-Tat peptides and water system were performed in order to investigate the mechanism of membrane translocation. Several systems differing in number and concentration of the peptides, phospholipids and water molecules were examined. The results of the molecular dynamics simulations showed that the bilayer becomes thinner as the Tat peptide concentration is increased. The penetration into the membrane starts with the attraction between the Arginine and Lysine side chains of the Tat peptide and the phosphate groups of the lipid bilayer. Water also penetrates as the side chains enter the membrane. At large timescales, the penetration of water causes formation of a transient water pore in the membrane. However, cell death because of a leakage is not observed because of the nature of the water [22].

All atom MD simulations were used to study the insertion and stabilization of a lipidated peptide. In their simulations, the authors applied an artificial force on the lipidated peptide to induce the insertion process. Once inserted, the applied force was turned off, and the lipidated peptide was allowed to stabilize. This approach, which is also known as steered molecular dynamics (SMD), was used to enhance the rate of insertion [20].

The use of SMD for uptake of peptides is valid as long as the applied force does not significantly destroy the model membrane during the simulations. If the membrane thickness, order parameters, or cross-sectional area of the membrane changes dramatically upon the insertion of the peptide, the SMD simulation is considered unrealistic. Therefore, selection of the magnitude of the pulling force or velocity is a critical parameter to be chosen. On the other hand, SMD is advantageous compared to MD simulations because of the time scale the insertion takes place [20].

The impact of three SMD parameters on the uptake mechanism such as spring elastic constant and the pulling group was investigated. For these purposes, a simplified model membrane was used. Three SMD simulations with different spring constants: k_1= 0.1, k_2= 0.6 and k_3=4 kcal/mol $Å^2$ were analyzed for the amino acid tryptophan. The pulling velocity was set to 0.015 Å/ps (1.5 m/s) and the pulling-group was one of the oxygen atoms of the C-terminal (COO^-). For the pentapeptide AcWLKLL, two SMD simulations were carried out with different pulling-groups which are the N- and C-terminal of this peptide and the extraction pathways and the system responses for these two pulling-groups were analyzed. As a result of these simulations, it was seen that exit pathways and interaction force values were conserved when the pulling velocity or the spring constant were varied. Moreover, different extraction pathways were followed when different conformations were compared or when different pulling-groups were considered for the same conformations. The SMD simulations demonstrated that the pulling group selection is quite important for determining the interaction pathway and consequently, diverse force responses. As a result, with the appropriate combination of the SMD parameters a precise analysis of any biological system may be performed [23].

1.4. *In-vivo* Peptide Uptake Studies

The kinetics and mechanism of peptide uptake have been examined using experiments, with focus on the uptake potential of different peptides. The uptake of fluorophore-labeled pVEC was compared to penetratin in four different cell lines, which are human aortic endothelial cells, brain capillary endothelial cells, Bowes melanoma cells and murine brain endothelial cells. Fluorescence microscopy was used to display the uptake of the peptides. It was determined that the intracellular concentration of pVEC was highest in the murine brain endothelial cells. For the comparison of the pVEC and the penetratin, all cell lines showed equal or slightly higher concentrations of pVEC that the penetratin. As a result, pVEC was determined to be a potent carrier peptide due to its efficient and rapid penetration characteristic into the cells [18].

In structure-activity relationship (S.A.R) experiments on pVEC, each residue of the original pVEC molecule was mutated to L -or D-alanine and the change in the cellular uptake of pVEC into the cells was examined to define the contribution of each residue to cellular uptake. The cellular uptakes of retro-pVEC with reversed sequence and the scramble pVEC, which has the same amine acid content with mixed sequence, were also studied. All the pVEC analogues are listed in Table 1.3. The pVEC and D-pVEC were treated with endocyctotic inhibitors: wortmannin, nystatin, heparinase III or EIPA in order to check whether translocation of pVEC occurred via endocytosis. Also, the cellular uptake of pVEC and D-pVEC in different temperatures was investigated [17].

Substitution of the first five amino acids in the N terminus of pVEC to L-alanine resulted in decrease of the cellular uptake values to 50-75% (Figure 1.5) suggesting that the hydrophobic N-terminus of the peptide was important for the cellular uptake. Significant reduction in uptake values was also spotted when the 9^{th} and 14^{th} residues of pVEC were mutated. The cellular uptake of the scramble pVEC was reduced the most [17].

Table 1.3. Sequences and properties of pVEC and its analogues [17].

Sequence	Name	Molecular mass (Da)	Rt (min ± S.D.)	Positive charges
LLIILRRRIRKQAHAHSK	pVEC	2208.7	22.1 ± 0.2	7
ALIILRRRIRKQAHAHSK	[Ala1]pVEC	2166.7	21.1 ± 0.9	7
LAIILRRRIRKQAHAHSK	[Ala2]pVEC	2166.7	20.9 ± 0.2	7
LLAILRRRIRKQAHAHSK	[Ala3]pVEC	2166.7	21.5 ± 0.3	7
LLIALRRRIRKQAHAHSK	[Ala4]pVEC	2166.7	21.7 ± 0.2	7
LLIIARRRIRKQAHAHSK	[Ala5]pVEC	2166.7	21.9 ± 1.4	7
LLIILARRIRKQAHAHSK	[Ala6]pVEC	2123.6	23.0 ± 0.4	6
LLIILRARIRKQAHAHSK	[Ala7]pVEC	2123.6	22.0 ± 0.7	6
LLIILRRAIRKQAHAHSK	[Ala8]pVEC	2123.6	25.5 ± 0.2	6
LLIILRRRARKQAHAHSK	[Ala9]pVEC	2123.6	21.5 ± 0.8	7
LLIILRRRIAKQAHAHSK	[Ala10]pVEC	2123.6	16.3 ± 0.9	6
LLIILRRRIRAQAHAHSK	[Ala11]pVEC	2151.6	22.3 ± 0.2	6
LLIILRRRIRKAAHAHSK	[Ala12]pVEC	2151.7	21.9 ± 0.2	7
LLIILRRRIRKQAHAHSK	[D-Ala13]pVEC	2208.7	21.6 ± 0.1	7
LLIILRRRIRKQAAAHSK	[Ala14]pVEC	2142.7	21.6 ± 0.5	7
LLIILRRRIRKQAHAHSK	[D-Ala15]pVEC	2208.7	16.4 ± 0.0	7
LLIILRRRIRKQAHAASK	[Ala16]pVEC	2142.7	22.4 ± 1.0	7
LLIILRRRIRKQAHAHAK	[Ala17]pVEC	2192.7	18.5 ± 3.2	7
LLIILRRRIRKQAHAHSA	[Ala18]pVEC	2151.6	17.6 ± 1.3	6
KSHAHAQKRIRRRLIILL	retro-pVEC	2208.7	16.5 ± 4.4	7
LLIILRRRIRKQAHAHSK	D-pVEC	2208.7	16.6 ± 0.0	7
IAARIKLRSRQHIKLRHL	scramble pVEC	2208.7	10.2 ± 0.01	7

When the effect of the endocytosis inhibitors was examined, it was seen that only wortmannin decreased pVEC uptake. Other inhibitors had no affect on pVEC and D-pVEC. For the effect of temperature on uptake, no important change was detected in the uptake when the temperature was decreased from 310 K to 281 K [17]. The overall uptake kinetics of three CPPs M918, TP10 and pVEC was studied using a quenched fluorescence assay. By this study, it is proved that different CPPs might exploit different pathways simultaneously. When cells are treated with different endocytosis inhibitors uptake levels and overall kinetic profile of the uptake is changed [24].

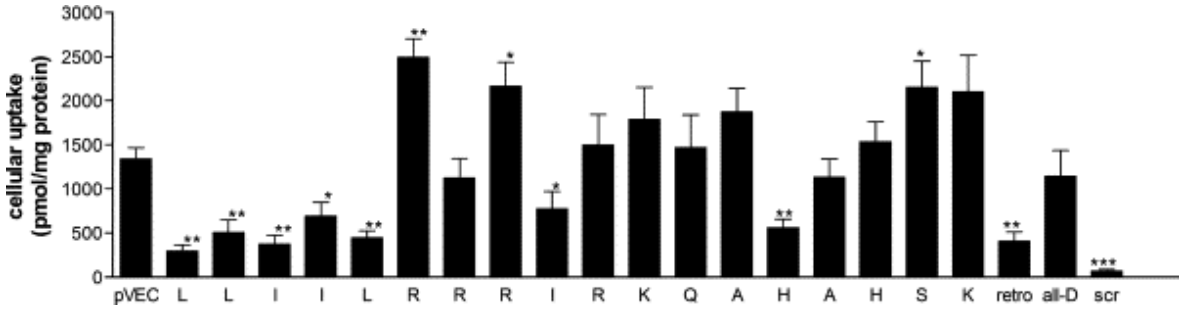

Figure 1.5. The cellular uptake values of the pVEC analogues [17].

There are a few studies that couple molecular dynamics with experimental methods which is a useful approach toward rational designs for therapeutic use. As an example, Indolicidin (IL) with the sequence H-ILPWKWPWWPWRR-NH_2 was studied to show that the presence of hydrophobic tryptophan residues leads to deeper insertion of the peptide while positive charges are critical to the peptide's adsorption. IL diffuses spontaneously from the aqueous phase to the water-lipid head group interface. Despite the results obtained for the POPC system, in which the tryptophan residues were positioned within the hydrophobic regions of the lipids, it was observed that some of the tryptophan residues are located at the water lipid interface of the POPG/POPC bilayer system. Thickness of the pure POPC lipid bilayer decreases when the peptide inserts into the hydrophobic region while the mixed POPG/POPC lipid bilayer becomes thinner upon the adsorption of IL at the water-lipid interfacial region. The zwitterionic POPC lipid bilayer became disordered mainly upon the insertion of IL and not upon its adsorption [25].

1.5. Motivation and Objective

The ultimate goal of this study is to design a BLIP based peptide that is not only able to penetrate into the cell lines, but also able to inhibit intracellular β-lactamase. For this aim, first the nature and uptake mechanism of the cell-penetrating peptide pVEC is examined. Also, the peptide is analyzed on a residue basis in order to be able to determine the significant residues that have an important role during the translocation of the peptide. For these analysis on pVEC, molecular dynamics and steered molecular dynamics simulations were used.

After understanding the translocation mechanism and significance of each residue of pVEC, it was aimed to investigate if these findings could be used to enhance the bacterial uptake of BLIP based peptides. For this part of the study, the effect of two BLIP based peptides and one other peptide which was proved to be a potent β-lactamase inhibitor, on the growth of antibiotic resistant *E. coli* K12 pUC18 cells was examined. *In-vivo* experiments using Peptide 1 (5-Fluorescein-NH-HA AGDYYAY- $CONH_2$), Peptide 2 (5/6-Fluorescein-NH-RRGHYY-COOH) and Peptide 3 (5/6-Fluorescein-NH-LLIILHAAGDYYAY- $CONH_2$) were carried out and the uptake of these fluorescein labeled peptides were visualized using fluorescence microscopy. The effect of addition of the five N-terminal residues (LLIIL) to the BLIP 45-53 residues (HAAGDYYAY) was examined to see if an antimicrobial peptide could be designed using an inhibitor protein and a cell-penetrating peptide.

2. MATERIALS AND METHODS

2.1. Computational Materials and Methods

2.1.1. Molecular Dynamics Simulations

Computer simulations are used as a bridge between the theoretical knowledge and the experimental applications and results. Molecular dynamics simulation (MD) method is one of the basic tools that can be used for computational simulations of model systems. Time dependent manner of a molecular system is calculated and measured by this method. Detailed information on the dynamics and conformational changes of proteins can be obtained from MD simulation trajectories [26, 27].

In MD Simulations, motions of atoms are simulated as a function of time according to Newton's equation of motion:

$$F = ma \tag{2.1}$$

where F is the force exerted on the particle, m is the mass of the particle and a is the acceleration of the particle.

The force can be also expressed as the gradient of the potential energy,

$$F = -\nabla V \tag{2.2}$$

By combining two equations the expression below is obtained;

$$F_i = -\frac{dV}{dr_i} = m_i \frac{d^2 r_i}{dt^2} \tag{2.3}$$

where r_i is the atomic coordinates of the particle, t is time and V is the potential energy of the system.

Newton's equation of motion can then relate the derivative of the potential energy to the changes in position as a function of time.

MD simulation of a protein includes three stages: minimization, equilibration and data collection stages. Energy minimization plays an essential role in starting dynamics simulations. The purpose is to bring the molecule to a conformation where its potential is at the minimum since the molecule is in a force field. The aim of equilibration is to bring the system to a favorable conformation at the target temperature and pressure.

2.1.1.1. CHARMM Force Field. In order to describe the relationship of chemical structure to energy, mathematical equations are applied in theoretical chemistry. Combined with statistical mechanics, all properties of a system can be calculated with this information. However, the energy of all possible conformations of a chemical system cannot be calculated. In order to handle this problem, simple mathematical functions must be used to treat the structure-energy relationship. This method is only valid for biological molecules with a molecular weight greater than 10 kDa and the aqueous environment must be included. This method is named as molecular mechanics or empirical force field calculations. However, the equation alone is not adequate to compute the structure-energy relationships. Parameters must be added in the mathematical equation. The empirical force field used in this study is CHARMM22 [28].

The intramolecular potential energy function is:

$$V_{intra} = \sum_{bonds} K_b(b - b_o)^2 + \sum_{angles} K_\theta(\theta - \theta_o)^2 + \sum_{torsions} K\phi(1 + \cos(n\phi - \delta)) + \sum_{impropers} K_\varphi(\varphi - \varphi_o)^2 + \sum_{Urey-Bradley} K_{UB}\left(r_{1,3} - r_{1,3,o}\right)^2 \quad (2.4)$$

The first term in Eq. 2.4 is the covalent bond stretching interaction where $b - b_o$ is the distance from equilibrium that the atom has moved and $K_b$is the bond force constant. The second term is associated with bond angles where $\theta - \theta_o$is the angle from equilibrium between 3 bonded atoms and $K_\theta$is the angle force constant. The third term is for the dihedral angle interaction where n is the multiplicity of the function, $\phi$is the dihedral angle, δ is phase shift and $K\phi$ is the dihedral force constant. The fourth term is associated with the impropers. $\varphi - \varphi_o$is the out of plane angle and K_φ is the impropers force constant. The fifth term is the Urey-Bradley component where $r_{1,3} - r_{1,3,o}$ is the distance between the 1, 3 atoms in the harmonic potential and $K_{UB}$is the force constant.

The intermolecular potential energy function is

$$V_{inter} = \sum_{electrostatic} \frac{q_i q_j}{r_{ij}} + \sum_{VDW} \varepsilon_{ij} \left[\left(\frac{R_{min,ij}}{r_{ij}} \right)^{12} - 2 \left(\frac{R_{min,ij}}{r_{ij}} \right)^{6} \right] \tag{2.5}$$

The first term in Eq. 2.5 corresponds to the electrostatics energy contribution and the second term is the van der Waals energy contribution. ε is the Lennard-Jones (vdW) well-depth. $R_{min}$is the Lennard-Jones radius and q is the partial atomic charge [28].

$$V = V_{intra} + V_{inter} \tag{2.6}$$

2.1.2. Steered Molecular Dynamics Simulations

Steered Molecular Dynamics (SMD) simulations are used to explain single molecule experiments, to overcome slow natural time scales and to explore putative conformational pathways. The idea behind any SMD simulation is to apply an external force to one or more atoms which are called the SMD atoms. There are two types of SMD simulations: constant velocity pulling and constant force pulling [29].

In the constant velocity pulling simulation, the SMD atom is attached to a dummy atom via a virtual spring. This dummy atom is moved at constant velocity and then the force between these two atoms is measured using:

$$\vec{F} = -\nabla V \tag{2.7}$$

$$V = \frac{1}{2}k[vt - (\vec{r} - \vec{r}_0) * \vec{n}] \tag{2.8}$$

In Eq. 2.7, $\vec{F}$ is the force applied and V is the potential energy. In Eq. 2.8, k is the spring constant, v is the pulling velocity, t is time, $\vec{r}$ is the actual position of the SMD atom, $\vec{r}_0$ is the initial position of the SMD atom and finally, $\vec{n}$ is the direction of pulling [29].

2.1.3. Simulation Systems

The peptide pVEC with the sequence LLIILRRRIRKQAHAHSK (wild-type), 8 pVEC mutants, retro-pVEC, which has the same sequence in reverse order (KSHAHAQKRIRRRLIILL) and scramble-pVEC, which has the same amino acid content in random order (IAARIKLRSRQHIKLRHL) were studied (Table 2.1).

The initial coordinates of the peptides were assigned randomly and were prepared manually through the Visual Molecular Dynamics (VMD) program [30]. The coordinates of the residues Histidine and Alanine of the pVEC peptides were assigned from the coordinates of HAAGDYYA peptide which is the sequence of BLIP 45-53 residues. Other residues were guessed by VMD. The mutant coordinates were obtained using psfgen package of VMD.

The pVEC peptide with the sequence LLIILRRRIRKQAHAHSK (or its mutants) was randomly placed into a water box of 10 Å x 10 Å x 10 Å dimensions. The water molecules 2.8 Å close to the peptide were removed. The water-peptide system was minimized for 1000 steps and equilibrated for 2 ns with constraints on peptide atoms. Then

all the atoms of the system were left free and the system was equilibrated for 2 ns further. Finally, the peptide was extracted from the water-box.

Table 2.1. The pVEC sequences used in the simulations and the mutated residue for each sequence.

Name	Sequence	Mutated residue
wt*	LLIILRRRIRKQAHAHSK	wild-type pVEC
L2A*	L**A**IILRRRIRKQAHAHSK	L2A
L5A	LLII**A**RRRIRKQAHAHSK	L5A
R6A	LLIIL**A**RRIRKQAHAHSK	R6A
R7A	LLIILR**A**RIRKQAHAHSK	R7A
R8A	LLIILRR**A**IRKQAHAHSK	R8A
I9A*	LLIILRRR**A**RKQAHAHSK	I9A
H14A*	LLIILRRRIRKQA**A**AHSK	H14A
S17A	LLIILRRRIRKQAHAH**A**K	S17A
r pVEC*	KSHAHAQKRIRRRLIILL	retro-pVEC
scr pVEC*	IAARIKLRSRQHIKLRHL	scramble pVEC

* Simulations marked with asterisk sign were carried out and analyzed in a previous study [31].

The membrane was created in 50 Å in x- and 50 Å in y-directions. The lipid of the membrane was chosen to be POPE in order to mimic the membrane of *E. coli* [32]. The membrane was solvated with TIP3P water molecules 80 Å in positive and negative z-directions. After solvation, the water-membrane system was equilibrated for 0.5 ns with constraints on the lipid tails and for 0.5 ns without any constrains.

The previously equilibrated peptide was placed into the water layer above the membrane manually such that the minimum distance between the peptide atoms and the membrane phosphate atoms was more than 10 Å.

The system composed of water, membrane, peptide and ions was ready for SMD simulation (Figure 2.1). Steered molecular dynamics simulations [29] were performed by applying force on the C_α atom of the first N terminal residue (SMD atom) of the peptide in

the z-direction to move the peptide from one side of the membrane to the other. For these simulations, the phosphorous heads of the lipid bilayer were fixed in z-direction while they were free to move in x- and y-directions.

The spring constant was set to 10 kcal/mol/$Å^2$ and the velocity of pulling was chosen as 0.0000050 Å/timestep which corresponds to 2.50 Å/ns with timestep=2.0 fs. The peptide traveled a total of 120 Å to completely traverse the membrane within about 50 ns or more simulation time.

The simulations were performed at 300 K and 1 atm pressure. In the configuration file, the simulation parameters and the extra parameters were manually adjusted. Periodic boundary conditions were modified according to the system size. The SMD data values were set to be printed out every 20 timesteps. The restart files and dcd files were printed out every 1000 timesteps, whereas, the energy and pressure values for the systems were calculated every 50 timesteps.

Throughout the MD and SMD simulations, NAMD2 program and CHARMM22 force field were used. NAMD2 is a parallel program aimed at utilizing large parallel machines in a scalable manner. The non-bonded force computations require calculation of pairwise interactions between atoms. In most common methods, a cutoff distance is used. Non-bonded interactions between atoms beyond this cutoff radius are not calculated or calculated rarely [33]. CHARMM22 force field calculates and prints out the properties of the systems such as coordinates of the atoms, force and energy values.

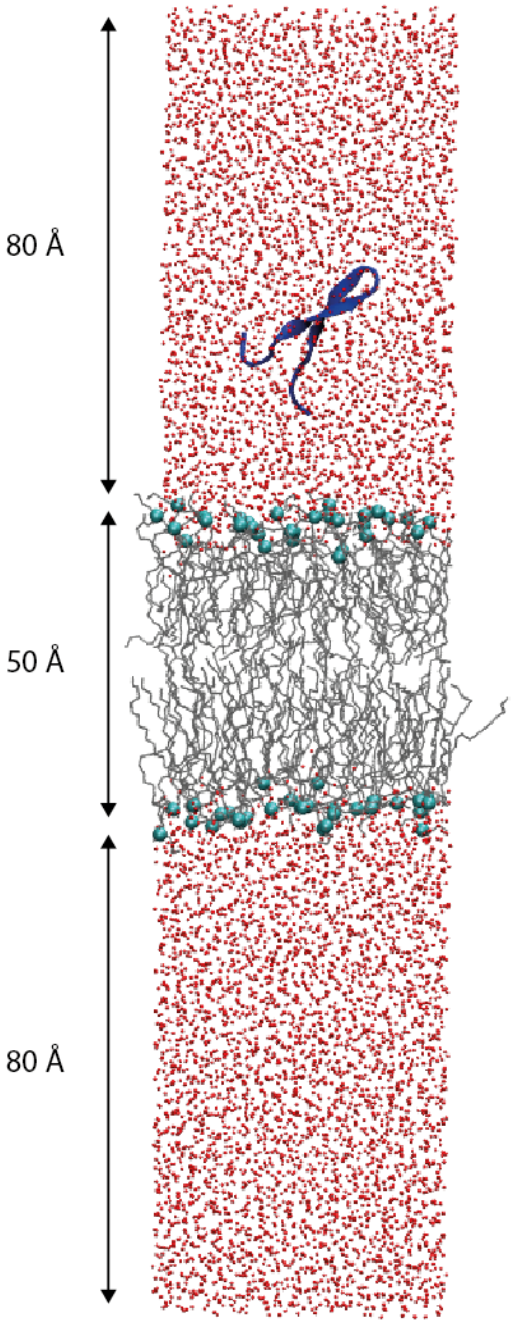

Figure 2.1. The structure of the system of water, membrane and peptide of wild-type pVEC before the SMD simulation.

2.2. Experimental Materials and Methods

2.2.1. Materials

2.2.1.1. Bacterial Strains and Plasmids. The experiments were performed with the *Escherichia coli* K12 strain. Cells were obtained from previously prepared laboratory stocks. β-lactamase expression was obtained from pUC18 plasmid carrying the gene for RTEM-1. pUC18 plasmid vector was also obtained from laboratory stocks.

2.2.1.2. Chemicals, Buffers and Solutions. All the chemicals and the solutions used in experiments were purchased from APPLICHEM (Germany), MERCK (Germany), MOLEKULA (Germany) and SIGMA (USA).

Potassium phosphate buffer was prepared and used for aliquoting the stock of peptides and tracers. Also, the buffer solution was used in the growth media for the control set and used as a wash buffer for the visualization of the cells under fluorescence microscopy.

The buffer solution was prepared both at 50 mM dilution and 1M dilution where necessary. In Table 2.2, the amount of acid and base used for the preparation of 1M of phosphate buffer at a pH of 7.0 is given.

Table 2.2. K^+PO_4 Buffer (1 M, pH 7.0).

Chemical	Amount
1M K_2HPO_4	450 ml
1M KH_2PO_4	550 ml

Ampicillin at a final concentration of 100 μg/ml was used in the growth media as the β-lactam antibiotic to select β-lactamase producing cells. Its stock solution was maintained at 100 mg/ml.

2.2.1.3. Laboratory Equipments. All used equipments during the experiments are are given in Table 2.3.

Table 2.3. The list of laboratory equipments.

Purpose	**Equipment**
Absorbance Measurement	DU 640 Spectrophotometer (Beckman, USA) Specord 200 (Analytikjena, UK)
Centrifugation	1-15 centrifuge (SIGMA, Germany)
Deep freezer	Ultra Low Temperature Freezer U410 Premium (New Brunswick Scientific, USA)
Incubation	FN500 Incubator (Nüve, Turkey)
Orbital Shaker	ZHWY-211B Shaker Incubator (ZHICHENG, China) Innova 4340 (New Brunswick Scientific, USA)
Sterilization	Steam Sterilizer OT40L (Nüve, TURKEY)
pH Measurement	pH meter (SCHOTT, Germany)
Pipetting	1-10, 10-100, 100-1000 µl pipettes (Thermo Electron Corporation, CANADA)
Power Supply	Power EC250-90 (Thermo Electron Corporation, CANADA)
Refrigerating	Refrigerator (RT59EBPN)
Sterile Environment	Microbiologic Safety Cabinet MN 120 (Nüve, Turkey)
Vortexing	Reax Top Vortex (Heidolph, Germany)
Water Purification Systems	MILLI-Q UF Plus (MILLIPORE, USA) MILLIPORE Elix® 5 UV (MILLIPORE, USA)
Weighing	Balance XB 220A (Precisa, Switzerland)
Magnetic Stirrer	CAT M6.1 (Germany)
Fluorescence Microscopy	Axio Observer A1 (Carl Zeiss Microscopy, GmbH Germany)

2.2.1.4. Growth Media. In all of the experiments, the cells were cultured in LB medium and plated in LB-agar medium. The contents of the LB and LB-agar medium are given in Table 2.4 and Table 2.5 respectively.

Table 2.4. LB medium.

Chemical	**Amount**
Peptone	10 g
Yeast extract	5 g
NaCl	10 g
Add dH_2O up to 1 liter	

Table 2.5. LB-agar medium.

Chemical	**Amount**
Peptone	10 g
NaCl	10 g
Yeast extract	5 g
Agar	15 g
Add dH_2O up to 1 liter	

2.2.1.5. Peptides and Tracers. For the experiments conducted, the peptides and tracer used along with their names, sequences and amount of stock are listed in Table 2.6.

The peptides and tracers were ordered from Thermo Fischer Scientific with > 95% purity. Stocks were stored dry, in the refrigerator at -20°C. The peptides and the tracers were then handled at appropriate conditions suggested in their user manuals and maintained at -20°C.

Peptide 1 and Peptide 3 were peptides based on BLIP 45-53 residues. Peptide 3, in addition to that, has the first 5 residues of the cell-penetrating peptide pVEC[17] in its N terminal. Both of the peptides have fluorescein attached as a tracer for the visualization under fluorescence microscopy. The peptides were delivered as powder in glassware and they were maintained at -20°C. They were both dissolved with 50 mM K^+PO_4 buffer

(pH=7.0) to a concentration of 1 mM and then aliquoted. After aliquoting, the stocks were kept in the refrigerator at -20°C.

Table 2.6. The name, sequence and amount of stock of the peptides and traces used.

Name	**Sequence/Molecular Formula**	**Amount of Stock**
Peptide 1	5-Fluorescein-NH-HAAGDYYAY- $CONH_2$	15.4 mg
Peptide 2	5/6-Fluorescein-NH-RRGHYY-COOH	10.0 mg
Peptide 3	5/6-Fluorescein-NH-LLIILHAAGDYYAY- $CONH_2$	10.0 mg
Kemptide Acetate Salt	LRRASLG ($C_{32}H_{61}N_{13}O_9$)	5.0 mg
Fluorescein Amine	$C_{20}H_{13}NO_5$	1.0 mg

Peptide 2 was previously shown to be a potent TEM-1 β-lactamase inhibitor with K_i of 136 μM [34]. The peptide was delivered as powder in glassware and was maintained at -20°C. Since the amino acid Arginine has a positively charged side chain, the peptide was dissolved in 50 mM K^+PO_4 buffer (pH=7.0) to a concentration of 1 mM and then acetic acid was added. The peptide was dissolved to a final concentration of 0.91 mM and aliquoted. After aliquoting, the stocks were kept in the refrigerator at -20°C.

Kemptide Acetate Salt was used as a negative control peptide which is expected not to inhibit the β-lactamase enzyme. The peptide was delivered as powder in glassware and was maintained at -20°C. It was dissolved with 50 mM K^+PO_4 buffer (pH=7.0) to a concentration of 1 mM and then aliquoted. After aliquoting, the stocks were kept in the refrigerator at -20°C.

Fluorescein Amine was used in order to determine the required fluorescein concentration for visualization by fluorescence microscopy. It was delivered as powder in dark brown glassware and was maintained at -20°C. It was dissolved with 1 M K^+PO_4 buffer (pH=7.0) to a concentration of 1 mM and then aliquoted. After aliquoting, the stocks

were kept in the refrigerator at -20°C away from sunlight. Due to the luminescence characteristic of Fluorescein Amine, stock, aliquotes and samples were always kept away from light.

2.2.2. Methods

2.2.2.1. Sterilization. All of the experiments were carried out using sterilized equipments. Tips, glassware, centrifuge tubes, solutions and culture media were sterilized at 1 atm and 121 °C for 15 minutes using a steam sterilizer. Stock solutions of antibiotics were filter sterilized through 45 μm pore sized membranes. Experiments that required sterile environment were carried out under laminar flow.

2.2.2.2. Preparation of Bacterial Stocks. 5 ml of sterile LB medium was inoculated with a single colony of bacteria from a master plate. Inoculation was carried out by a sterile tip. Preculture was incubated overnight in an orbital shaker that was adjusted to 37 °C and 180 rpm. LB medium was supplemented with ampicillin. Grown cells were added at 1:1 v/v ratio to sterile centrifuge tubes containing 50% sterile glycerol and stocks were stored at -80 °C.

2.2.2.3. Preparation of Preculture. 2 ml of sterile liquid medium supplemented with the appropriate antibiotic, was inoculated with 30 μL frozen stock culture.

2.2.2.4. Growth Conditions. Preculture was pipetted into sterile fresh growth media and cultures were grown in orbital shakers at 37 °C and 180 rpm. In order to provide efficient aeration, culture volume was adjusted to a maximum of one fifth of the test tube volume. All of the experiments were carried out in LB medium which was supplemented with ampicillin for the selection of pUC18 harboring cells. Growth of the cells was monitored by measuring the OD at a wavelength of 600 nm using a spectrophotometer.

2.2.2.5. Determination of Growth Profiles. Optical densities of *E. coli* cells were measured at a wavelength of 600 nm using a spectrophotometer in order to determine the growth profile of *E. coli* cultures. LB medium was used for both the blank and diluting the samples

to keep the spectroscopic readings within the reliable range of 0.2 to 0.8.

2.2.2.6. *In-vivo* β-lactames Inhibition by Peptides. *E. coli* K12 cells harboring plasmid pUC18 were grown in LB medium at 37 °C and 180 rpm in the presence of peptides. The cells were grown in 2 ml tubes and were treated with peptides or tracer (Peptide 1, Peptide 2, Peptide 3, Kemptide acetate salt, Fluorescein Amine) at a final concentration of 100 μM, in early logarithmic phase (OD_{600} nm ~ 0.2). Cell growth was monitored every hour at OD_{600} and bacterial cell samples were plated to determine the difference in the number of colony forming units after introduction of the inhibitor peptide or tracer to examine their inhibitory effects. Bacterial samples grown in the absence of the peptides were also plated on LB-agar plates as a control set.

2.2.2.7. Viable Cell Count. Bacterial samples were plated to determine the difference in the number of colony forming units for the control set and after inhibitor peptide induction. For a ten-fold dilution, 100 μl of the bacterial sample taken at the desired time interval was transferred into a centrifuge tube containing 900 μl of fresh LB medium and vortexed to homogenize. In order to obtain desired dilution, this procedure was repeated with the currently diluted sample. Finally, 1 ml of the appropriate dilution was deposited in a sterile Petri dish and LB-agar containing ampicillin was poured into Petri dishes. The sample and the liquid agar were mixed gently by moving the plates through an eight-shaped path. The plates were left to cool to harden and then incubated overnight at 37 °C. The colonies were counted to determine the colony forming units in Petri dishes. Average values from plates were calculated.

2.2.2.8. Visualization of Bacterial Uptake of the Peptides. For the visualization of the bacterial uptake of peptides and tracer, fluorescence microscopy was used. The peptides labeled with fluorescein (Peptide 1, Peptide 2, Peptide 3) and Fluorescein Amine are able to emit UV light and hence can be traced under microscopy. The cultures in 2 ml tubes that contained cells which were treated with peptides or tracer were used to analyze bacterial uptake at each hour of growth. A sample from the culture is extracted to be visualized under fluorescence microscopy. The culture was centrifuged at 8000 rpm for 10 minutes to separate the cells from its medium. The medium was then extracted and a sample was

taken to be visualized. The precipitated cells were washed with potassium phosphate buffer (pH=7.0) and centrifuged at 8000 rpm for 5 minutes. Cells were washed 3 times and the final precipitated cells were dissolved in 10 μL potassium phosphate buffer in order to obtain a liquid sample to be analyzed under fluorescence microscopy.

3. RESULTS AND DISCUSSION

3.1. Computational Results

The aim of this study is to investigate the translocation mechanism of the cell-penetrating peptide pVEC and to analyze the peptide on a residue basis in order to determine the structural parts that are significant for bacterial uptake. The wild-type pVEC, eight mutants, retro- and scramble pVEC were studied using molecular dynamics and steered molecular dynamics simulations. The experimental uptake values of these peptides were determined by Elmquist et al. [17]. Since no raw data on bacterial uptake values were found, the uptake of mutant pVEC peptides are presented relative to that of wild-type according to Figure 1.5. The uptake values, names and sequences of the peptides used in the simulations are given in Table 3.1.

Table 3.1. The pVEC sequences used in the simulations, the mutated residue for each sequence and *in vivo* cellular uptake values.

Name	**Sequence**	**Mutated residue**	**Uptake[a] Potential**
wt*	LLIILRRRIRKQAHAHSK	wild-type pVEC	-
L2A*	L**A**IILRRRIRKQAHAHSK	L2A	< wt
L5A	LLII**A**RRRIRKQAHAHSK	L5A	<< wt
R6A	LLIIL**A**RRIRKQAHAHSK	R6A	>> wt
R7A	LLIILR**A**RIRKQAHAHSK	R7A	≈ wt
R8A	LLIILRR**A**IRKQAHAHSK	R8A	>> wt
I9A*	LLIILRRR**A**RKQAHAHSK	I9A	< wt
H14A*	LLIILRRRIRKQA**A**AHSK	H14A	< wt
S17A	LLIILRRRIRKQAHAH**A**K	S17A	>> wt
r pVEC*	KSHAHAQKRIRRRLIILL	retro-pVEC	<< wt
scr pVEC*	IAARIKLRSRQHIKLRHL	scramble pVEC	< wt

a: The uptake potential of the peptides measured by fluorescently labeled peptide accumulation are reported with respect to the uptake of the wild-type pVEC [17].

* Simulations marked with asterisk sign were carried out in a previous study [31].

Five new SMD simulations and one MD simulation were performed in this study and the simulations were compared with previously performed simulations [31]. The system of wild-type pVEC was studied using both MD and SMD simulations. The systems of mutant pVEC peptides were studied by using SMD simulations and compared.

3.1.1. Dynamics and Interactions of the wild-type pVEC Peptide in MD Simulations

Wild-type pVEC system was studied using MD simulations for up to 170 ns simulation time without any constraints on any atoms. At the end of the simulation time, the initial penetration of wild-type pVEC into the membrane was still not observed. The distance between the center of mass of the peptide and the center of mass of the lipid bilayer was plotted as a function of simulation time and is shown in Figure 3.1.

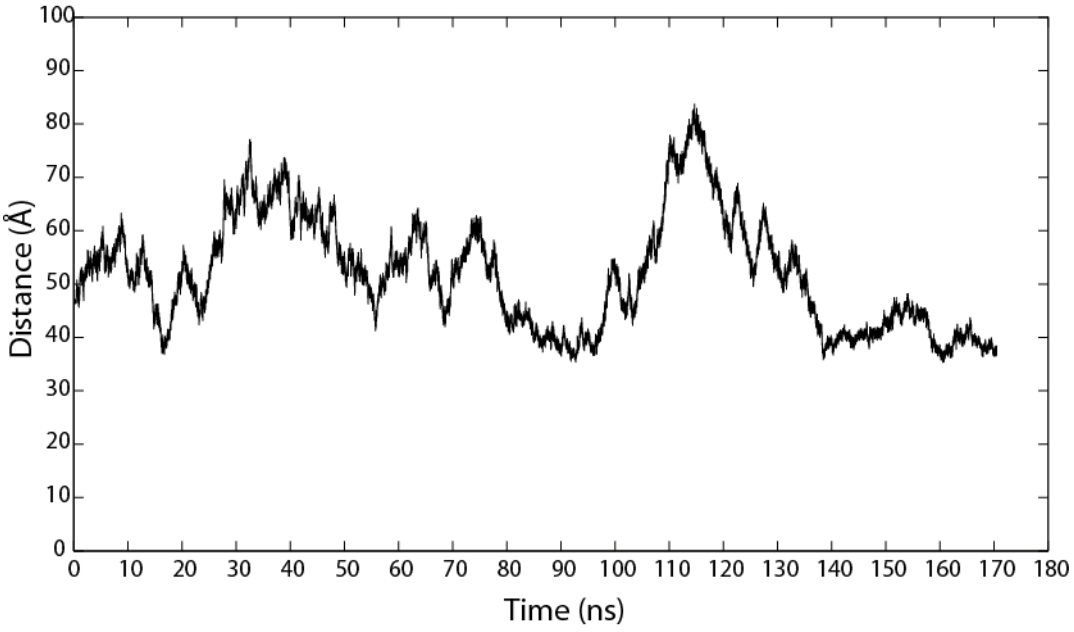

Figure 3.1. Distance between the center of mass of wild-type pVEC and center of mass of lipid bilayer plotted as a function of simulation time.

The minimum distance between the center of mass of the peptide and center of mass of the lipid bilayer was 35.3 Å at t=160.6 ns. Considering the membrane thickness is around 50 Å, the distance between the center of mass of the peptide and the upper phosphate heads of the lipid bilayer is about 10 Å. On the other hand, the maximum distance between the center of mass of the peptide and center of mass of the lipid bilayer

was 83.7 Å at t=114.7 ns. The snapshots taken at the time of minimum and maximum distance between the peptide and the membrane are shown in Figure 3.2.

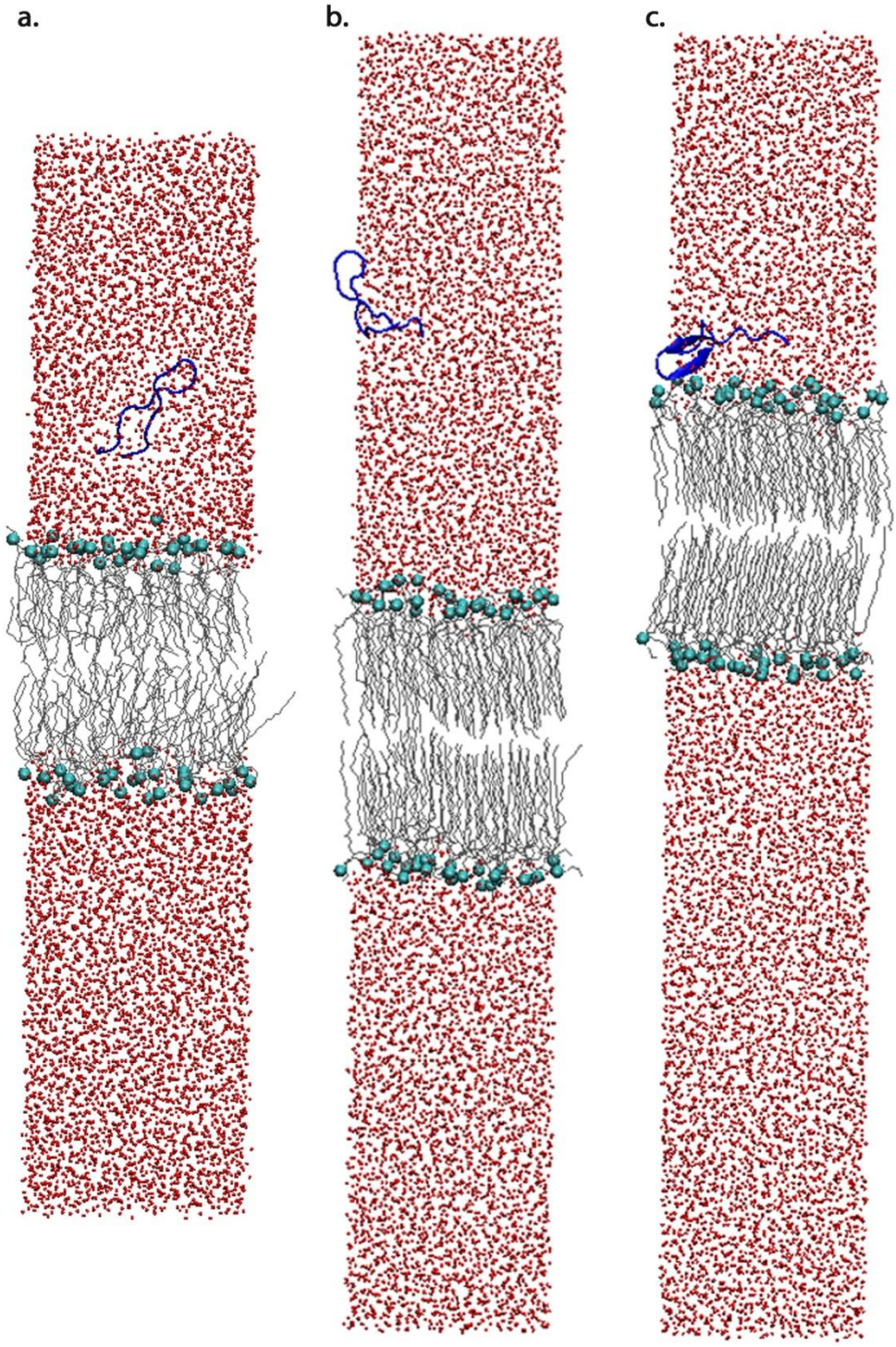

Figure 3.2. The structure of the system of wild-type pVEC in MD simulations at (a) t=0ns, (b) t=114.7ns and (c) t=160.6ns.

During the MD simulations, wild-type pVEC approaches the membrane several times. The interactions between the pVEC and the peptide was examined and it was observed that residues R6, R7, R8, R9 and R10 are frequently in contact with the membrane when the distance between the peptide and the membrane is minimum. At the absolute minimum distance between the peptide and the membrane, residue R10 is touching the upper phosphate heads and residues K11 and Q12 are in contact with the upper phosphate heads (Figure 3.2 (c)).

It was observed that pVEC does not penetrate the membrane and the system size in z-direction changes throughout the simulation. Although the thickness of the membrane stays around 54-56 Å during the simulation, the membrane moves toward positive or negative z-directions upon interacting with the peptide. Since there are no constraints on any atom of the system, the movement of the membrane results in the change of the center of the system and penetration of the peptide is not observed even at the end of a 170 ns simulation. Since no penetration of the wild-type pVEC is observed after 170 ns of MD simulations, the SMD simulations seem to be the appropriate approach for analyzing the translocation mechanism of wild-type pVEC and its mutants.

3.1.2. SMD Simulations on wild-type pVEC and Mutants

SMD simulations were performed on wild-type pVEC and mutant pVEC systems by applying force on the N terminal C_α atom (SMD atom) of the peptide in the negative z-direction to move the peptide from one side of the membrane to the other. The phosphate heads of the lipid bilayer were fixed in z-direction while they were free to move in x- and y-directions. The spring constant was set to 10 kcal/mol/Å^2 and the velocity of pulling was chosen as 0.0000050 Å/timestep which corresponds to 2.50 Å/ns with timestep=2.0 fs. Simulations were performed for minimum 50 ns in order for the peptides to complete their exit out of the membrane.

To study the dynamics of the peptide, first the displacement of the peptides was calculated. In Figure 3.3, the displacement of the SMD atom was plotted as a function of

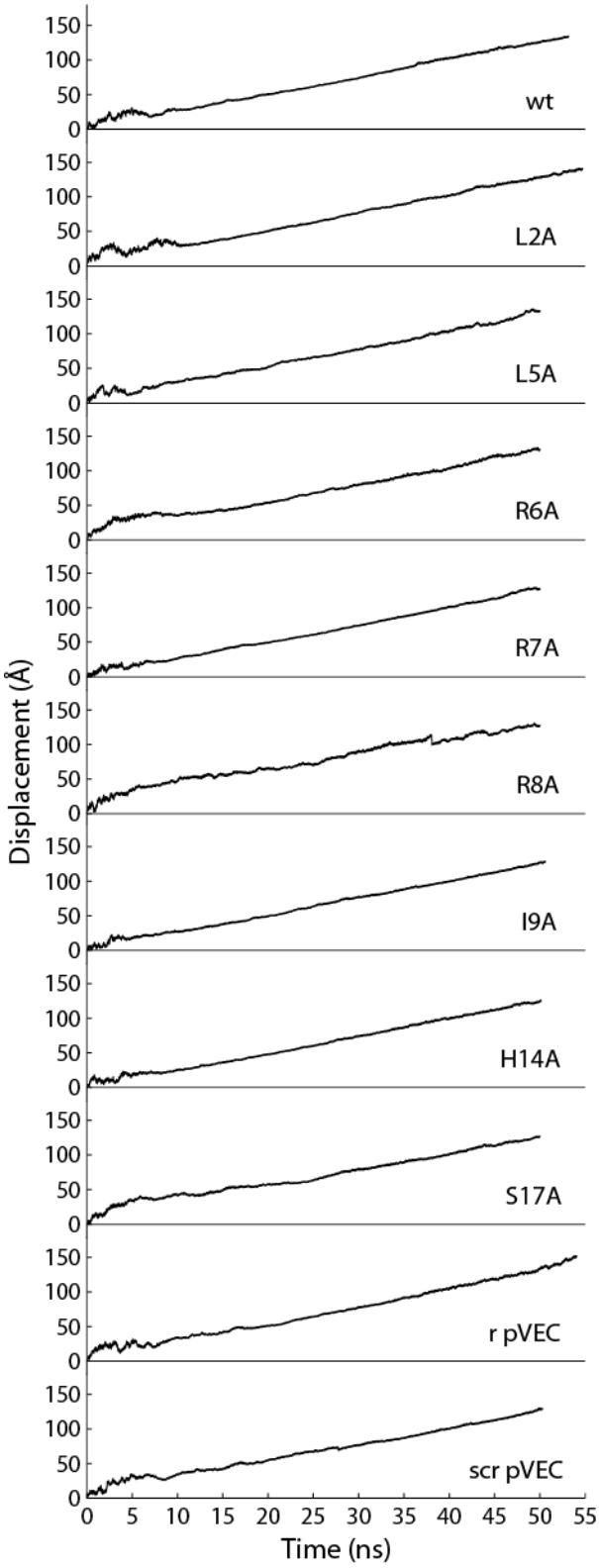

Figure 3.3. Displacement of the peptide for the systems of wt (wild-type pVEC), L2A, L5A, R6A, R7A, R8A, I9A, H14A, S17A, r pVEC (retro-pVEC) and scr pVEC (scramble pVEC).

simulation time for all the simulation systems. The displacement profiles help in understanding the movement of the peptides and verifying the pulling effect is the same for all of the systems.

When the displacement profiles of all 11 peptides (Figure 3.3) were compared, some fluctuations in the first 10-15 ns period were observed for all of the simulations. After this period, all of the profiles became almost linear with the same slope because all of the peptides were pulled with the same velocity. Some small fluctuations were still observed towards the end of the simulation time for most of the simulation systems. The initial coordinates of the peptides were not identical and for some of the peptides the simulations were extended so that the peptide completed its movement. In the first 10 ns of the simulations some fluctuations were observed. These were caused by the movements of the peptide not only in z direction, but also in the x-y plane before the penetration into the lipid bilayer. Mobility in the x-y plane is reduced in the lipid membrane environment compared to the water phase. Thus, after 10 ns, the displacement profiles became almost linear since the unfolding was completed and the extended peptide movement through the membrane was in a straight line only in negative z direction. Towards the end of the simulations, some small fluctuations were observed due to the folding of the peptides back into their initial form after they left the membrane. Due to the difference in the simulation time, these small fluctuations were not clearly observed for all of the simulation systems.

3.1.2.1. Interactions Between pVEC and the Membrane. To reveal the translocation mechanism of wild-type pVEC, first, the interaction between the SMD atom and phosphate heads of the lipid bilayer was analyzed. For the selections of C_α of the SMD atom and phosphate heads of the lipid bilayer, the interaction energy, van der Waals and electrostatic energy values were calculated and plotted as a function of z coordinate of the SMD atom in Figure 3.4a, Figure 3.4b and Figure 3.4c respectively. Simulation snapshots taken at the labeled points in the interaction energy plot in Figure 3.4a corresponding to the major changes in interaction energy profile are shown in Figure 3.5.

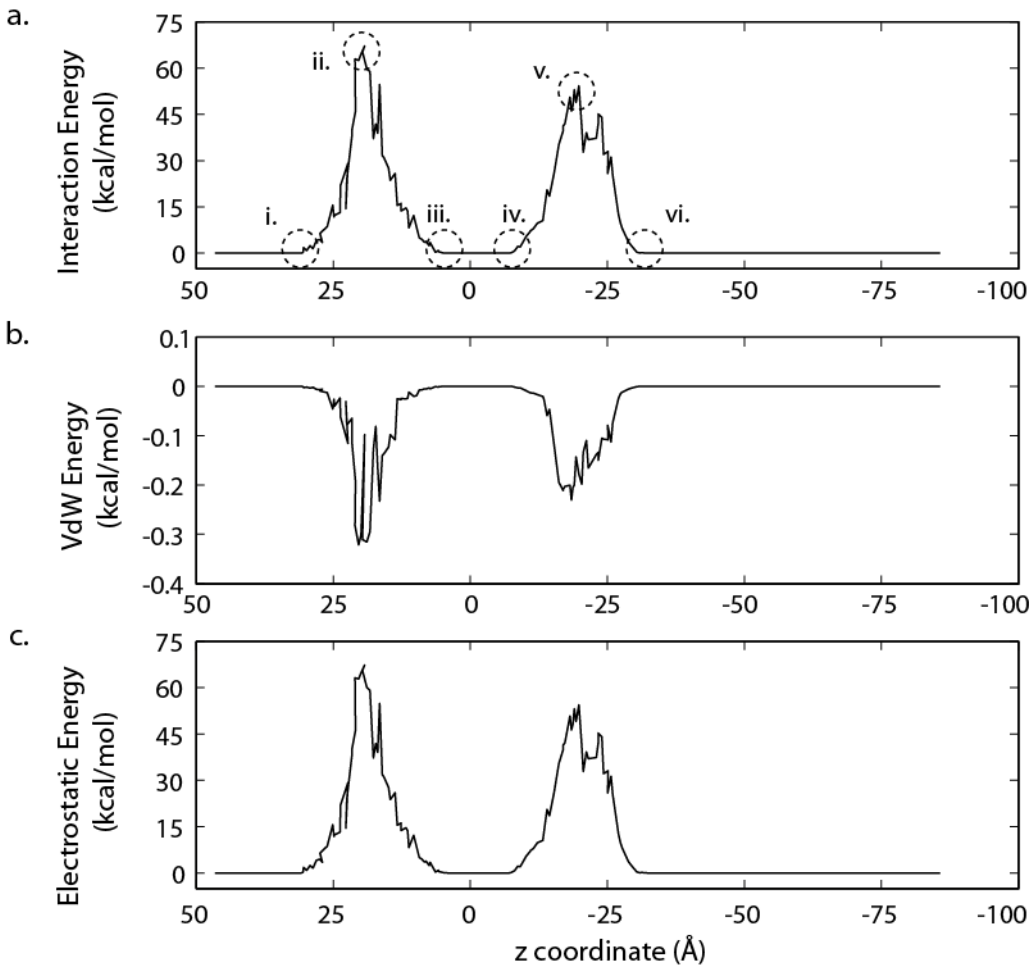

Figure 3.4. (a) The interaction energy (b) van der Waals energy and (c) electrostatic energy between the SMD atom and phosphate heads of the lipid bilayer of the wild-type pVEC system as a function of the z-coordinate of the SMD atom.

The peptide is represented in red and NewRibbons representation, the phosphate heads are shown as cyan spheres and lipid tails are highlighted in gray and Lines representation in Figure 3.5. The rendering was carried out using VMD. The same color scheme is used in Figure 3.7, Figure 3.9 and Figure 3.14.

The initial interaction energy between the SMD atom and the phosphate heads is zero at t=0 ns of the simulation. When the peptide is moving in the upper water layer, there is no interaction between the SMD atom and the upper phosphate heads. The interaction does not occur until the SMD atom, thus the peptide is in contact with the top of the membrane. After (i) z=31.2 Å and t=6.2 ns the interaction and electrostatic energy starts to increase (Figure 3.4a (i) and Figure 3.5 (i)).

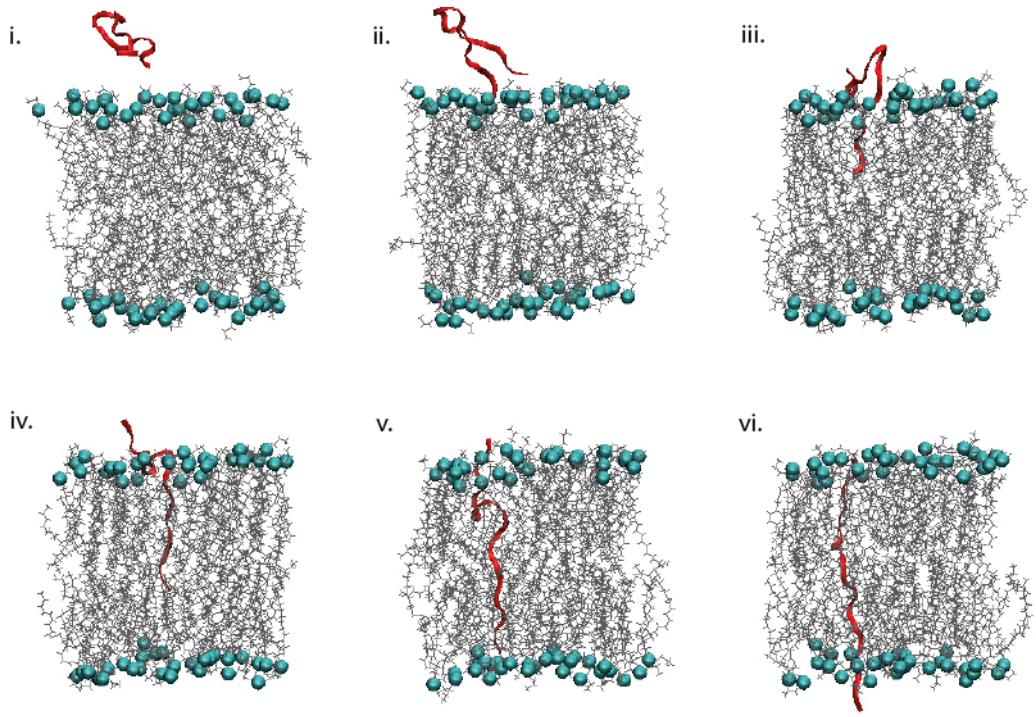

Figure 3.5. The structure of the system of wild-type pVEC at (i) z=31.2 Å and t=6.2 ns, (ii) z=19.3 Å and t=11.2 ns, (iii) z=4.1 Å and t=17.3 ns, (iv) z=-7.1 Å and t=21.9 ns, (v) z=-19.8 Å and t=27.3 ns, (vi) z=-32.3 Å and t=31.9 ns.

The interaction energy increases as the SMD atom moves toward the membrane and reaches a maximum value of 67.2 kcal/mol at (ii) z=19.3 Å and t=11.2 ns when the SMD atom is nestled between the phosphate heads which corresponds to the insertion of the peptide (Figure 3.4a (ii) and Figure 3.5 (ii)). After this point, the peptide moves through the membrane and the interaction energy decreases from 67.2 kcal/mol to 0 kcal/mol between (ii) and (iii). Between (iii) z=4.1 Å, t=17.3 ns and (iv) z=-7.1 Å, t=21.9 ns the SMD atom is located in the center of the membrane away from the phosphate atoms and the peptide is embedded in the membrane. Thus, the interaction, van der Waals and electrostatic energy are 0 kcal/mol again (Figure 3.4a (iii) and (iv), Figure 3.5 (iii) and (iv)). As the SMD atom heads toward the lower phosphate layer of the membrane the interaction energy increases once more and reaches a second maximum value of 54.3 kcal/mol at (v) z=-19.8 Å and t=27.3 ns where the SMD atom is nestled between the phophate heads of the lower layer of the membrane (Figure 3.4a (v) and Figure 3.5 (v)). As the SMD atom and thus the peptide leaves the membrane, the interaction energy decrases

and reaches the value of zero once more. Starting from the point (vi) z=-32.3 Å and t=31.9 ns, the interaction between the SMD atom and the phophate heads is zero until the end of the simulation (Figure 3.4a (vi) and Figure 3.5 (vi)).

The electrostatic energy profile between the SMD atom and the phosphate heads of the membrane for resembles that of the interaction energy profile suggesting that electrostatic energy is the major contributor to interaction energy between the SMD atom and phosphate heads of the lipid bilayer. On the other hand, the van der Waals energy profile contributes to the interaction energy only up to -0.3 kcal/mol during the insertion and exit of the SMD atom where the interaction energy is maximum.

Once the overall behavior of the SMD atom was established by measuring its displacement (Figure 3.3) and its interactions (Figure 3.4), the interaction between the peptide and the membrane was analyzed and calculated to obtain information about the behaviour of the peptide as it moves across the bilayer. The interaction energy, van der Waals energy and electrostatic energy are plotted as functions of the z coordinate of the SMD atom for the wild-type pVEC system in Figure 3.6a, Figure 3.6b and Figure 3.6c respectively. Simulation snapshots taken at the labeled points in the interaction energy plot in Figure 3.6a corresponding to the major changes in interaction energy profile are shown in Figure 3.7.

Mapping of the interaction energy profile onto the snapshots gives an idea about the uptake mechanism of peptide. The interaction energy plot has two valleys observed in Figure 3.6a which correspond to regions in which the peptide and the membrane are in high interaction (ii) initial contact of peptide with the membrane and (iv) complete insertion of peptide with N-terminal interacting with lower phosphate head layer. On the other hand, two plateaus are observed in Figure 3.6a (iii) and Figure 3.6a (v) which correspond to movement of the peptide between lipid tails.

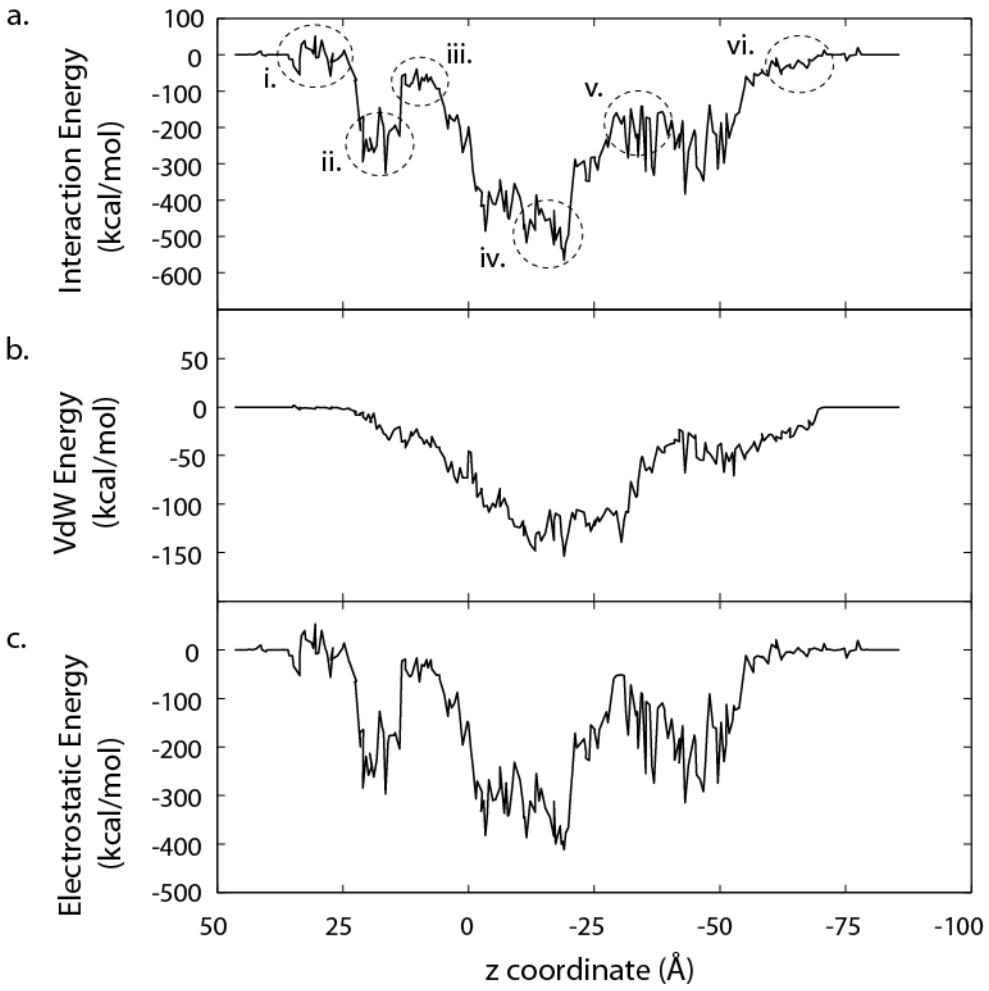

Figure 3.6. (a) The interaction energy profile (b) the van der Waals energy profile and (c) the electrostatic energy profile between the peptide and the lipid bilayer as a function of the z coordinate of the SMD atom for the system of wild-type pVEC.

When the individual time points are examined in detail, more detailed information about the barriers to motion is obtained. In Figure 3.7 (i) at z=31.2 Å, the peptide was close to the membrane; however, there was no contact between the peptide and the membrane and the interaction energy between the peptide and the membrane was around 0 kcal/mol. Figure 3.7(ii) shows the initial contact of the peptide with the membrane at z=19.3 Å. At this stage, the interaction energy reached its first maximum value and the first barrier was seen at the insertion of the N terminus into the bilayer with the C terminus also was in contact with the lipid bilayer (Figure 3.7(ii)). The interaction energy started to increase to about -300 kcal/mol as the positively charged amino group of the N-terminus and the negatively charged phosphate heads interacted. At z=10.3 Å, the N terminus has passed the

P heads of the membrane, the interaction energy decreased back to about -100 kcal/mol and the peptide insertion had started. The C terminus was also still in contact with the P heads (Figure 3.7 (iii)). In Figure 3.7 (iv) at z=-25.9 Å, the peptide was completely embedded in the membrane. The N terminus is in contact with the lower P heads while the C terminus is in contact with the upper P heads. The second barrier was seen at this stage as the whole peptide was included inside the membrane and the interaction energy reached its overall maximum point around -500 kcal/mol (Figure 3.7 (iv)). In Figure 3.7 (v), the peptide was moving out of the lipid bilayer. At this point, at z=-32.3 Å, interaction between the peptide and the membrane decreased back to about -300 kcal/mol and stayed at this value until the peptide exits the membrane. At this stage, the third barrier was seen and the interaction weakened but the oscillations could be seen as the peptide tried to find its way out of the membrane (Figure 3.7 (v)). Figure 3.7 (vi) shows the peptide as it completed its exit. The interaction between the peptide and the membrane was maintained until the peptide completely leaved the membrane at z=-63.2 Å and started to fold again.

The electrostatic and van der Waals energies between the peptide and the membrane were also calculated to identify the contribution of each to the total interaction energy. The electrostatic energy contribution to the interaction energy profile was found to be higher and the valleys and plateaus observed in the interaction energy profile were also observed in the electrostatic energy profile (Figure 3.6). Maximum electrostatic energy value of at around -400 kcal/mol is attained when the peptide is completely immersed inside the membrane (Figure 3.7 (iv)). At this point, the van der Waals energy also contributes -100 kcal/mol to total energy.

The analysis of the interaction energy profile for the system of wild-type pVEC suggests that the peptide transport occurs in three main stages. The first barrier is the insertion of the N terminus into the bilayer where the interaction reaches its first maximum value. The second barrier is the inclusion of the whole peptide inside the membrane where the interaction between the peptide and the membrane reaches its ultimate maximum value. Finally, the third barrier is observed as the N terminus of the peptide exits from the bilayer.

The maximum interaction observed between z values of 0 and -25 Å (Figure 3.6a (iv)) is due to the interaction of the positively charged region (wild-type pVEC residues 6-11) with the upper phosphate layer and of the N-terminus with the lower phosphate layer.

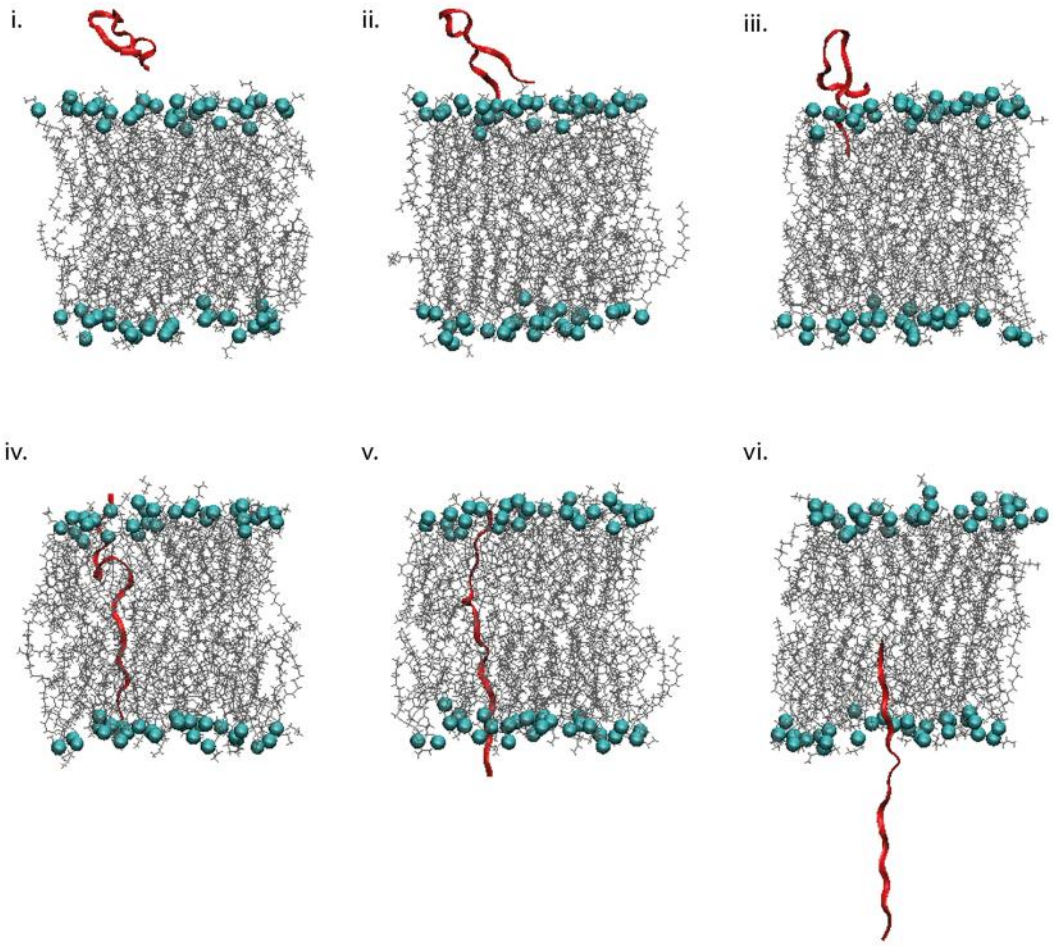

Figure 3.7. The structure of the system of wild-type pVEC at (i) z=31.2 Å and t=6.2 ns, (ii) z=19.3 Å and t=11.2 ns, (iii) z=10.3 Å and t=15.0 ns, (iv) z=-19.8 Å and t=27.3 ns, (v) z= -32.3 Å and t=31.9 ns, (vi) z= -63.2 Å and t=43.9 ns.

3.1.2.2. Analysis of SMD Force and Work Applied During the SMD Simulations. To determine the possible energy barriers in the process that required the use of higher force, the SMD force applied to the wild-type pVEC in the negative z-direction during the simulations was calculated and plotted as a function of the z coordinate of the SMD atom (Figure 3.8). Snapshots at labeled time points corresponding to different regions in the force profile are shown in Figure 3.8.

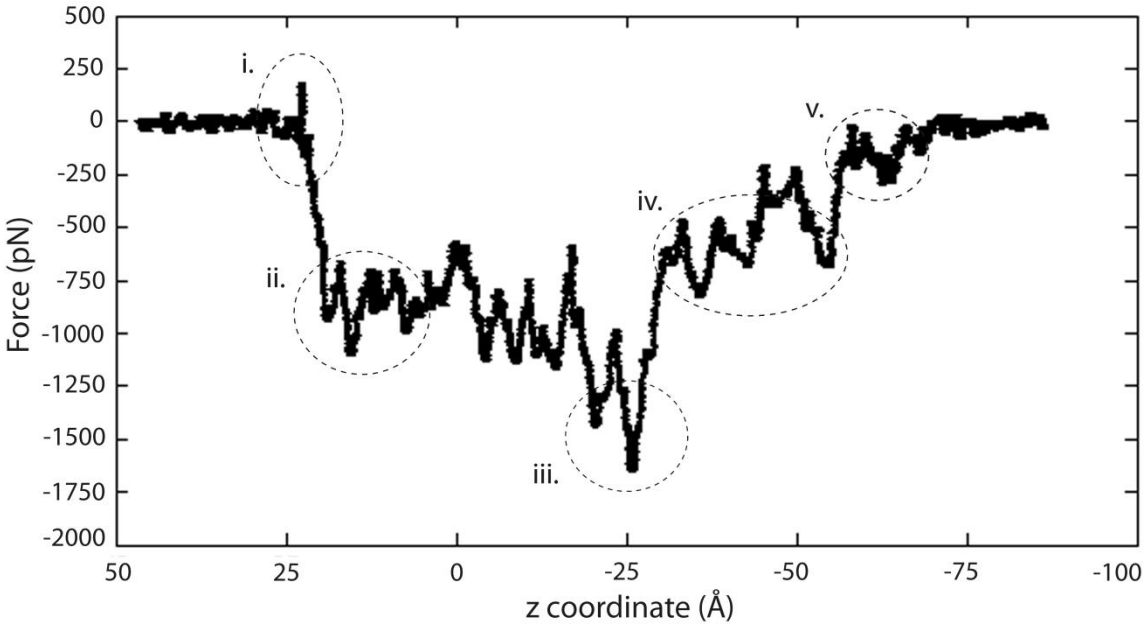

Figure 3.8. Force applied on the peptide plotted as a function of z coordinate of the SMD atom for the system of wild-type pVEC.

At the beginning of the simulation, as the peptide moves through the water layer the magnitude of the force applied is 0 pN (Figure 3.9 (i)). At around z = 20 Å a sudden increase in the force is observed as the peptide contacts the membrane. The membrane resists this penetration of the peptide and to overcome this resistance, force has to be applied to the peptide. At this stage, the first barrier of the translocation mechanism previously identified in interaction energy analysis is verified by the force profile (Figure 3.8 (ii) and Figure 3.9 (ii)). The force value reaches a maximum at around z = -25 Å when the peptide is totally immersed in the membrane and the N terminus starts to exit the membrane (Figure 3.9 (iii)). After this checkpoint, the peptide starts to leave the membrane. As more of the peptide enters the water layer, the applied force decreases (Figure 3.9 (iv)). After the peptide is out of the membrane and moving through the water layer, the magnitude of the force applied is 0 pN again (Figure 3.9 (v)).

The three main stages of the uptake mechanism observed in the interaction energy profiles are also present in the force profiles. The force applied on the SMD atom is abruptly increased upon entrance and exit of the N-terminal.

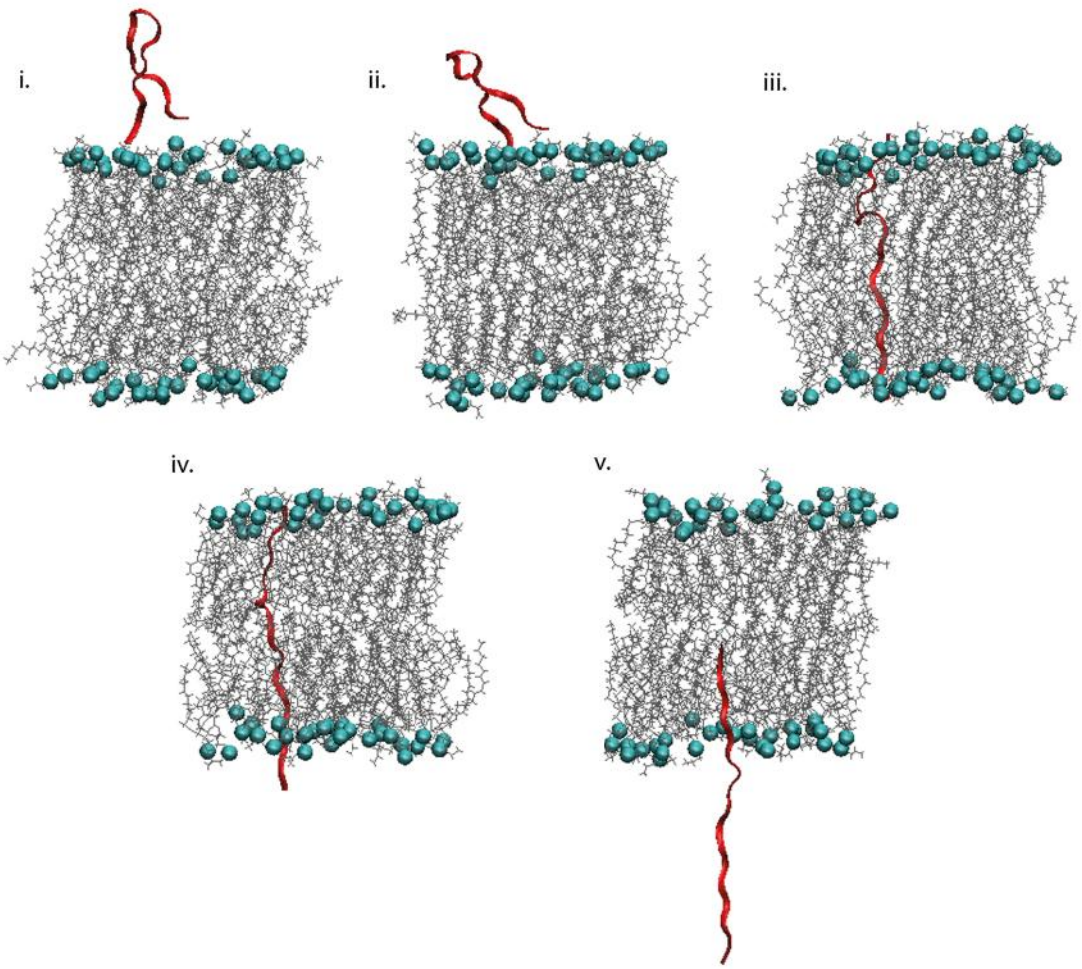

Figure 3.9. The structure of the system of wild-type pVEC at (i) z=22.3 Å and t=9.4 ns, (ii) z=19.3 Å and t=11.2 ns, (iii) z= -25.9 Å and t=29.9 ns, (iv) z= -32.3 Å and t=31.9 ns, (v) z= -63.2 Å and t=43.9 ns.

In Figure 3.10 the work done on the peptide is plotted as a function of the z coordinate of the SMD atom for the wild-type pVEC system. Work was calculated using;

$$Work = \int F\, v\, dt \tag{3.1}$$

where F is pulling force, v is pulling velocity and dt is timestep.

The work done on the peptide was stable and 0 kcal/mol up to about z = 20 Å where the SMD atom contacted the membrane. The peptide moved without accumulating

any work from the beginning of the simulation (z = 50 Å) until the first contact is seen (at z = 20 Å). The reason for this observation is that the peptide moved easily through the water layer and no force was needed to be applied. At around z = 20 Å, the work performed on the peptide started to increase as the peptide started to penetrate the membrane. The work done by pulling the peptide through the membrane continued to increase until around z = -75 Å. This location was critical since the peptide was out of the membrane, when the SMD atom was at this location, the force became zero again and no more force was necessary to be applied to the peptide because peptide is once again in the water layer. Therefore, no more work was required and done.

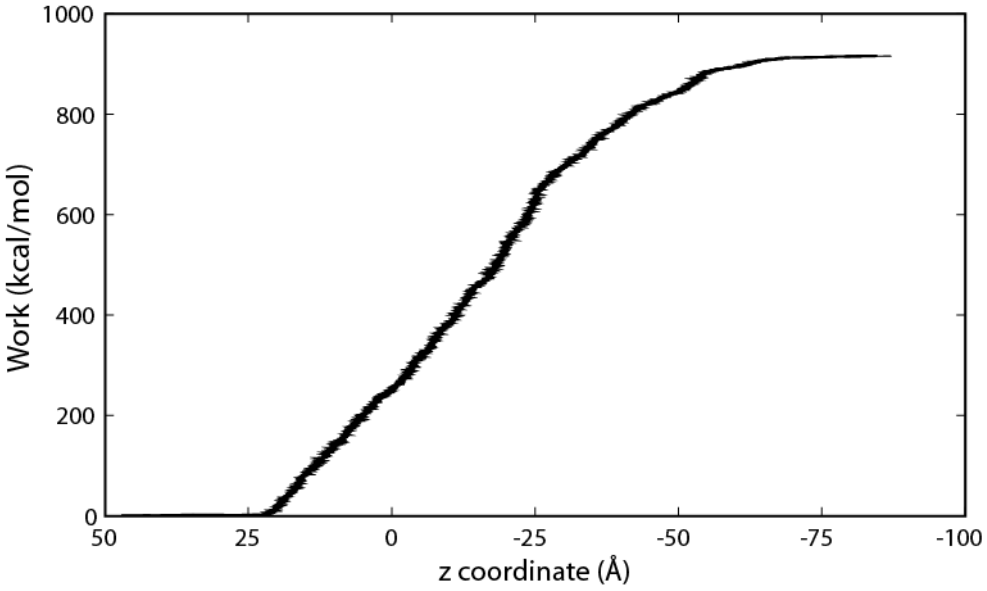

Figure 3.10. Work done on wild-type pVEC throughout the simulation.

In order to obtain detailed information about the mechanism of the translocation, the residues that contribute to the interaction were identified. For this aim, the interaction and electrostatic energy between each residue (backbone and side chain) and the lipids were calculated for the wild-type pVEC system and shown in Figure 3.11 and Figure 3.12.

The interaction energy profiles of residues were compared and it was observed that residues L1, R6, R7, R8, R10, K11 and K18 contribute to the interaction of the wild-type pVEC with the lipid bilayer (Figure 3.11). Among all the residues, residue K18 reaches the maximum interaction energy value of -209.1 kcal/mol at around z=-30 Å, followed by L1, R7 and R10 which reach interaction energy values at around -150 kcal/mol. The other

residues have comparatively lower interactions with the lipid bilayer during the simulation. The residues that have the lowest interaction energy are A13, I9 and A15 with -8.9, -15.0 and -17.7 kcal/mol respectively.

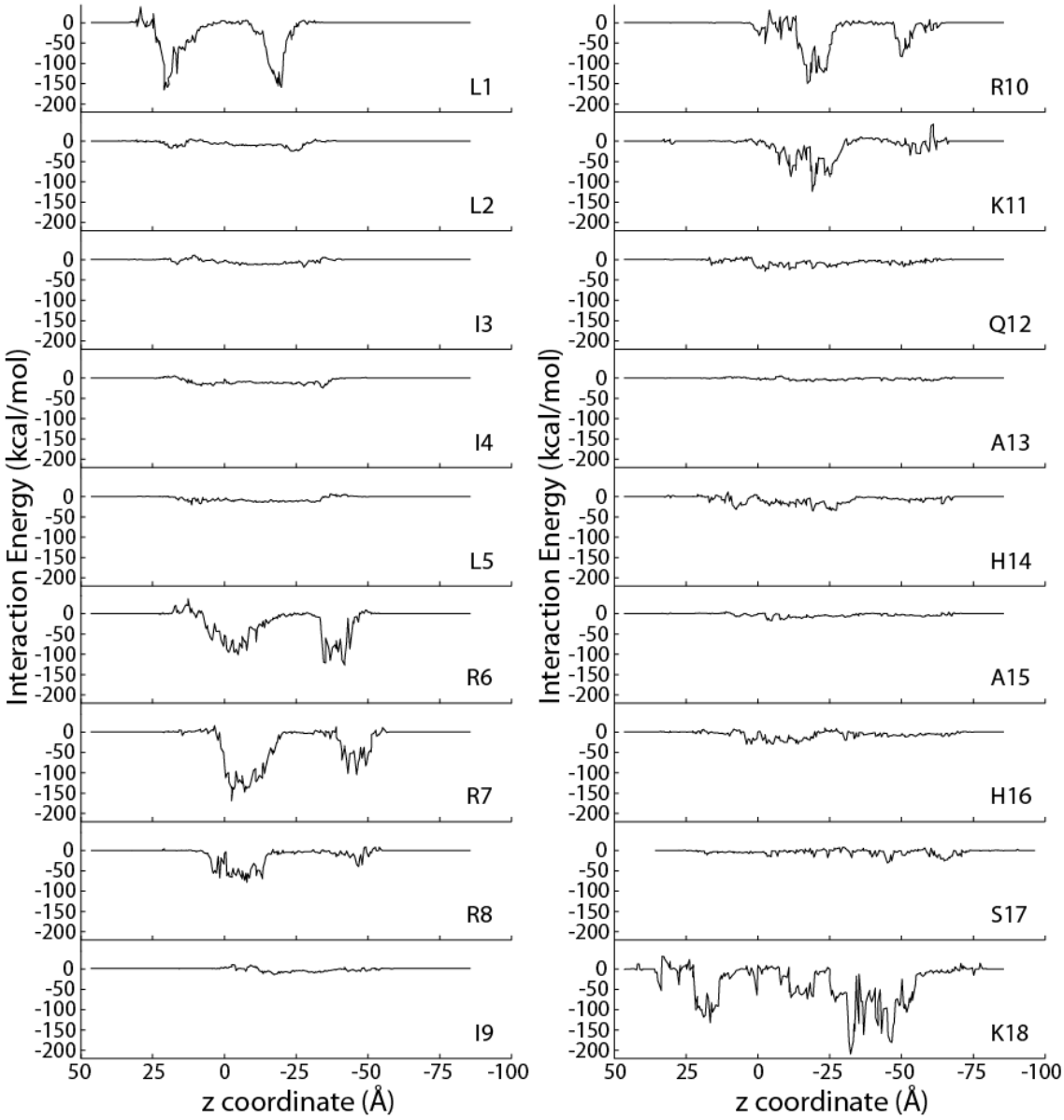

Figure 3.11. Interaction energy analysis for wild-type pVEC system on a residue basis.

The analysis of individual residue contributions to lipid- pVEC interactions shows that Arginine and Lysine, amino acids with polar and positively charged side chains, have strong interactions with the lipid bilayer as observed both in the interaction energy and electrostatic energy profiles (Figure 3.11 and Figure 3.12). L1, which also has high

interactions, has a neutral sidechain. However, the peptide used in the simulations are not capped and therefore contain a positively charged N-terminus and a negatively charged C-terminus. As a result, the interaction observed for L1 is not due to the sidechain but it is due to the backbone amino group.

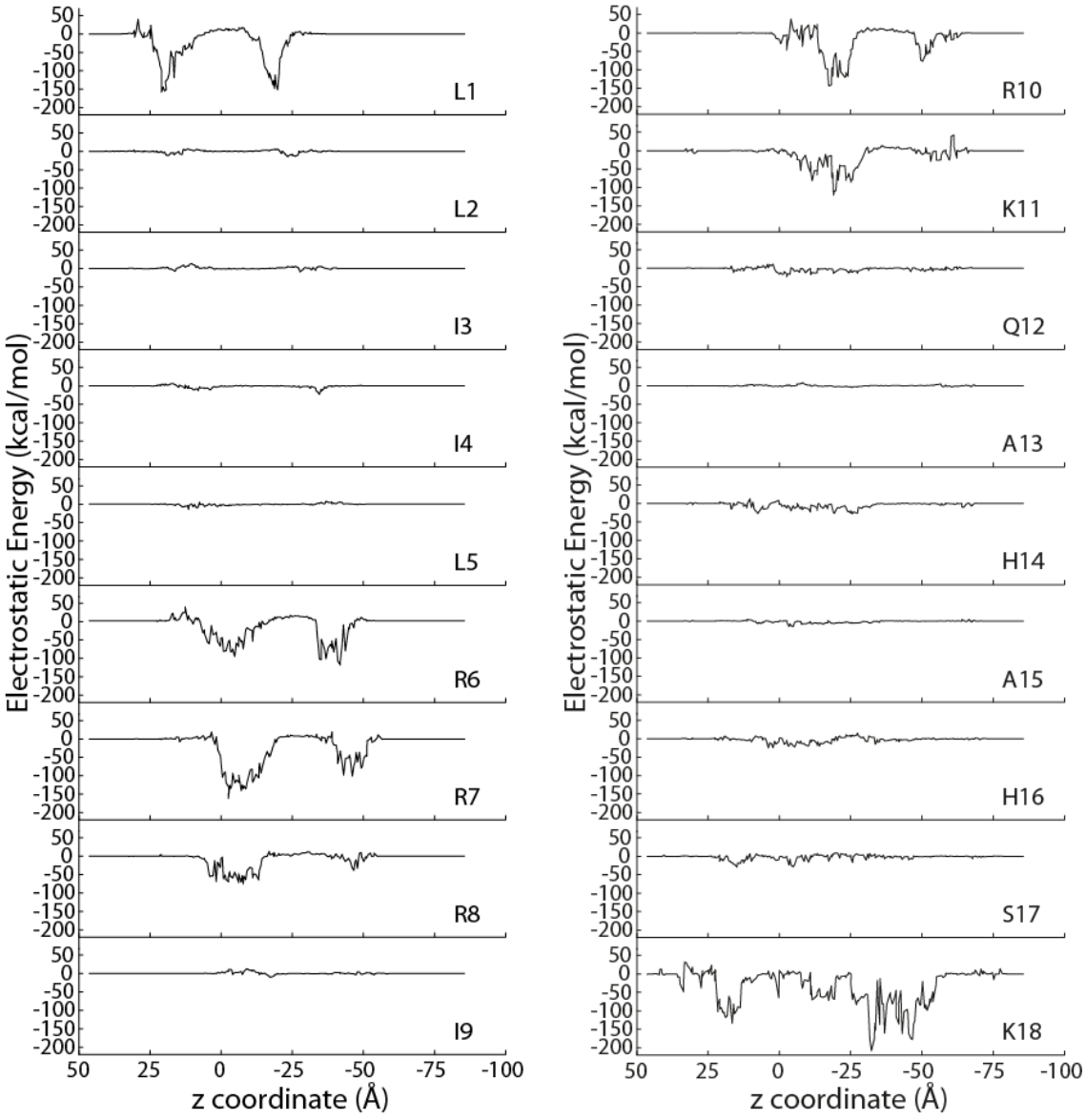

Figure 3.12. Electrostatic energy analysis for wild-type pVEC system on a residue basis.

On the other hand, the weak interaction for residues A13, I9, A15, I3, I4, L2 and L5 can be on account of the non-polar and neutral charged side chains of Alanine, Isoleucine and Leucine amino acids. The residues Q12, H14 and S17 which also have weak interactions with the lipid bilayer have polar and neutral side chains.

The comparison of the Figure 3.11 and Figure 3.12 shows that electrostatic energy makes the highest contribution to the interaction between the residues and the lipid bilayer and the van der Waals energy contributes only around -5 to -10 kcal/mol.

3.1.2.3. Analysis of Membrane Dynamics in the SMD Simulations on wild-type pVEC. The transport of the peptide causes changes in the structure and dynamics of the membrane. In order to verify that the membrane remained intact, the thickness of the membrane was first measured. The thickness profile of wild-type pVEC system is plotted as a functon of time in Figure 3.13a.

The membrane thickness stayed between 52 Å and 58 Å during the wild-type pVEC simulation and the membrane did not undergo any major change in thickness. In some simulations, the membrane structure was disrupted by lipid tails leaving the membrane during peptide transport. Those simulations were not analyzed because they were not realistic.

The number of water molecules that penetrate into the cell membrane was analyzed in order to investigate the distortion and stability of the membrane upon peptide insertion. In Figure 3.13b, the number of water molecules that enters the membrane bilayer was plotted as a function of z-coordinate of the SMD atom for the wild-type pVEC system and snapshots are taken for corresponding points of the simulation. Snapshots at labeled time points corresponding to different regions in the number of water molecules in mambrane profile are shown in Figure 3.14.

At the beginning of the simulation, the peptide is embedded in the water layer above the membrane and the initial number of water molecules in the membrane is equal to zero. The number of water molecules is at a minimum and mostly equal to zero until the peptide starts to penetrate into the membrane at z= 13.8 Å (Figure 3.13 (i) and Figure 3.14 (i)). As peptide insertion starts, the cavity formed by the peptide is filled by about 30 water molecules causing the small shoulder observe at z = -8.1 Å. (Figure 3.13 (ii) and Figure 3.14 (ii)). As the insertion of the peptide continues and the SMD atom approaches the lower layer of the membrane, thus opening a way out for some of the water molecules

grouped around the first residues of the peptide (z = -13.2 Å, Figure 3.13 (iii) and Figure 3.14 (iii)). After that point, the SMD atom starts to leave the membrane, but the C terminal of the peptide is in contact with the upper layer of the membrane. This interaction causes the peptide to extend and lets the β hairpin loop to unfold as the peptide is embedded in the membrane. As the unfolding takes place, the number of water molecules in the membrane increases and reaches its maximum at around 70 at z = - 40.2 Å (Figure 3.13 (iv) and Figure 3.14 (iv)).

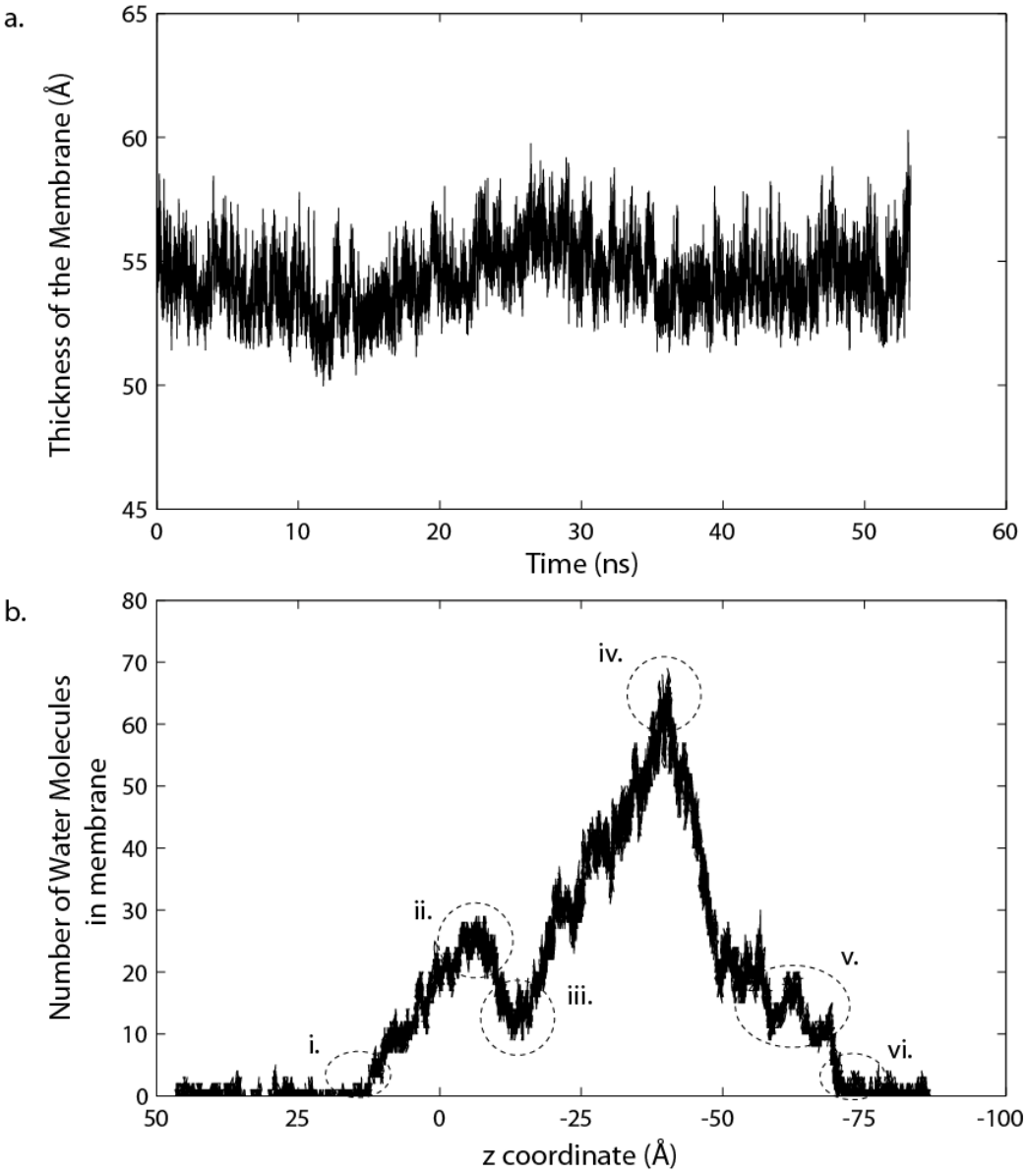

Figure 3.13.(a) Change in thickness of the membrane throughout the simulations for the system of wild-type pVEC and (b) Number of water molecules in the membrane as a function of z coordinate of the SMD atom for the system of wild-type pVEC.

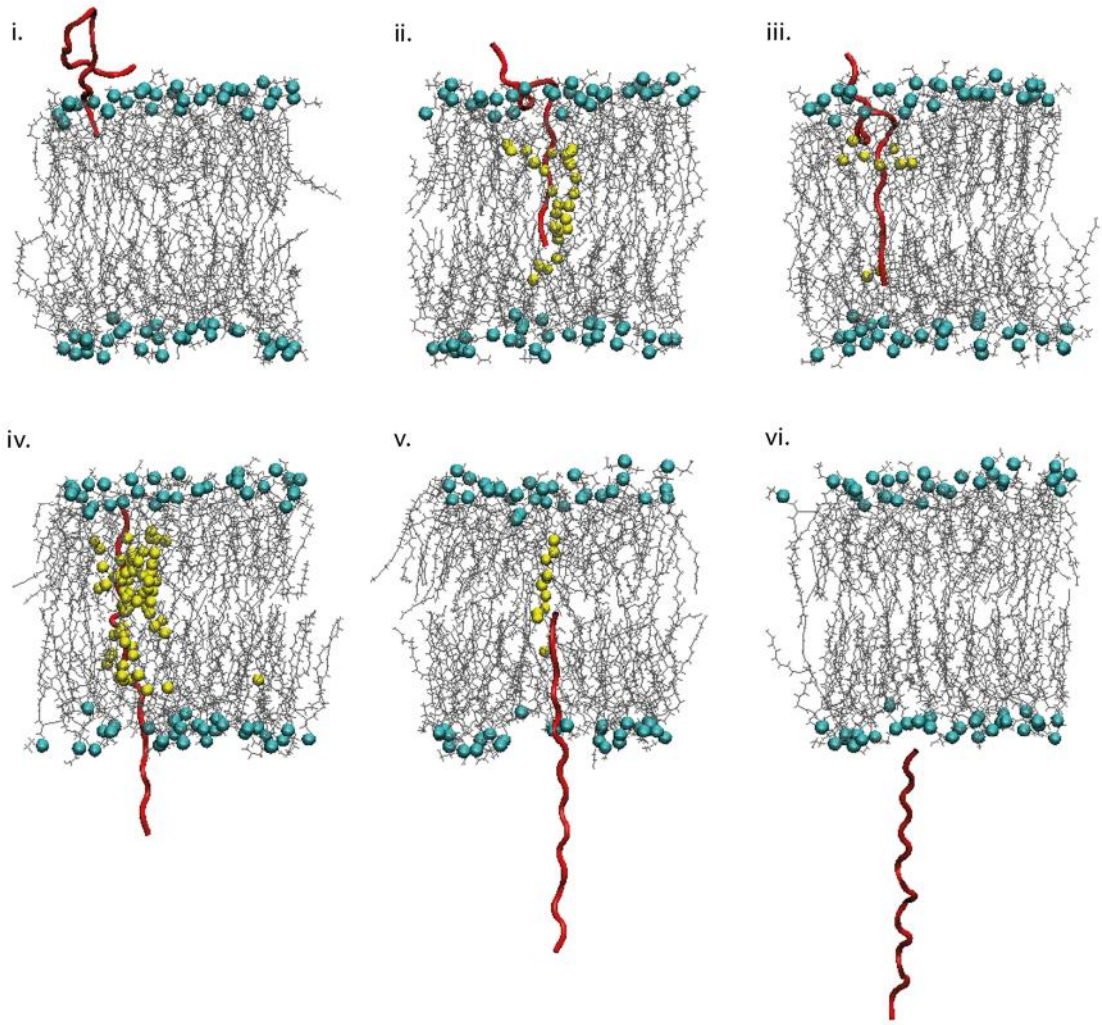

Figure 3.14. The structure of the system of wild-type pVEC at (i) z=13.8 Å and t=14.1 ns, (ii) z= -8.1 Å and t=22.0 ns, (iii) z= -13.2 Å and t=24.6 ns, (iv) z= -40.2 Å and t=35.1 ns, (v) z= -58.3 Å and t=42.2 ns, (vi) z= -71.0 Å and t=47.1 ns.

After this peak, at z = -58.3 Å, the number of water molecules decreases as the peptide starts to exit the membrane and water molecules leave the membrane with the peptide. Although most of the water molecules leave the membrane with the N terminal of the peptide, some water molecules tend to enter the membrane from the upper layer of P heads where the entrance of the C terminal causes a cavity. This results in some oscillations in the profile instead of a steep decrease (Figure 3.13 (v) and Figure 3.14 (v)). The number water molecules continues to decrease and finally becomes 0 when the last residue LYS18 leaves the membrane at z= -71.0 Å (Figure 3.13 (vi) and Figure 3.14 (vi)).

3.1.3. Comparison of Dynamics and Interactions of the Mutant pVEC Peptides

After the analysis of peptide and membrane dynamics and interactions for the system of wild-type pVEC, the systems of mutant pVEC peptides were analyzed. These analysis yield results of the effects of mutations on pVEC and help in understanding the importance of specific residues of wild-type pVEC.

The interaction of the SMD atom with the phosphate heads of the lipid bilayer was analyzed for all the simulation systems. In Figure 3.15, the interaction energy between the SMD atom and the phophate heads are plotted as a function of z coordinate of the SMD atom for all of the simulation systems.

The peaks observed in the interaction energy profile for the wild-type pVEC system are valid in the profiles of all the simulations systems. These two peaks correspond to the insertion of the peptide when the SMD atom is nestled between the phosphate heads and the exit of the peptide as the SMD atom heads toward the lower phosphate layer of the membrane as previously mentioned.

The maximum interaction energy values are seen in the systems of wild-type pVEC as 67.24 and 54.28 kcal/mol for the first and second peaks respectively. The maximum interaction energy values of wild-type pVEC system are followed by the systems of S17A and r pVEC which have the absolute maximum interaction energy values of 56.74 and 53.68 kcal/mol.

The interaction of the peptide with the membrane was analyzed for all the simulation systems. In Figure 3.16, the interaction energy, electrostatic energy and van der Waals energy between the peptide and the membrane are plotted as a function of z coordinate of the SMD atom for all of the simulation systems.

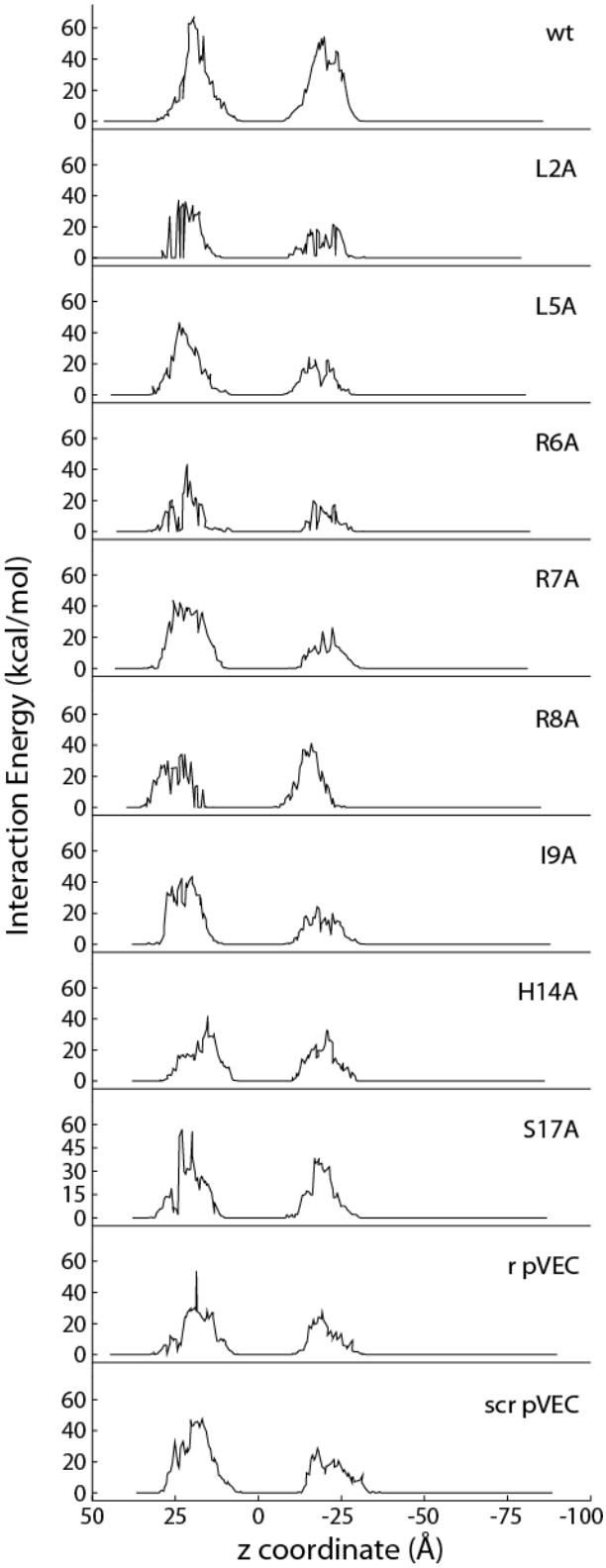

Figure 3.15. Interaction energy between the SMD atom and phosphate heads of the membrane for the systems of wt (wild-type pVEC), L2A, L5A, R6A, R7A, R8A, I9A, H14A, S17A, r pVEC (retro-pVEC) and scr pVEC (scramble pVEC).

Comparison of the interaction energy profiles as a function of z-coordinate of SMD atom for the different simulations systems (Figure 3.16) shows that the interaction energy profiles of R7A, R8A, I9A, H14A and S17A systems are similar to that of wild-type pVEC in terms of the maximum value attained (at around or less than -550 kcal/mol), as well as the number of maxima as the peptide moves through the membrane. On the other hand, the retro-pVEC (r pVEC) interaction energy profile is different as it has one maximum at a higher value and no other maxima. Also, the systems with mutated residues L2A, L5A and R6A and the scramble-pVEC (scr pVEC) show a different trend in the interaction energy profiles.

For those peptides with a different interaction energy profile,the profile is more flat therefore the maximum interaction energy value reached is lower compared to the wild-type pVEC system. The maximum interaction energy values are tabulated in Table 3.2 for each simulation.

Comparison of the force profiles as a function of z-coordinate of SMD atom for the different simulations systems is shown in Figure 3.17. For the compared force profiles of mutant pVEC systems, it was observed that the profiles are similar trend but the maximum force applied values differ. For the systems of L2A, R6A, R7A and I9A, the maximum force values were very close to each other and that of wild-type pVEC system. Therefore, it can be suggested that mutation on residues L2, R6, R7 and I9 alanine did not affect the required force to pull the peptide. The resistance of the membrane was almost same for these mutants. For the systems of L5A, R8A, H14A and scr pVEC the maximum force applied are lower than that of wild-type pVEC suggesting that mutations on L5, R8, H14 and mixing the sequence of pVEC requires less force to be applied for the translocation of the peptides. On the contrary, the systems of S17A and r pVEC required higher amount of force compared to the wild-type pVEC system for translocation. The maximum force applied on the peptide for each simulation system is tabulated in Table 3.2.

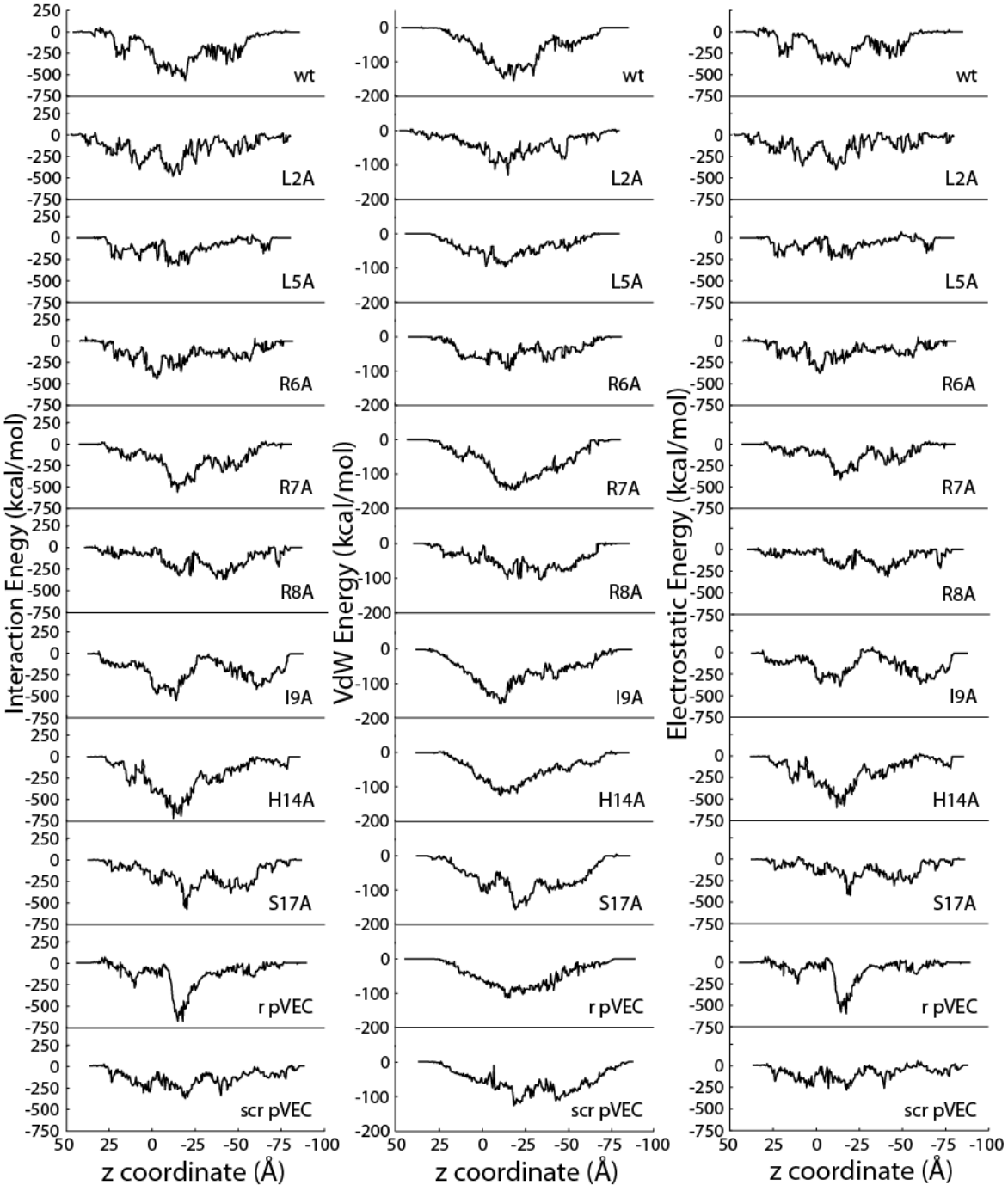

Figure 3.16. The interaction, VdW and Electrostatic energy between the peptide and the membrane for systems of wt (wild-type pVEC), L2A, L5A, R6A, R7A, R8A, I9A, H14A, S17A, r pVEC (retro-pVEC) and scr pVEC (scramble pVEC).

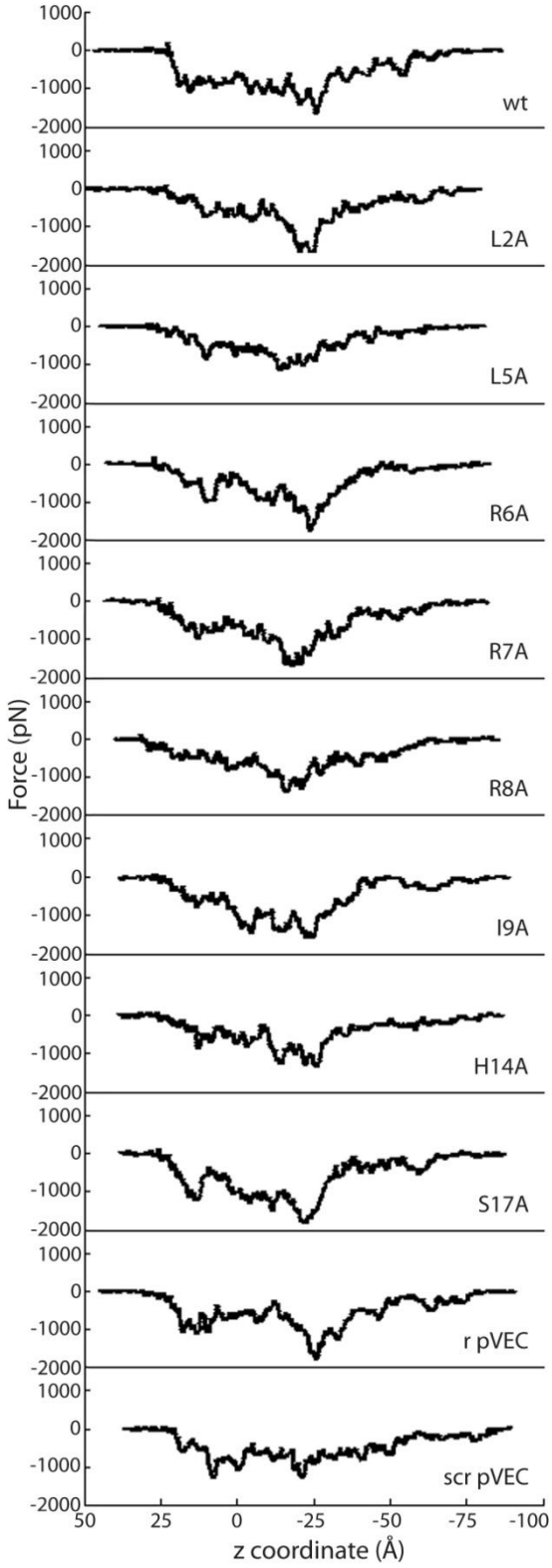

Figure 3.17. The force applied to the SMD atom for the systems of wt (wild-type pVEC), L2A, L5A, R6A, R7A, R8A, I9A, H14A, S17A, r pVEC (retro-pVEC) and scr pVEC (scramble pVEC).

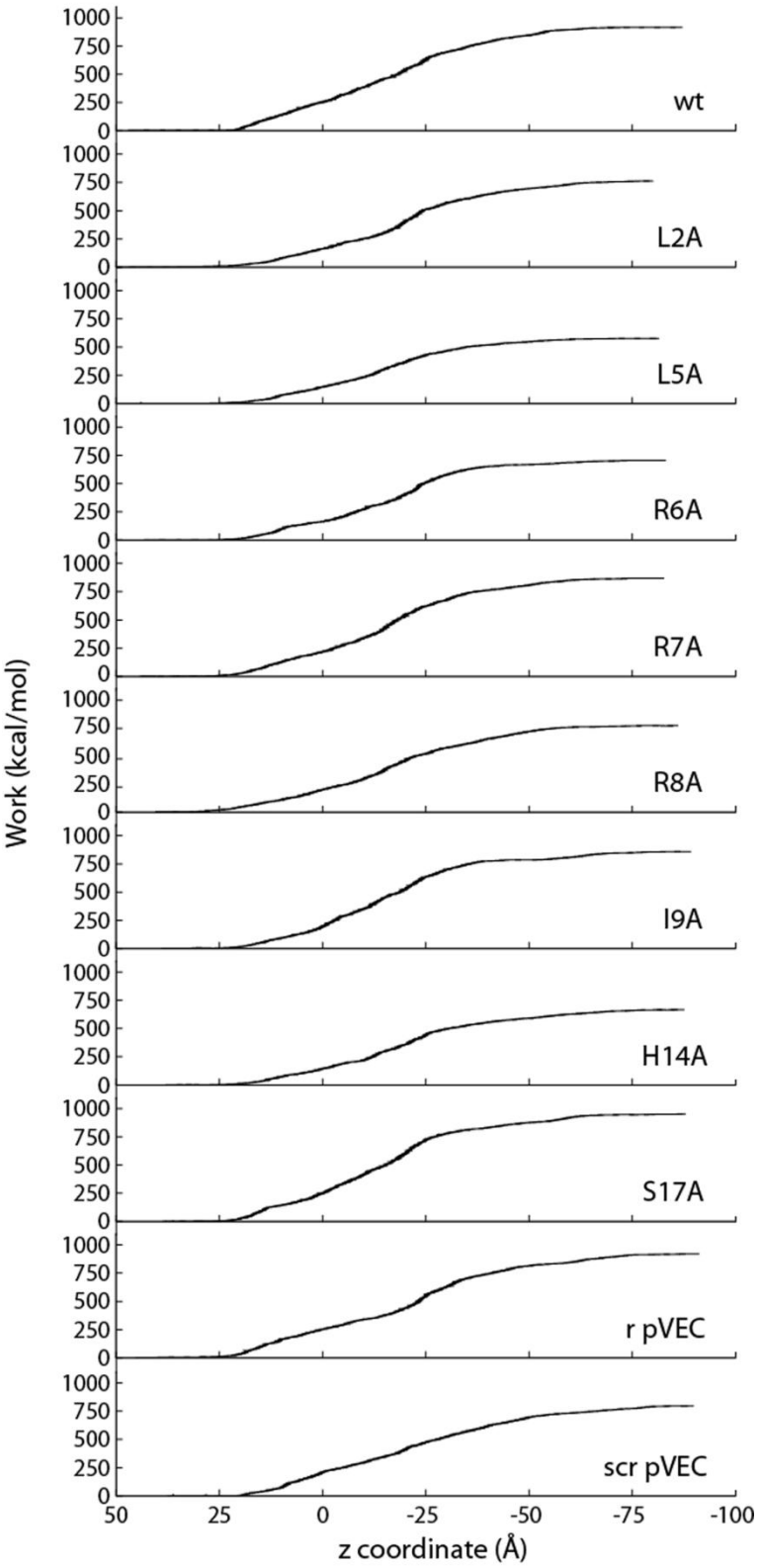

Figure 3.18. The work done on the peptide for the systems of wt (wild-type pVEC), L2A, L5A, R6A, R7A, R8A, I9A, H14A, S17A, r pVEC (retro-pVEC) and scr pVEC (scramble pVEC).

Comparison of the work profiles as a function of z-coordinate of SMD atom for the different simulations systems is shown in Figure 3.18. For the work profiles of all simulations systems, initially the SMD atom, the N terminal alpha carbon atom of each system, was located at around z = 50 Å. The work was stable up to about z = 20 Å in all the simulations. The peptides moved without accumulating any work in the z = 50 Å to z = 20 Å region because it moved easily through the water layer and no force was needed to be applied. At the z = 20 Å checkpoint, the work performed on the peptides started to increase as the peptides started to penetrate the membrane. The work done by pulling the peptide through the membrane continued to increase until z = -75 Å when the peptides completed their translocation and were out of the membrane. After that point, no more force was required since the peptides once again, moved easily through the water. The mutant pVEC peptides R7A, r pVEC, I9A yielded approximately the same amount of work requirements of that of wild-type pVEC. L2A, L5A, R6A, H14A and scr pVEC on the contrary, require less amount of work done on the peptide for translocations. Only the system of S17A required higher amount of work done than the system of wild-type pVEC. The maximum work done on the peptide for each simulation system is tabulated in Table 3.2.

In Table 3.2, the maximum force values and maximum work done on the peptide are tabulated as well as the minimum interaction energy and maximum work done for all the simulations. For comparison, the uptake values for the peptides measured [17] are given with respect to the uptake value of wild-type pVEC.

When all the simulations are compared, it can be determined that for higher maximum force values the work done is higher too. On the other hand, for scr pVEC (scramble-pVEC), a continuously low force is applied throughout the simulation, hence increasing the work without a pronounced peak in the force profile.

When the work performed and cellular uptake values are compared for all the simulations, it can be distinguished that for those peptides with increased uptake potential, the work performed was higher.

Table 3.2. The minimum interaction energy, maximum force applied and maximum work done values for the 11 pVEC simulations.

Name	**Minimum interaction energy (kcal/mol)**	**Maximum force applied in negative z direction (pN)**	**Maximum work done (kcal/mol)**	**Uptake[a] Potential**
wt*	-565	1653	916	-
L2A*	-481	1675	762	< wt
L5A	-337	1147	577	<< wt
R6A	-438	1773	705	>> wt
R7A	-559	1708	871	≈ wt
R8A	-370	1404	765	>> wt
I9A*	-540	1587	857	< wt
H14A*	-715	1357	666	< wt
S17A	-575	1838	952	>> wt
r pVEC*	-685	1803	919	<< wt
scr pVEC*	-380	1308	797	< wt

a: The uptake potential measured by fluorescently labeled peptide accumulation. The uptake potential of the peptides are reported with respect to the uptake of the wild-type pVEC [17].

* Simulations marked with asterisk sign were carried out and analyzed in a previous study [31].

Figure 3.19 shows the change in the thickness of the membrane throughout the simulation for all of the simulation systems. The existence of rapid increases and drops in the thickness profile verifies a disorder in the membrane such as lipid tails that hang out of the membrane. For this reason, the simulations were considered appropriate or failed according to the thickness profiles. The simulations that were considered as failed mutations are not taken into consideration and analyzed.

Since the simulations with disrupted membrane systems were considered failed and not analyzed, the simulation systems with thickness profiles shown in Figure 3.19 have mean thickness values close to that of wild-type pVEC system (54.3Å). Among the thickness profiles of all simulations systems, R8A outstands since fluctuations are observed at a higher range. The lipid tails that are in interaction with the peptide caused those fluctuations, but the membrane is not disrupted at the end of the simulation.

The profiles of the number of water molecules plotted as a function of the z coordinate of the SMD atom were compared and shown in Figure 3.20. Although the profiles are mostly similar, some pVEC mutants show a profile rather shifted or a peak missing due to their structure and translocation mechanism. For I9A, L5A and R6A systems, the third peak is missing in the profile due to the structure of the pVEC forming in the membrane. When the first residues lead to the exit of the membrane, the last residues (C terminal) are embedded in the membrane already because the peptide does not unfold as it penetrates, but only unfolds as it exits the membrane. The r pVEC (retro-pVEC) shows a different and a rather mirror image-like profile as expected due to its sequence. As the peptide approaches the membrane, the hairpin loop between residues 13-17 forms and enters the membrane as folded. The loop only unfolds as the peptide exits the membrane. The scr pVEC (scramble-pVEC) shows a different profile too. Instead of sharp peaks, the profile includes some increases and decreases with oscillations. At the beginning of the simulation, when the SMD atom touches the upper layer of the membrane, residue LEU18 touches the upper layer of the membrane too. The hairpin loop formed before the insertion (residues 7-12) starts to unfold as the residue LEU7 touches the upper layer of the membrane and completely unfolds as the loop is embedded in the membrane.

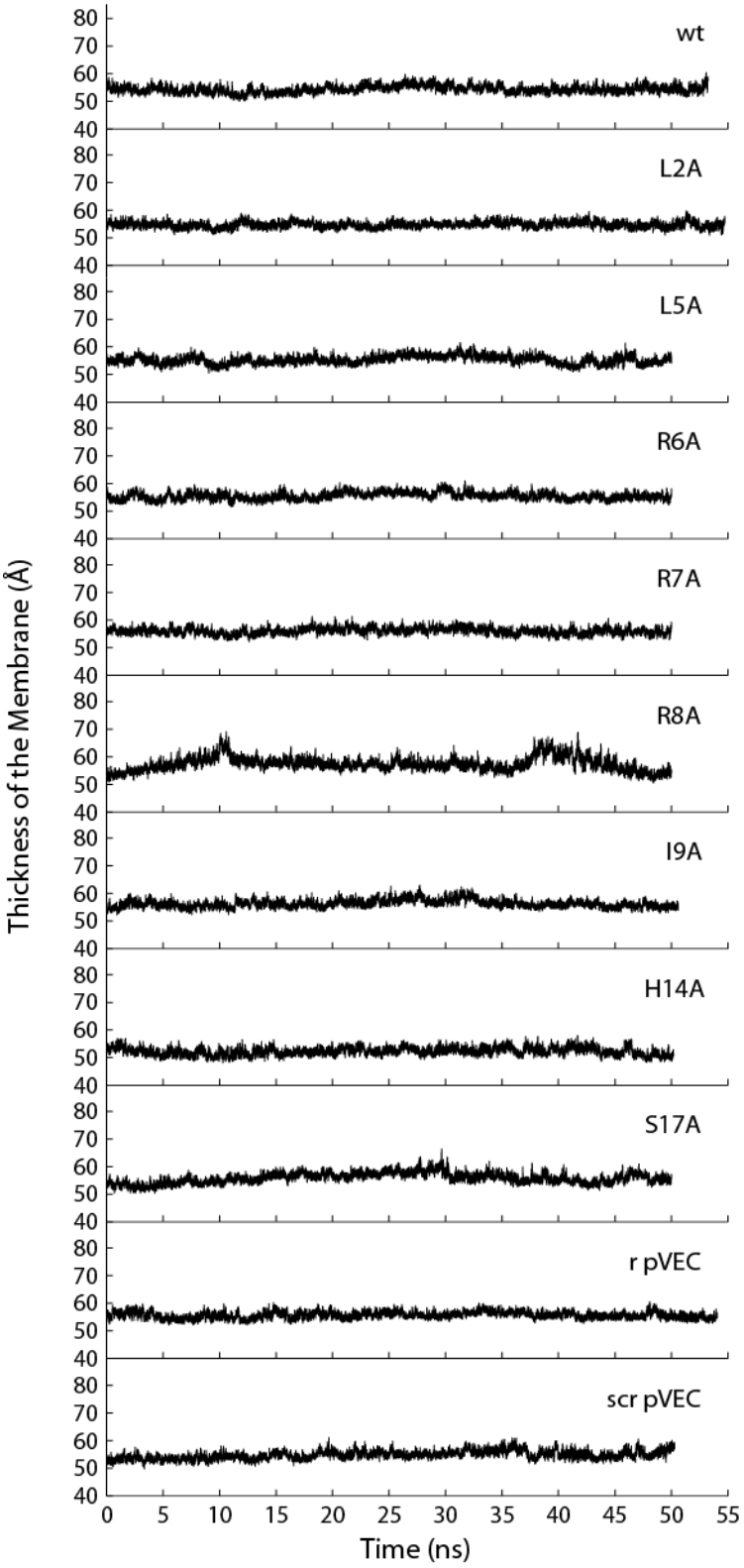

Figure 3.19. The thickness of the membrane for the systems of wt (wild-type pVEC), L2A, L5A, R6A, R7A, R8A, I9A, H14A, S17A, r pVEC (retro-pVEC) and scr pVEC (scramble pVEC).

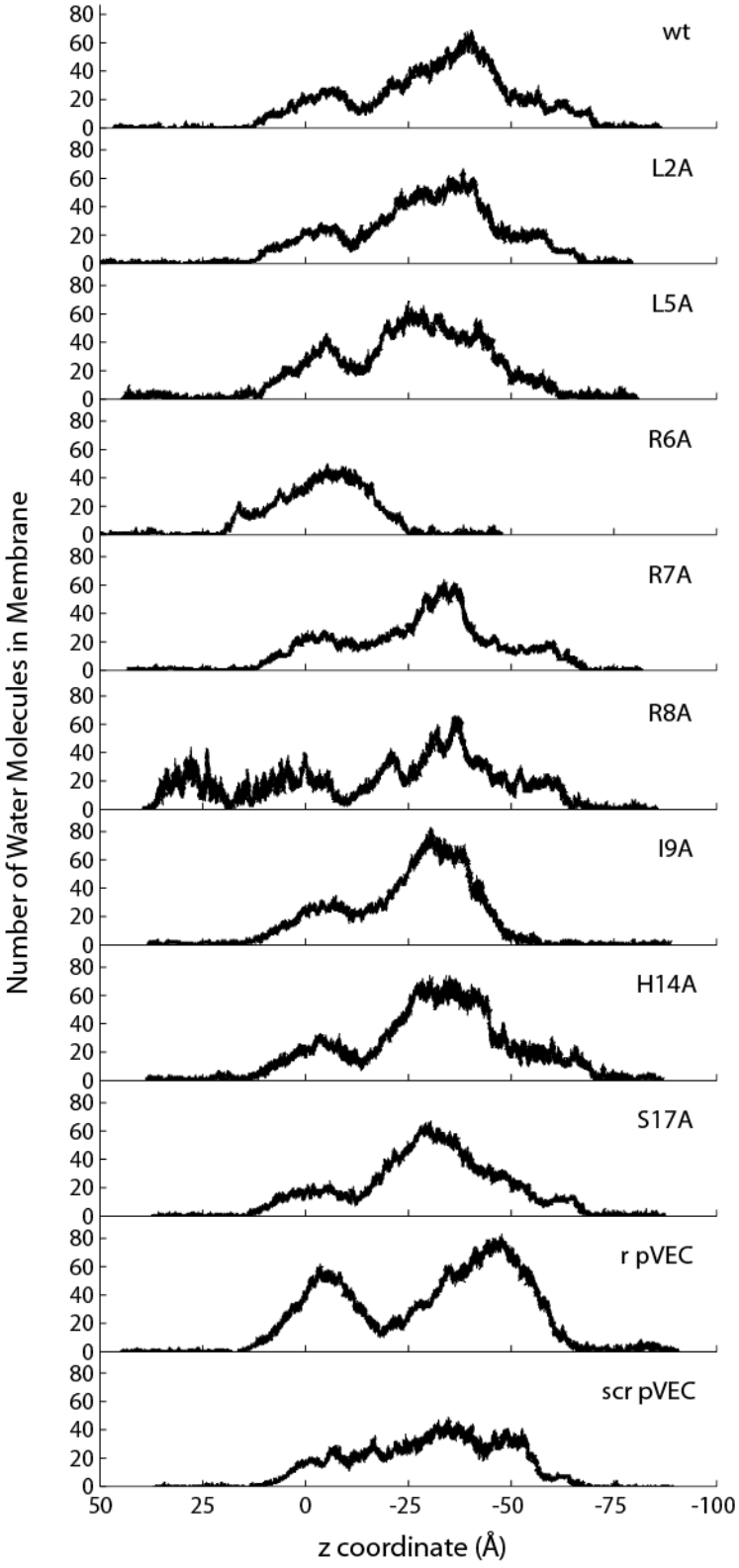

Figure 3.20. The number of water molecules in the membrane for the systems of wt (wild-type pVEC), L2A, L5A, R6A, R7A, R8A, I9A, H14A, S17A, r pVEC (retro-pVEC) and scr pVEC (scramble pVEC).

3.2. Experimental Results

The effect of Peptide 1 (5-Fluorescein-NH-HAAGDYYAY- $CONH_2$), Peptide 2 (5/6-Fluorescein-NH-RRGHYY-COOH) and Peptide 3 (5/6-Fluorescein-NH-LLIILHAAGDYYAY- $CONH_2$) on growth of *E. coli* K12 pUC18 cells expressing β-lactamase was examined. The bacterial uptake of the fluorescein labeled peptides (Peptide 1 and Peptide 3) was visualized by using fluorescence microscopy.

Peptide 1 (5-Fluorescein-NH-HAAGDYYAY- $CONH_2$) and Peptide 3 (5/6-Fluorescein-NH-LLIILHAAGDYYAY- $CONH_2$) were peptides with BLIP 45-53 residues. Peptide 3, in addition to that, has the first 5 residues of the cell-penetrating peptide pVEC [17] in its N terminal. The aim was to compare their inhibitory effects and their potential to be taken into the bacterial cell lines. Peptide 2 (5/6-Fluorescein-NH-RRGHYY-COOH) was previously shown to inhibit TEM-1 β-lactamase with a K_i of 136 μM and it was used as a positive control. On the other hand, Kemptide Acetate Salt was used as a negative control peptide which was expected not to inhibit the β-lactamase enzyme. Fluorescein Amine was used in order to determine the required fluorescein concentration for visualization using fluorescence microscopy.

3.2.1. Effect of Peptide 1 Addition on Cell Growth

In order to investigate the effect of Peptide 1 (5-Fluorescein-NH-HAAGDYYAY-$CONH_2$) on antibiotic resistant *E. coli* cells, growth experiments were carried out. *E. coli* K12 cells harboring pUC18 plasmid were precultivated at 37°C and 180 rpm overnight. The precultivated cells were added to 2 mL fresh LB medium in test tubes and incubated at 37°C and 180 rpm. As OD_{600} nm reached 0.2, peptides were added to sample sets and phosphate buffer was added to the control set. The cells in test tubes were harvested one by one at 1, 2 and 3 hours after peptide addition. OD_{600} nm of cells in each tube was measured before harvesting and the values obtained were plotted in Figure 3.21.

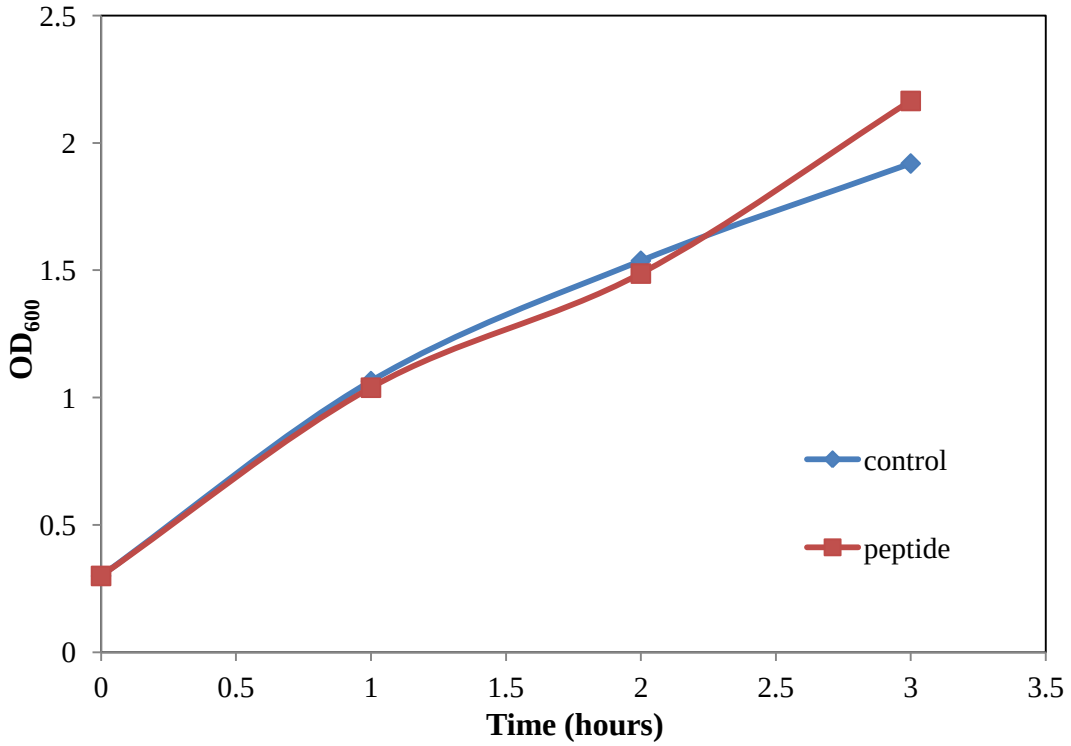

Figure 3.21. Growth profile of *E. coli* K12 pUC18 cells for the control set and for the peptide set in the presence of Peptide 1.

In order to determine the number of live cells, viable cell count was performed. Production of β-lactamase confers antibiotic resistance to the cells, and it may be hypothesized that the addition of a β-lactamase inhibitor should eliminate this resistance, by inhibiting the intracellular β-lactamase, hence leading to cell death. Therefore, comparison of the number of live cells in the samples with and without peptide addition may provide information about the inhibition of β-lactamase by Peptide 1. After 100 μM peptide addition, the cells were grown for a total of three hours and plated in one hour intervals to count viable cells. Cell viability plotted as a function of time is given in Figure 3.22. It was observed that cells continued to grow almost equally in the control set and the peptide set. The cell viability profiles of the cells incubated with the peptide did not have a significant change after peptide addition, suggesting that under the conditions used, Peptide 1 did not have an inhibitory effect on the cellular β-lactamase.

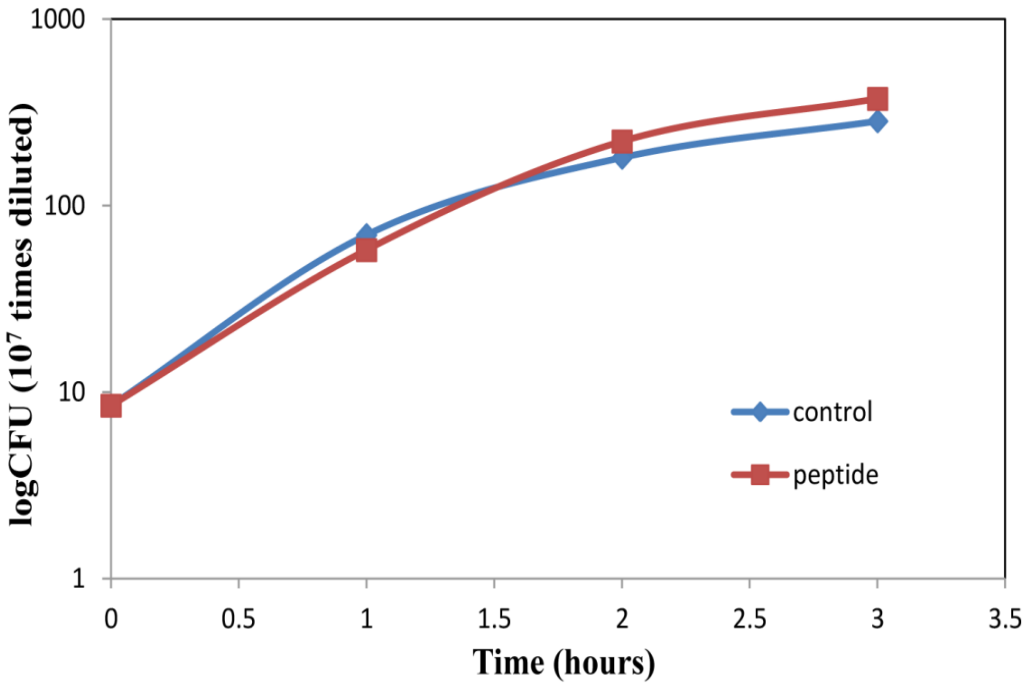

Figure 3.22. Cell viability profiles of *E. coli* K12 (pUC18) cells for the control set and sample set incubated with Peptide 1.

3.2.2. Determination of the Required Fluorescein Concentration

The peptide would be effective only if it can reach and bind to the cellular beta-lactamase, which is located in the periplasmic space. There was no major change in cellular growth as Peptide 1 was added, either because it was a poor inhibitor or because it was not able to cross the cell membrane efficiently. Therefore, the up-take of fluoresceinated Peptide 1 by *E. coli* cells was investigated using fluorescence microscopy.

Fluorescein labeling is a commonly used method for tracing proteins, peptides and molecules that translocate through the cell membranes. As a first step, the required fluorescein concentration for visualization under fluorescence microscopy was determined. To this end, *E. coli* K12 pUC18 cells were grown in 2 mL test tubes until OD_{600} nm value reached 0.2. After that point, different concentrations of Fluorescein amine were added to three sets of cells for comparison of the fluorescein concentration. Fluorescein amine stocks of 1 mM were used. 3 sets were prepared so that the final fluorescein concentration would be 10 µM, 50 µM and 100 µM in the tubes.

One hour after the addition of fluorescein amine, each sample was centrifuged to precipitate cells and separate them from the medium. Then, to be able to analyze the cell extract as well as the sample of the medium under the microscope, the precipitate was dissolved in 10 µL potassium phosphate buffer of 1 M.

Figure 3.23 and Figure 3.24 show the fluorescence microscopy captures for the cell and media samples from each set after one hour of incubation with Fluorescein amine. One drop of each sample was analyzed without the cover glass since it would thin the droplet and decrease the intensity. The captures were taken under 5X zoom and different exposure values as 25ms, 50ms, 100ms and 200ms.

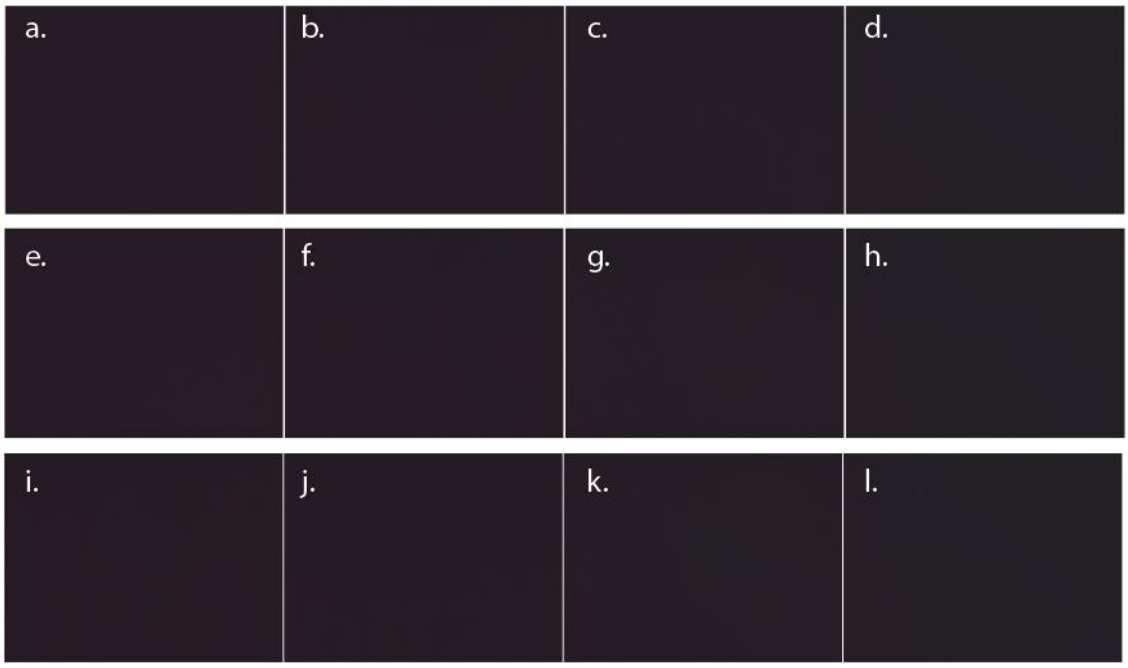

Figure 3.23. Captures of the cells with 10µM fluorescein concentration under (a) 25ms, (b) 50ms, (c) 100ms, (d) 200ms exposure, 50µM concentration (e) 25ms, (f) 50ms, (g) 100ms, (h) 200ms and 100µM concentration (i) 25ms, (j) 50ms, (k) 100ms, (l) 200ms.

Figure 3.23 shows that after one hour of the addition of the Fluorescein amine, no fluorescence was observed. This may be due to lack of Fluorescein amine penetration into the cells or insufficient amount of Fluorescein amine concentration used in the experiment.

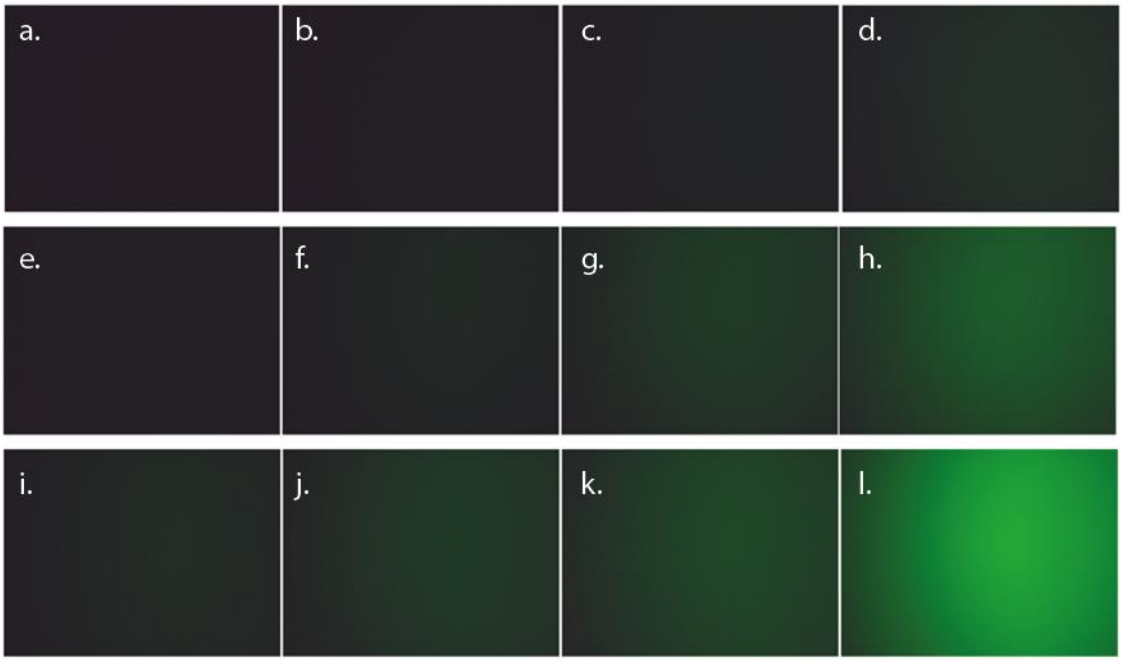

Figure 3.24. Captures of the medium with 10µM fluorescein concentration under (a) 25ms, (b) 50ms, (c) 100ms, (d) 200ms exposure, 50µM concentration (e) 25ms, (f) 50ms, (g) 100ms, (h) 200ms and 100µM concentration (i) 25ms, (j) 50ms, (k) 100ms, (l) 200ms.

To check whether fluorescein uptake occurs, the medium was analyzed for the presence of fluorescence. Figure 3.24 shows that enough fluorescein is present in media hence it could be detected with fluorescence microscopy.

10µM of Fluorescein amine was insufficient to be detected by fluorescence microscopy. On the other hand, 50µM and preferably 100µM concentration were chosen to be the sufficient amounts for analysis under 100ms and 200ms exposure. Finally 100µM fluorescein-labeled peptide concentration was chosen to be used for further uptake experiments.

3.2.3. Determination of the Effect of Buffer Concentration on Growth

The Fluorescein amine stock was dissolved in 1 M potassium phosphate buffer. On the other hand, the peptide stocks were prepared with 50 mM potassium phosphate buffer. In order to investigate whether the buffer concentration has an effect on the cell growth, 2 sets of experiments were carried out.

In the first experiment, tubes with 2 mL growth media were used. The preculture was incubated in an orbital shaker at 37°C and 180 rpm overnight, then the cells were transferred to these 2mL fresh LB media and incubated. When the measured OD_{600} of the cells reached 0.2 water, 50mM buffer or 1M buffer was added to the tubes. OD_{600} of all three sets were measured for 3 hours and plotted in Figure 3.25.

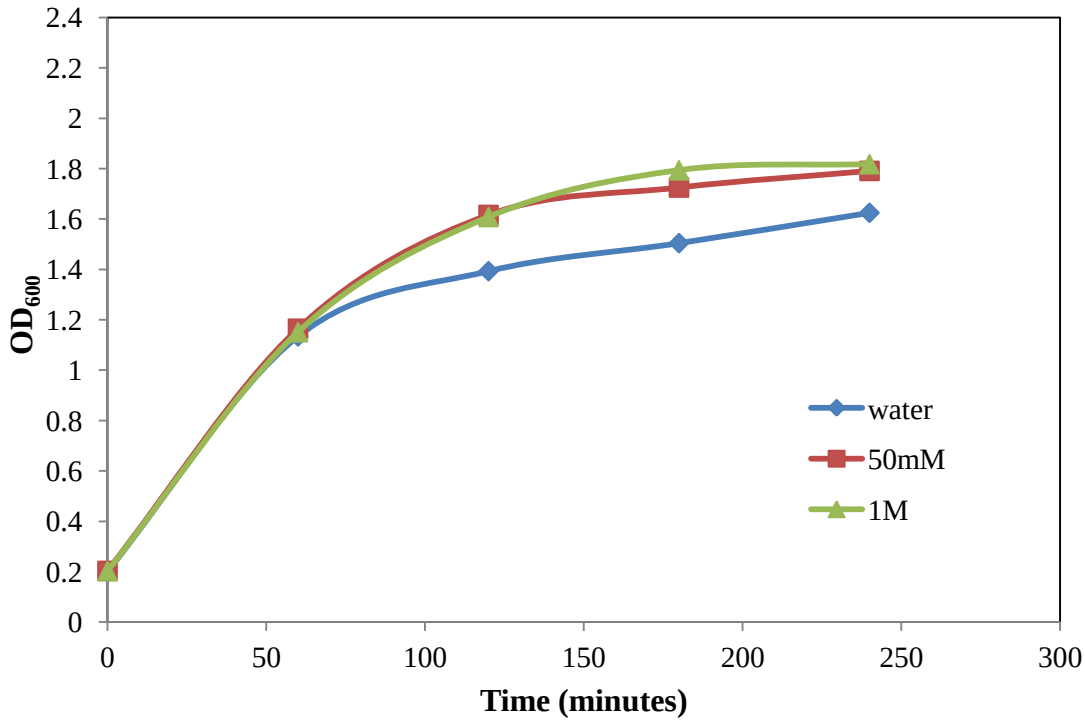

Figure 3.25. Growth profile of *E. coli* K12 pUC18 cells in LB medium that contained water, 50 mM potassium phosphate buffer and 1 M potassium phosphate buffer.

The culture was diluted and smeared on agar+LB media for viable cell count. Cell viability as a function of time is plotted in Figure 3.26.

The log scale in Figure 3.26 showed that there was no significant effect of the concentration of the buffer on cell growth. After 3 hours, it is seen that the cell growth is slightly higher in the sets that contained potassium phosphate buffer than the set that contained only water. This can be reasoned with the consumption of phosphate by the cells during growth and ATP formation.

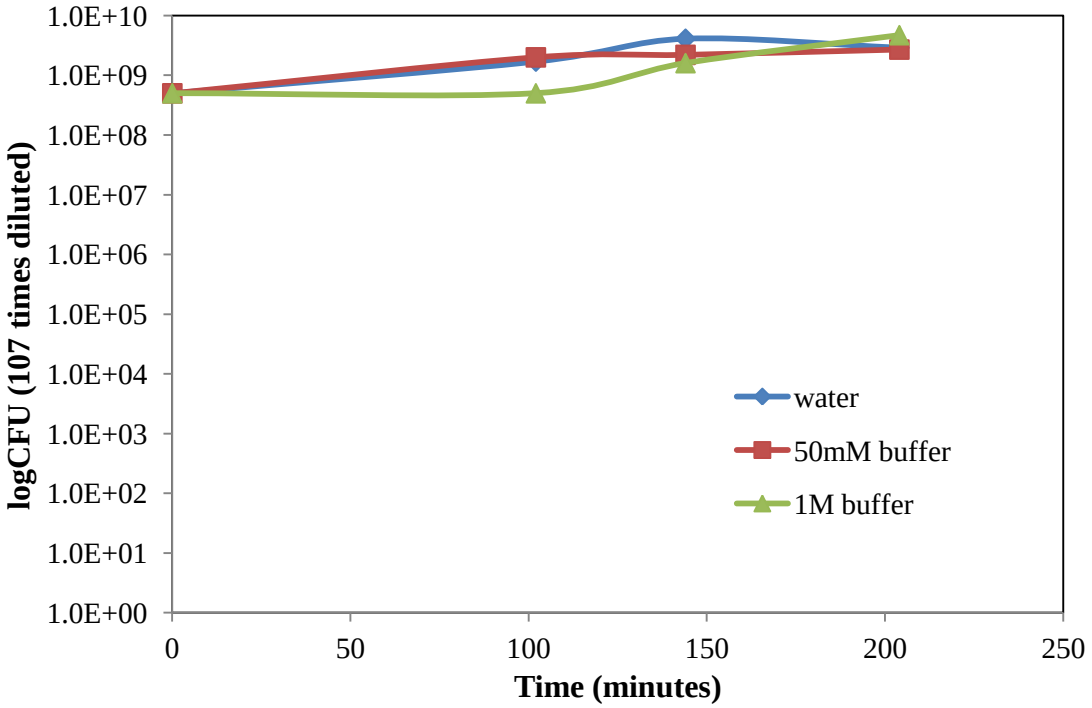

Figure 3.26. Cell viability profiles of *E. coli* K12 (pUC18) cells in LB medium that contained water, 50 mM potassium phosphate buffer and 1 M potassium phosphate buffer.

3.2.4. Bacterial Uptake of Peptide 1

For the investigation of the uptake of the peptide derived from the 45-53 loop of β-Lactamase inhibitory protein (BLIP), the fluorescein labeled peptide 1, with the sequence of 5(6)-Fluorescein-NH-HAAGDYYAY- $CONH_2$ was used. *E.coli* K12 pUC18 cells were grown in 2 mL test tubes until OD_{600} was equal to 0.2. After that point, 200 µL of the peptide stock of 1 mM concentration was added to each tube so that the final peptide concentration would be 100 µM. The samples were analyzed every hour for 3 hours following the addition of the fluoresceinated peptide. Each sample was centrifuged to precipitate and separate the cells from the medium. Then, to be able to analyze the precipitated cells as well as the media under the microscope, the precipitate was dissolved in 10µL potassium phosphate buffer of 1M.

The intensity of the medium was expected to be higher than the intensity of the cells. In addition to this, increasing intensity in the cells with time should mean that the amount of fluorescein labeled peptide that penetrates the cell increase with time. This

would point efficient bacterial peptide uptake.

Figure 3.27 and Figure 3.28 show the fluorescence microscopy captures of the cells and media after the addition of the peptide in one hour intervals. For visualization, 1 drop from each sample was analyzed without the cover glass since it would thin the droplet and decrease the intensity. The captures were taken under 5X, 20X and 40X zoom and different exposure values as 10ms, 20ms and 40ms.

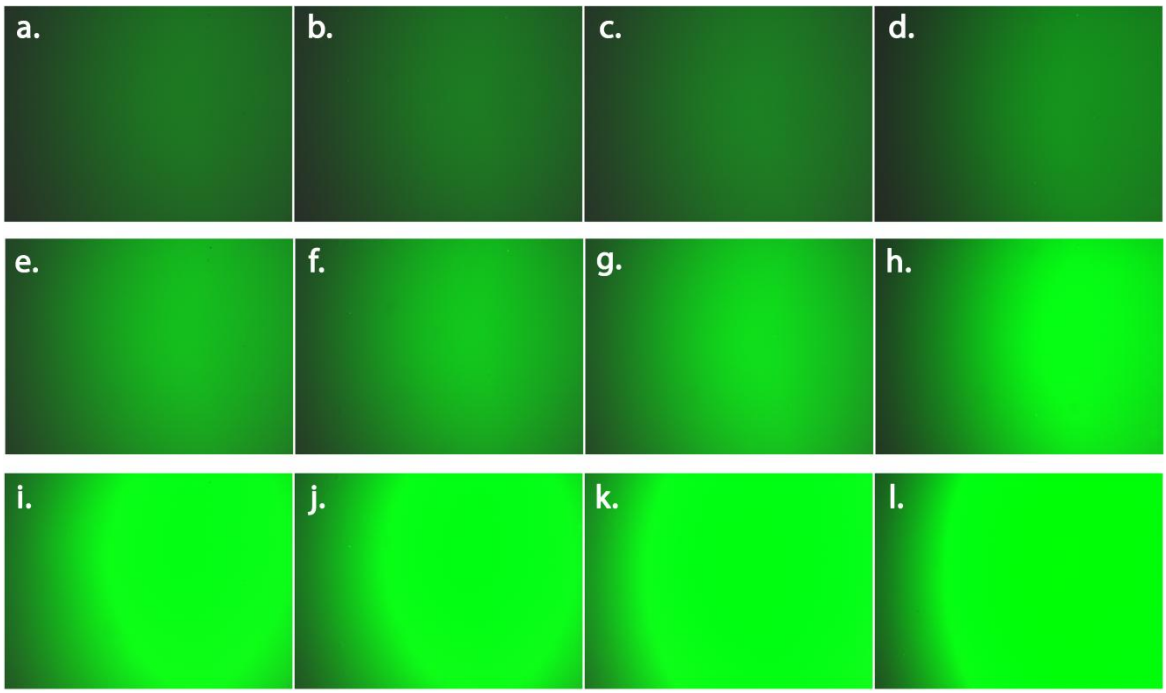

Figure 3.27. Fluorescence microscopy captures for the medium samples observed 3 hours after incubation under 5X zoom at 10 ms for (a) 0h, (b) 1h, (c) 2h, (d) 3h, at 20 ms (e) 0h, (f) 1h, (g) 2h, (h) 3h and at 40 ms (i) 0h, (j) 1h, (k) 2h and (l) 3h.

The media captures which can be seen in Figure 3.27 indicate a fair amount of intensity. Although the highest amount of fluorescein labeled peptide was expected to be observed in the initial stage of growth, this difference in intensity cannot be clearly seen in the captures.

In Figure 3.28 the cell captures at 5X zoom can be seen. The cells cannot be seen individually because 5X zoom was not sufficient for the observation of bacteria. The 5X captures are about 2600-2700 micrometers long horizontally, but a typical *E. coli* cell is

only 2 micrometers long and 0.5 micrometers in diameter. Although the cells cannot be seen individually in Figure 3.28, some intensity was observed. Here, it is important to mention that the intensity observed could either be from the peptides that actually penetrated into the cells or from the peptides that were absorbed onto the outer surface of the cell membrane. This deduction may be made when the cell extract is analyzed under fluorescence microscopy.

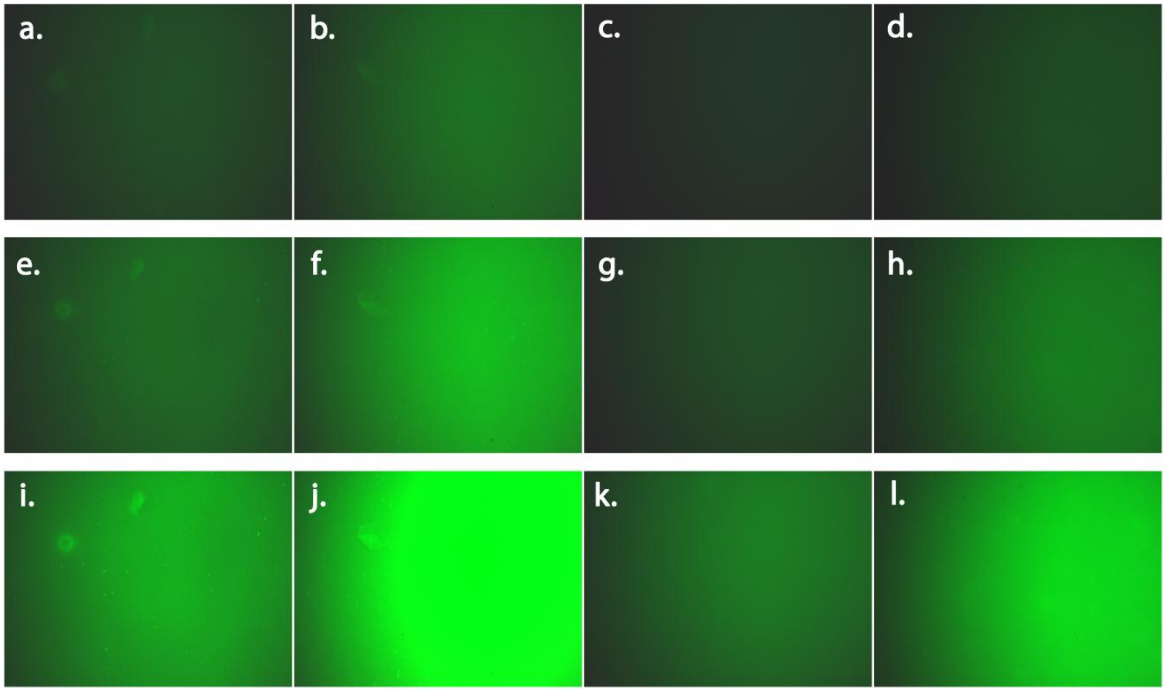

Figure 3.28. Fluorescence microscopy captures for the cell samples observed 3 hours after incubation under 5X zoom at 10 ms for (a) 0h, (b) 1h, (c) 2h, (d) 3h, at 20 ms (e) 0h, (f) 1h, (g) 2h, (h) 3h and at 40 ms (i) 0h, (j) 1h, (k) 2h and (l) 3h.

The decrease in the intensity observed for the cells incubated one and two hours with the peptide was probably a result of the incomplete washing procedure. The cells were not washed thoroughly in the first two samples. From then on, cells were washed three times with potassium phosphate buffer resulting in a slight decrease in the intensity.

In order to analyze the cells more accurately, fluorescence microscopy was used at 20X and 40X zoom and images were taken under 40ms exposure. In Figure 3.29 and Figure 3.30 the cell captures taken from samples after two and three hours of incubation with the peptides under 20X and 40X zoom can be seen.

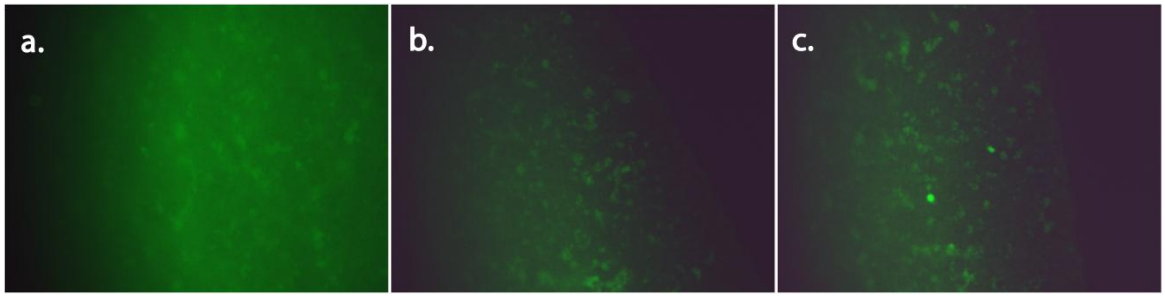

Figure 3.29. Captures for the cells observed after 2 hours of addition of Peptide 1 under 40ms exposure with 20X zoom. The capture (a) is taken from the middle of the sample drop and the captures (b) and (c) are taken from the edges of the sample drop.

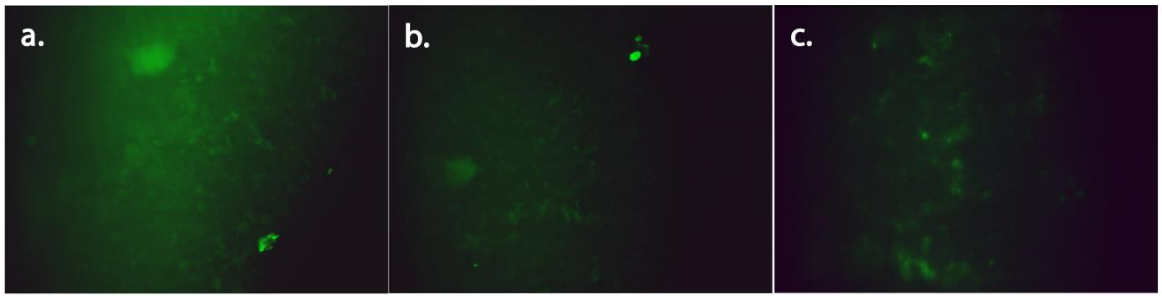

Figure 3.30. Captures for the cells observed 3 hours after the addition of Peptide 1 under 40ms exposure. The captures in (a) and (b) are taken under 20X zoom, the capture in (c) is taken under 40X zoom.

Figure 3.29 and Figure 3.30 show close up captures of the cells. The size of the capture under 20X zoom is 600-700 micrometers horizontally.

In Figure 3.29, the cells were observed 2 hours after the addition of the peptide, at 40 ms exposure under 20X zoom. Capture (A) was the middle part of the drop analyzed while captures (B) and (C) were from the edges of the drop. In the initial analysis, the cover glass was not used in order not to decrease the intensity, however a homogenous analysis of the sample to compare intensities may necessitate the use of a cover glass.

Similarly, the captures in Figure 3.30 were from cells 3 hours after the addition of Peptide 1 under exposure of 40 ms. The capture (C) is taken under 40X zoom while captures (A) and (B) were taken under 20X zoom. Although individual cells were not clearly differentiated even under 40X zoom, groups of cells could be seen.

Figure 3.31 and Figure 3.32 are the fluorescence microscopy captures from the cells, media and culture two hours after the addition of the peptide. In this case during analysis, cover glass was used in order to obtain a thin film of the sample. The captures were taken under 40X zoom and different exposure values as 50 ms, 100 ms and 200 ms. As expected, cell captures had lower intensity than the media samples.

Figure 3.31. The fluorescence microscopy captures for the samples of (a) cell, (b) culture and (c) medium taken under 40X zoom and 100 ms exposure.

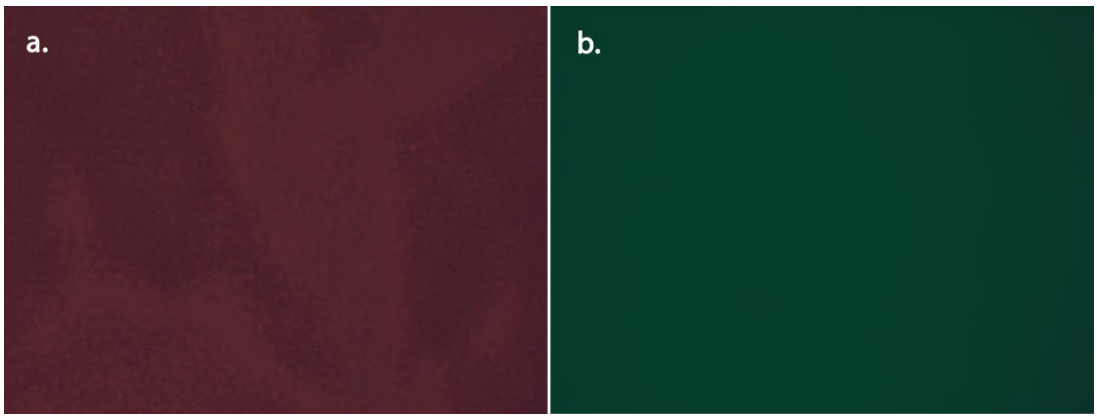

Figure 3.32. The cell captures taken under (a) sun light and (b) UV light.

In Figure 3.32, the same cell sample is analyzed both under sun light and UV light. The idea behind this was to see if some regions on the sample with higher density of cells would reflect UV light more and stand out in the capture under UV light. Although in the capture under sun light, the regions with higher cell density could be distinguished, the intensity was equally distributed in the capture taken under UV light.

3.2.5. Effect of Peptide 2 Addition on Cell Growth

In order to investigate the effect of Peptide 2 (5/6-Fluorescein-NH-RRGHYY-COOH) on antibiotic resistant *E. coli* cells, growth experiments were carried out. *E. coli* K12 cells harboring pUC18 plasmid were precultivated at 37°C and 180 rpm overnight. The precultivated cells were added to 2 mL fresh LB media and incubated in test tubes at 37°C and 180 rpm. Peptide was added to the sample sets as OD_{600} nm reached 0.2 while phosphate buffer and acetic acid was added to the control set. The peptide was previously dissolved in 50 mM phosphate buffer and acetic acid and aliquoted. The amounts of buffer and acid were kept the same in the control set. In order to adjust the pH of the peptide stock to 7.0, 10065 µl of KOH was used for 600 µl of the peptide stock prepared. The content of the control set medium and peptide set medium are given in Table 3.3.

Table 3.3. Contents of medium for control and experimental sets

Control set	**Peptide set**
2 mL LB	2 mL LB
2 µl ampicillin	2 µl ampicillin
19.2 µl acetic acid	4 mL peptide+KOH (for 100 µl final peptide concentration)
200.7 µl phosphate buffer	
4150 µl 1M KOH	

Acetic acid, phosphate buffer, KOH for the control set and peptide and KOH for sample set were added when the cells were grown in the LB medium until the OD_{600}nm reached 0.2. Following the addition of the acetic acid, potassium phosphate buffer, KOH and Peptide 2, the OD_{600} values were measured for 4 hours. Figure 3.33 shows the change in OD_{600} for the addition of Peptide 2.

In order to determine the number of viable cells, colony forming unit (CFU) were counted. The samples were plated and incubated at 37°C for 24 hours. The control set samples were too dense in cells because the samples were not diluted enough prior to plating, the viable cell count was too many on plates after 2 hours. Upon Peptide 2

addition, the viable cell count converged to zero after 1 hour of incubation. The number of CFU for control and sample sets are given in Table 3.4.

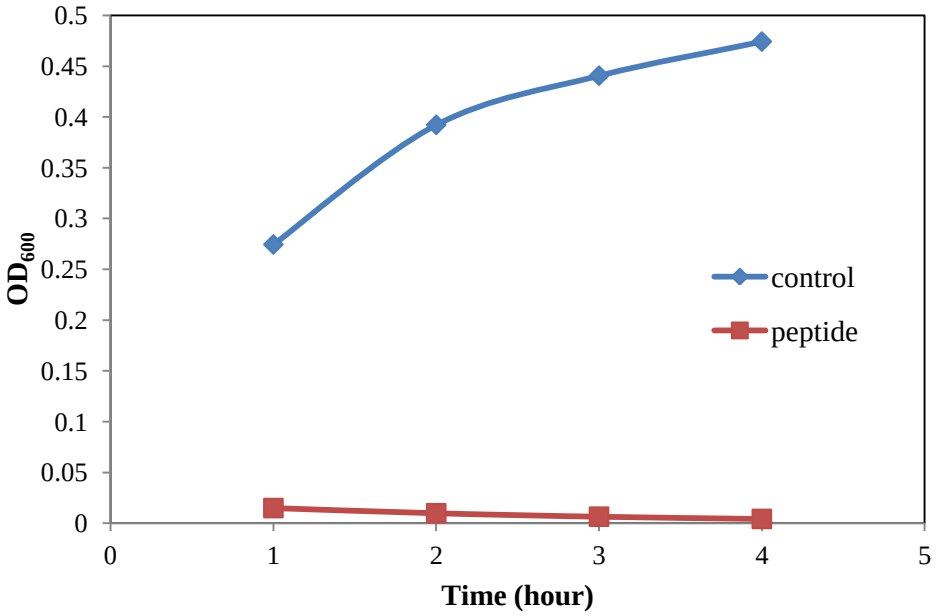

Figure 3.33. Growth profile of *E. coli* K12 pUC18 cells for the control set and for the peptide set in the presence of Peptide 2.

Although the initial CFU analysis was done just at the time of Peptide 2 addition, the difference in the initial CFU count for control and peptide set shows that the peptide has already started to take action and inhibit β-lactamase when the cells were smeared on the agar+LB added petri dishes. The death of the cells in the peptide set proved that Peptide 2 is a potent inhibitior of β-lactamase enzyme.

Table 3.4. The viable cell count for control and experiment sets.

	Control set	**Peptide set**
initial	744 x 10^4	328 x 10^1
1 h	cells viable but too many	0
2 h	cells viable but too many	0
3 h	cells viable but too many	0
4 h	cells viable but too many	0

3.2.6. Effect of Kemptide Acetate Salt Addition on Cell Growth

In order to investigate the effect of Kemptide acetate salt on antibiotic resistant *E. coli* cells, growth experiments were carried out. *E. coli* K12 cells harboring pUC18 plasmid were precultivated at 37°C and 180 rpm overnight. The precultivated cells were added to 2 mL fresh LB media and incubated in test tubes at 37°C and 180 rpm. Peptide was added to the sample sets as OD_{600} nm reached 0.2 and phosphate buffer was added to the control set. OD_{600} was measured and samples were harvested 1, 2, 3 and 4 hours after peptide addition. Growth as a function of OD_{600} nm is plotted in Figure 3.34.

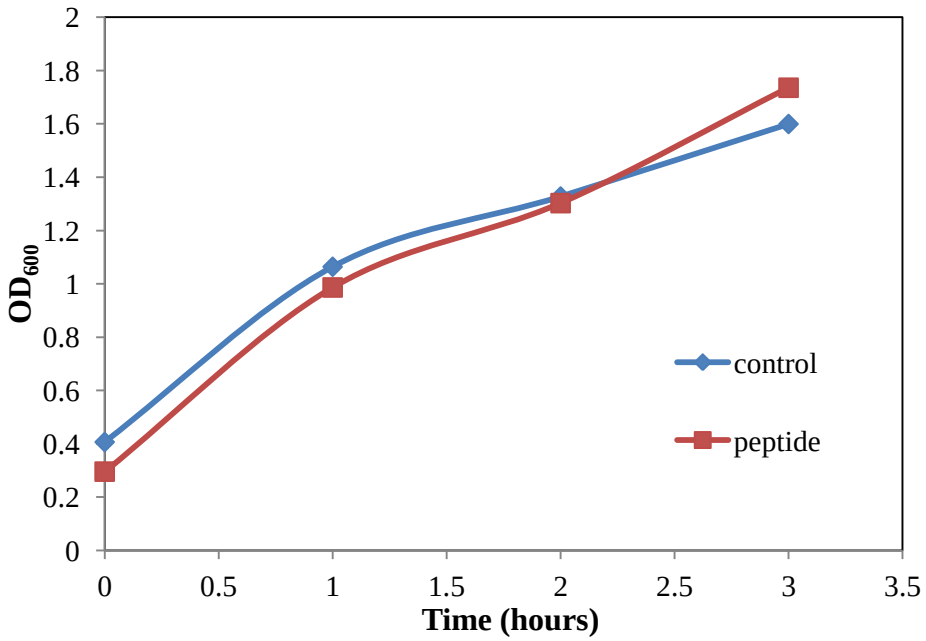

Figure 3.34. Growth profile of *E. coli* K12 pUC18 cells for the control set and for the peptide set in the presence of Kemptide acetate salt.

As reported in literature, Kemptide acetate salt possesses no inhibitory potential for β-lactamase. Hence Kemptide was used as a negative control in the experiments.

Figure 3.35 shows the viable cell profiles plotted as a function of time for the control and sample sets when Kemptide acetate salt was added. As it was expected, the viable cell numbers showed that there was no significant difference in the control and sample sets using Kemptide acetate salt as the inhibitor.

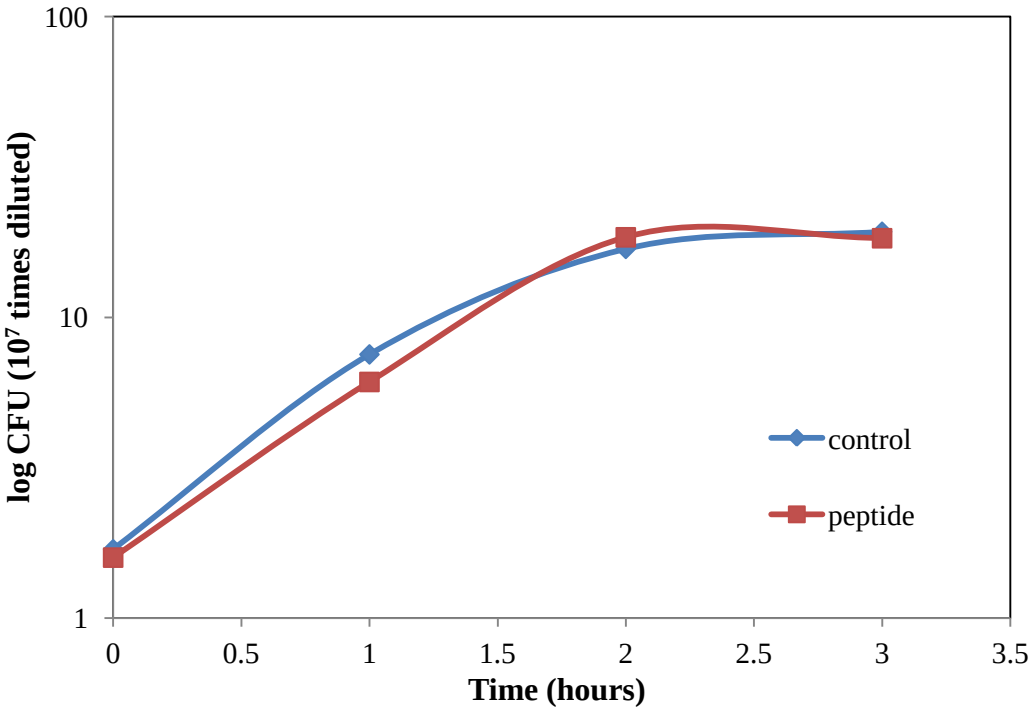

Figure 3.35. Cell viability profiles of *E. coli* K12 (pUC18) cells for the control set and peptide set incubated with Kemptide acetate salt.

3.2.7. Effect of Peptide 3 Addition on Cell Growth

Peptide 3 (5/6-Fluorescein-NH-LL IIL HAA GDY YAY- $CONH_2$ (fluorescein-LLIIL-BLIP residues 45-53)) is based on BLIP 45-53 as well as Peptide 1. It has the first 5 residues (LLIIL) of the cell-penetrating peptide pVEC in its N-terminus. Previously, it was shown that the substitution of the first five amino acids in the N-terminus of the cell-penetrating peptide pVEC to L-alanine resulted in decrease of the cellular uptake values to 50-75%. Thus, the hydrophobic N-terminus of the peptide was determined to be important for the cellular uptake [17]. The addition of LLIIL to the N-terminus of BLIP 45-54 residues was expected to enhance the bacterial uptake of the designed peptide. For the visualization of the bacterial uptake by using fluorescence microscopy, the peptide has fluorescein attached as a tracer.

In order to investigate the effect of Peptide 3 on antibiotic resistant *E. coli* cells, growth experiments were carried out. *E. coli* K12 cells harboring pUC18 plasmid were precultivated at 37°C and 180 rpm overnight. The precultivated cells were added to 2 mL

fresh LB medium in test tubes and incubated at 37°C and 180 rpm. As OD_{600} nm reached 0.2, peptides were added to sample sets and phosphate buffer was added to the control set. The cells in test tubes were harvested one by one 1, 2, and 3 hours after peptide addition. OD_{600} nm of cells in each tube was measured before harvesting and the values obtained were plotted as a function of time in Figure 3.36. Although the initial OD_{600} of the cultures were equal to each other (~0.2) before the incubation, the fluorescein attached at the N-terminus of Peptide 3 resulted in the difference of OD_{600} at the time of incubation due to the emission.

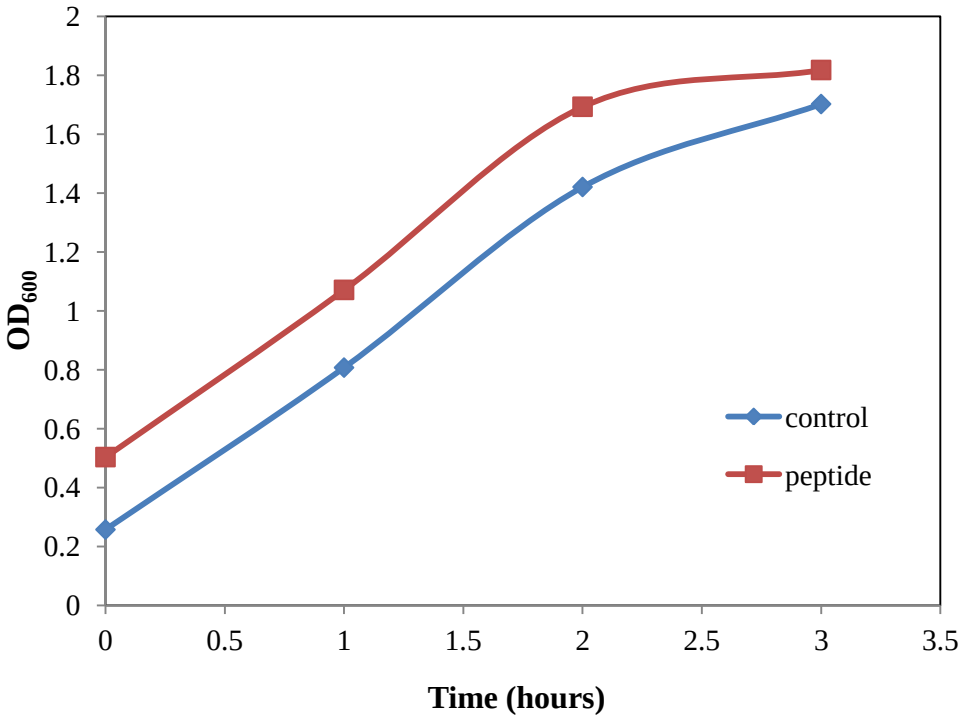

Figure 3.36. Growth profile of *E. coli* K12 pUC18 cells for the control set and for the peptide set with the addition of Peptide 3.

In order to determine the number of live cells, viable cell count was performed. After 100 µM peptide addition, the cells were grown for a total of three hours and plated in one hour intervals to count viable cells. Cell viability plotted as a function of time is given in Figure 3.37. It was observed that cells continued to grow almost equally in the control set and the peptide set in the first hour of incubation. The cell viability profiles of the cells incubated with the peptide started to decrease after the second hour of incubation,

suggesting that under the conditions used, Peptide 3 is a potent inhibitior of β-lactamase enzyme.

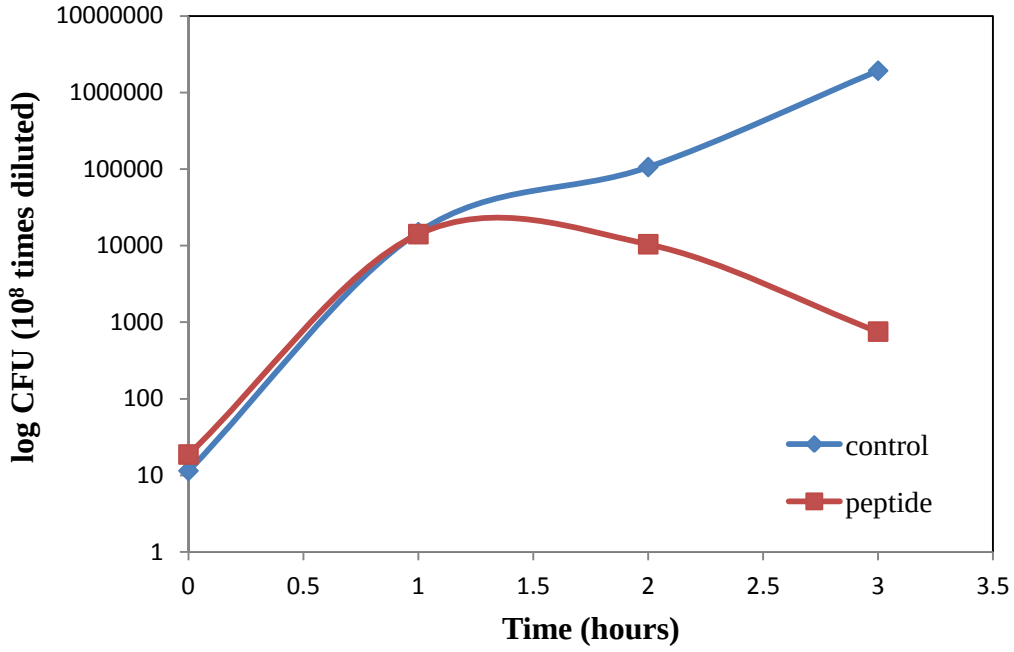

Figure 3.37. Cell viability profiles of *E. coli* K12 (pUC18) cells for the control set and peptide set incubated with Peptide 3.

3.2.8. Bacterial Uptake of Peptide 3

For the investigation of the uptake of a peptide, the fluorescein labeled Peptide 3 with the sequence of 5/6-Fluorescein-NH-LL IIL HAA GDY YAY- $CONH_2$ (fluorescein-LLIIL-BLIP residues 45-53) was used. *E. coli* K12 pUC18 cells were grown in 2 mL LB media in test tubes. When OD_{600} nm reached 0.2, 200 µL of the peptide stock of 1 mM concentration was added to each tube so that the final peptide concentration would be 100 µM. The samples were analyzed in one hour intervals for 2 hours after the addition of the fluoresceinated peptide. Each sample was centrifuged to precipitate and separate cells from the medium. The precipitated cells were then washed with potassium phosphate buffer three times and centrifuged to remove excess medium and peptide stuck on the outer of the cells. The precipitated cells were then dissolved in 10 µL potassium phosphate buffer of 50 mM in order for analysis under the microscope.

For efficient bacterial peptide uptake, intensity of the cells should increase with time as more of the fluorescein labeled peptide would penetrate though the cell membrane.

Figure 3.38, Figure 3.39 and Figure 3.40 show the fluorescence microscopy captures for the culture, media and cell samples after the addition of the peptide in one hour intervals. For analysis, cover glass was used. The captures were taken under 40X zoom and 200 ms exposure.

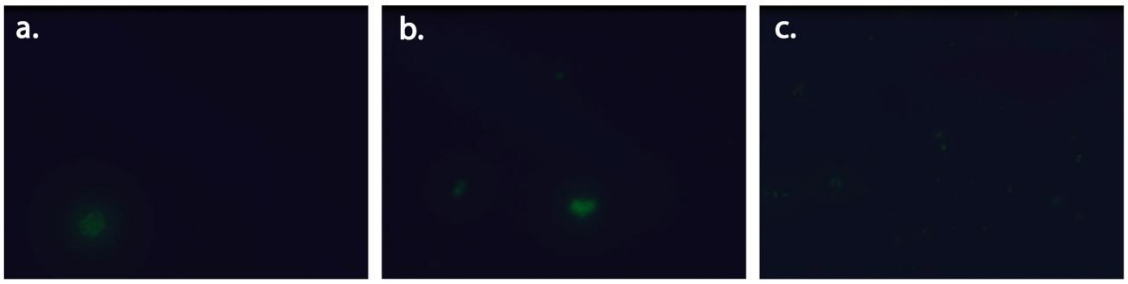

Figure 3.38. Fluorescence microscopy captures for the culture samples observed 2 hours after incubation with the peptide under 40X zoom and 200 ms for (a) 0h, (b) 1h and (c) 2h.

Figure 3.38 shows the fluorescence microscopy captures of the culture samples that were analyzed for a total of 2 hours after the addition of Peptide 3. The intensities of three captures do not have a significant difference. On the other hand, the regions that outstand in the captures with higher intensity are the regions with higher density of cells and are clearly visible.

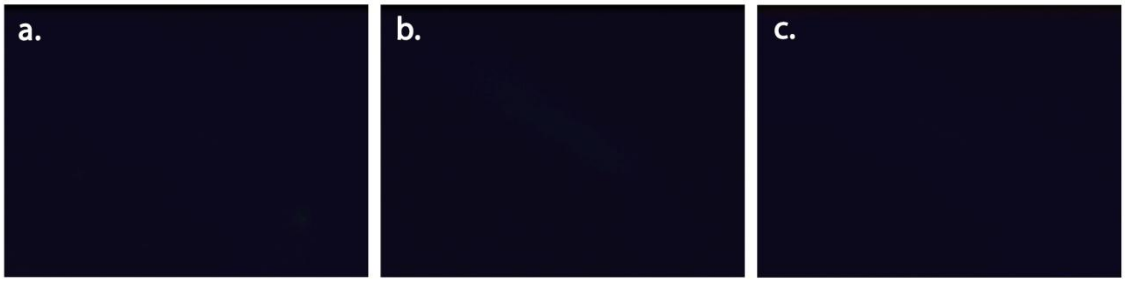

Figure 3.39. Fluorescence microscopy captures for the medium samples observed 2 hours after incubation with the peptide under 40X zoom and 200 ms for (a) 0h, (b) 1h and (c) 2h.

Figure 3.39 and Figure 3.40 show the fluorescence microscopy captures for the media and cell samples respectively. It was found that the intensity of the medium dropped

to almost zero 2 hours after the addition of Peptide 3. This has led to the conclusion that Peptide 3 was taken-up by the cells. In Figure 3.40, it can clearly be seen that the intensity of cell captures increased with time, also an indication of their intracellular location (Figure 3.40(a) and Figure 3.40(c)).

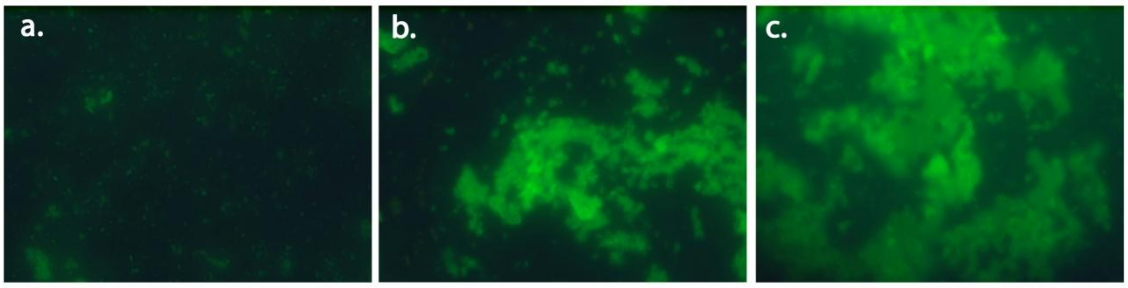

Figure 3.40. Fluorescence microscopy captures for the cell samples observed 2 hours after incubation with the peptide under 40X zoom and 200 ms for (a) 0h, (b) 1h and (c) 2h.

The difference between Peptide 1 and Peptide 3 was the extra first five residues LLIIL which were also comprised the N-terminal residues of the cell-penetrating peptide pVEC. The intensity differences in the cell captures for Peptide 1 and Peptide 3 (Figure 3.28 and Figure 3.40) showed that the residues LLIIL have an important role in the penetration of the peptides.

4. CONCLUSIONS AND RECOMMENDATIONS FOR FUTURE STUDIES

4.1. Conclusions

In the computational part of the study, the translocation mechanism of the cell-penetrating peptide pVEC is investigated and the peptide is analyzed on a residue basis in order to determine the structural elements that are significant for bacterial uptake. For this aim, the wild-type pVEC, eight mutants, retro- and scramble pVEC were studied using molecular dynamics and steered molecular dynamics simulations. When MD simulations were carried out with the wild-type pVEC, no penetration of the peptide was observed after 170 ns of simulation time. Therefore, SMD simulations, in which an extra potential is added to the molecular mechanics forcefield to move the peptide from one side of the membrane to the other side, were employed to analyze the translocation mechanism of wild-type pVEC and its mutants.

The SMD simulations carried out for the system of wild-type pVEC were analyzed in detail. The change in interaction energy was plotted as a function of the SMD atom displacement and the interaction energy profile combined with visual analysis of the simulation trajectory gave an idea about the uptake mechanism of peptide. The interaction energy plot had two valleys that correspond to regions in which the peptide and the membrane are in high interaction (initial contact of peptide with the membrane) and complete insertion of peptide with N-terminal interacting with lower phosphate head layer. On the other hand, two plateaus were observed which correspond to motion of the peptide between lipid tails. The electrostatic energy contribution to interaction energy was found to be higher than the van der Waals energy contribution. The electrostatic energy profile resembled that of the total interaction energy, with maximum electrostatic energy value of at around -400 kcal/mol attained when the peptide is completely immersed inside the membrane for the system of wild-type pVEC. The analysis of the interaction energy profile for the system of wild-type pVEC suggests that the peptide transport occurs in three main stages. The first barrier is the insertion of the N terminus into the bilayer where the

interaction reaches its first maximum value. The second barrier is the inclusion of the whole peptide inside the membrane where the interaction between the peptide and the membrane reaches its ultimate maxiumum value. Finally, the third barrier is observed as the N terminus of the peptide interacts with the lower layer and exits from the bilayer. The three main stages of the uptake mechanism observed in the interaction energy profiles are also present in the force profiles. The force applied on the SMD atom is abruptly increased upon entrance (first barrier) and exit of the N-terminal (third barrier).

The peptide conformation varied in different simulations during the translocation through the membrane. The I9A, L5A and R6A peptides maintained their hairpin loop structure after they penetrated into the membrane and the C-terminus was already inside the membrane as the first residues exit the membrane. The hairpin unfolded upon exit in these systems. Similarly, as r pVEC (retro-pVEC) approached the membrane, the hairpin loop between residues 13-17 (corresponding to the same region) was formed and the peptide entered the membrane as folded. The loop only unfolded as the peptide exit the membrane. For the system of scr pVEC (scramble-pVEC), at the beginning of the simulation, when the SMD atom touched the upper layer of the membrane, residue LEU18 had an interaction with the upper layer of the membrane too. The hairpin formed before the insertion (residues 7-12) started to unfold as residue LEU7 touched the upper layer of the membrane and completely unfolded as the loop was embedded in the membrane.

Comparison of the interaction energy profiles for the different simulations systems showed that the interaction energy profiles of R7A, R8A, I9A, H14A and S17A systems were similar to that of wild-type pVEC in terms of the maximum value attained (at around or less than -550 kcal/mol) and the number of maxima as the peptide moves through the membrane. On the other hand, the retro-pVEC (r pVEC) interaction energy profile was different as it had one maximum at a higher value and no other maxima. Also, L2A, L5A and R6A peptides and the scramble-pVEC (scr pVEC) showed a different trend in the interaction energy profiles. For those peptides with a different interaction energy profile, the profile was more flat, and the maximum interaction energy value reached was lower compared to the wild-type pVEC system. Force profile also followed a similar trend, with valleys and peaks observed in similar locations with the interaction energy profile. When

all the simulations were compared, it was determined that for higher maximum force values the work done is higher too. On the other hand, for scr pVEC (scramble-pVEC), a continuously low force was applied throughout the simulation, hence increasing the work without a pronounced peak in the force profile. When the work performed and cellular uptake values were compared for all the simulations, it was distinguished that for those peptides with increased uptake potential, the work performed was higher.

In order to analyze wild-type pVEC on a residue basis, the interaction energy profile of each residue with the lipid bilayer was compared and it was observed that residues L1, R6, R7, R8, R10, K11 and K18 contributed the most to the interaction of the wild-type pVEC with the lipid bilayer. The analysis showed that Arginine and Lysine, amino acids with polar and positively charged side chains, had strong interactions with the lipid bilayer as observed both in the interaction energy and electrostatic energy profiles. The high interaction of the L1 residue was due to the charged N-terminus.

In the experimental part of the study, the effect of Peptide 1 (5-Fluorescein-NH-HAAGDYYAY- $CONH_2$), Peptide 2 (5/6-Fluorescein-NH-RRGHYY-COOH) and Peptide 3 (5/6-Fluorescein-NH-LLIILHAAGDYYAY- $CONH_2$) on growth of antibiotic resistant *E. coli* K12 pUC18 cells, which express beta-lactamase, was examined. The bacterial uptake of the fluorescein labeled peptides (Peptide 1 and Peptide 3) was investigated using fluorescence microscopy.

The addition of Peptide 1 to the medium at OD_{600} = 0.2 which is the early growth phase of *E. coli* cells, did not have any effect on the growth of *E. coli* cells, which continued to grow almost equally in the control set and the peptide set. The cell viability profiles of the cells incubated with peptide did not have a significant change after peptide addition, either, suggesting that under the conditions used, Peptide 1 did not have an inhibitory effect on the cellular β-lactamase.

The bacterial uptake of Peptide 1 was carried out by visualizing the medium and cell samples using fluorescence microscopy. Intensity of the medium samples was higher than the intensity of the cell samples. Although intensity was observed in the cell samples,

the intensity observed could either be from peptides that actually penetrated into the cells or from the peptides that were stuck on the outer surface of the cell membrane. Under 40X magnification, it was not possible to observe single cells.

Experiments with Kemptide, a kinase inhibitor that was previously shown to have no inhibitory effect on beta-lactamase, were carried out to be used as the negative control. As expected, the viable cell count proved that there was no significant difference in the control and peptide set. This analysis verified the validity of the experimental procedure that was followed.

For the bacterial uptake investigation of Peptide 3, cell, culture and medium samples were visualized under fluorescence microscopy. The cell sample exhibited fluoresence, while the intensity of the medium sample is almost zero after two hours of Peptide 3 incubation, suggesting that Peptide 3 was taken into the cells. The difference between Peptide 1 and Peptide 3 was the first five residues LLIIL, the five N-terminal residues of the cell-penetrating peptide pVEC. These five residues were previously shown to be crucial for cellular uptake of pVEC. The intensity differences in the cells captures for Peptide 1 and Peptide 3 showed that the residues LLIIL had an important role in the uptake of the peptides as cargo.

4.2. Recommendations for Future Studies

For the future computational studies, pVEC simulations can be repeated with the peptides acetylated at the N-terminus and with the peptides both acetylated at the N-terminus and amidated at the C-terminus. Since the peptides used in the experiments are delivered as capped at the C-terminus, comparison of the SMD simulations and the experiments will be more consistent. Also, since the charged N- and C- terminals will be neutralized when the peptide is capped, the interaction energy profile, the force applied and the work done on the peptides may change, so the translocation mechanism can be revealed more accurately.

For the future studies, it is recommended that sonication method should be used in order to distinguish the peptide that actually penetrates into the cells and the peptide that

was stuck on the outer membrane of the cells. The cell extract samples prepared by sonication method should be visualized under greater magnification (100X desired) in order to observe single cells. Also, the intensity profiles should be plotted using the software of the Axio Observer so that the intensity of the samples could be compared quantitatively. Fluoremeter could also be used for quantitative analysis in the sample solutions of medium and cells.

APPENDIX A: VMD SCRIPTS

trial.tcl

```
resetpsf
package require psfgen
topology top_all27_prot_lipid.inp
pdbalias residue HIS HSE
pdbalias atom ILE CD1 CD
segment A {
residue 1 LEU
residue 2 LEU
residue 3 ILE
residue 4 ILE
residue 5 LEU
residue 6 ARG
residue 7 ARG
residue 8 ARG
residue 9 ILE
residue 10 ARG
residue 11 LYS
residue 12 GLN
residue 13 ALA
residue 14 HSE
residue 15 ALA
residue 16 HSE
residue 17 SER
residue 18 LYS
}
coordpdb peptide.pdb A
writepsf newpeptide.psf
```

```
guesscoord
writepdb newpeptide.pdb
```

code.tcl

```
mol delete all
package require solvate
solvate newpeptide.psf newpeptide.pdb -o new_pep_sol -t 10
mol load psf new_pep_sol.psf pdb new_pep_sol.pdb
set all [atomselect top all]
$all set beta 0
set clash [atomselect top "resname TIP3 and same residue as (within 2.8 of protein)"]
$clash set beta 1
set clashwater [atomselect top "name OH2 and beta > 0"]
set seglist [$clashwater get segid]
set reslist [$clashwater get resid]
mol delete all
package require psfgen
readpsf new_pep_sol.psf
coordpdb new_pep_sol.pdb
foreach segid $seglist resid $reslist {
delatom $segid $resid
}
writepdb pep_VdW.pdb
writepsf pep_VdW.psf
mol delete all
mol load psf pep_VdW.psf pdb pep_VdW.pdb
```

membrane_equilibrate.tcl

```
mol delete all
resetpsf
```

```
package require membrane
membrane -l POPE -x 50 -y 50
set all [atomselect top all]
$all moveby [vecinvert [measure center $all]]
$all writepdb centered.pdb
mol delete all
package require solvate
solvate membrane.psf centered.pdb -o membrane_water_TEMP -minmax {{-24 -24 -80}
{24 24 80}}
set all [atomselect top all]
$all set beta 0
set seltext "segid WT1 to WT99 and same residue as abs(z) <10"
set sel [atomselect top $seltext]
$sel set beta 1
set badwater [atomselect top "name OH2 and beta > 0"]
set seglist [$badwater get segid]
set reslist [$badwater get resid]
mol delete all
#mol load psf membrane_water.psf pdb membrane_water.pdb
package require psfgen
readpsf membrane_water_TEMP.psf
coordpdb membrane_water_TEMP.pdb
foreach segid $seglist resid $reslist {
delatom $segid $resid
}
writepdb membrane_water.pdb
writepsf membrane_water.psf
#file delete membrane_water_TEMP.psf
#file delete membrane_water_TEMP.pdb
mol load psf membrane_water.psf pdb membrane_water.pdb
```

manipulation.tcl

```
mol load pdb finalsnapshot.pdb
mol load pdb protein_pVEC.pdb
package require psfgen
readpsf membrane_water.psf
coordpdb finalsnapshot.pdb
## created manually by save coordinates
readpsf protein_pVEC.psf
coordpdb peptidemanipulated.pdb
## created manually by save coordinates
writepdb manipulated.pdb
writepsf manipulated.psf
mol load pdb manipulated.pdb
set all [atomselect top all]
$all set beta 0
set clash [atomselect top "resname TIP3 and same residue as (within 2.8 of protein)"]
$clash set beta 1
set clashwater [atomselect top "name OH2 and beta > 0"]
set seglist [$clashwater get segid]
set reslist [$clashwater get resid]
foreach segid $seglist resid $reslist count_water_in_membrane.out}}"
writepdb memb_wat_pep.pdb
writepsf memb_wat_pep.psf
mol delete all
mol load pdb memb_wat_pep.pdb
```

count_water_in_membrane.tcl

```
puts "count_water_in_active_site {{molid top} {outputfile
count_water_in_membrane.out}}"
puts "For Example"
```

```
puts "count_water_in_membrane top  count_water_in_membrane.out \n"
proc count_water_in_membrane {{molid top} {outputfile
count_water_in_membrane.out}} {
set selection ""
set selection "abs(z)<10 and water and name OH2"
set fid [open $outputfile "w"]
set total_frame [molinfo $molid get numframes]
for {set frame 0} {$frame < $total_frame} {incr frame} {
set sel1 [atomselect top $selection frame $frame]
set a [$sel1 get resid]
puts $fid [llength $a]
set a ""
}
close $fid
}
```

thickness_of_memb.tcl

```
puts "thickness_of_memb {{molid top} {outputfile thickness_of_memb.out}}"
puts "For Example"
puts "thickness_of_memb top  thickness_of_memb.out \n"
proc thickness_of_memb {{molid top} {outputfile thickness_of_memb.out}} {
set fid [open $outputfile "w"]
set total_frame [molinfo $molid get numframes]
for {set frame 0} {$frame < $total_frame} {incr frame} {
set sel [atomselect top lipid frame $frame]
set m [measure minmax $sel]
set z1 [lindex $m 0 2]
set z2 [lindex $m 1 2]
set r [expr $z2 - $z1]
puts $fid $r
}
```

```
close $fid
}
```

distance.tcl

```
proc distance {seltext1 seltext2 N_d f_r_out f_d_out} {
set sel1 [atomselect top "$seltext1"]
set sel2 [atomselect top "$seltext2"]
set nf [molinfo top get numframes]
set outfile [open $f_r_out w]
for {set i 0} {$i < $nf} {incr i} {
  puts "frame $i of $nf"
  $sel1 frame $i
  $sel2 frame $i
  set com1 [measure center $sel1 weight mass]
  set com2 [measure center $sel2 weight mass]
  set simdata($i.r) [veclength [vecsub $com1 $com2]]
  puts $outfile "$i $simdata($i.r)"
}
close $outfile

set r_min $simdata(0.r)
set r_max $simdata(0.r)
for {set i 0} {$i < $nf} {incr i} {
  set r_tmp $simdata($i.r)
  if {$r_tmp < $r_min} {set r_min $r_tmp}
  if {$r_tmp > $r_max} {set r_max $r_tmp}
}
set dr [expr ($r_max - $r_min) /($N_d - 1)]
for {set k 0} {$k < $N_d} {incr k} {
  set distribution($k) 0
}
```

```
for {set i 0} {$i < $nf} {incr i} {
  set k [expr int(($simdata($i.r) - $r_min) / $dr)]
  incr distribution($k)
}
set outfile [open $f_d_out w]
for {set k 0} {$k < $N_d} {incr k} {
  puts $outfile "[expr $r_min + $k * $dr] $distribution($k)"
}
close $outfile
}
```

APPENDIX B: THE MATLAB SCRIPTS

displacement_time.m

```
A=load('smdforces.out');
for i=1:length(A(:,1))
   B(i,1) = sqrt((A(i,2)-A(1,2))^2+(A(i,3)-A(1,3))^2+(A(i,4)-A(1,4))^2);
end
plot((A(:,1)*2*10^(-6)),B(:,1))
xlabel('Time (ns)')
ylabel('Displacement (A)')
```

energy_coor.m

```
x=load('energy_profile');
Nonbond=x(:,5);
Total=x(:,6);
z=load('smdforces.out');
plot(abs(z(1:50.0050:end,4)),Total)
xlabel('z coordinate (A)')
ylabel('Interaction Energy')
```

force_coor_av.m

```
x=load('smdforces.out');
windowsize = 5000;
runningavgF=filter(ones(1,windowsize)/windowsize,1,x(:,7));
plot(x(:,4),runningavgF(:,1));
xlabel('z coordinate (A)');
ylabel('Force (pN)');
```

thickness_of_memb.m

```
x=load('thickness_of_memb.out');
plot(((1:1:length(x))/1000*2),x)
xlabel('Time (ns)')
ylabel('Thickness of the membrane (A)')
```

water_coor.m

```
x=load('count_water_in_membrane.out');
y=load('smdforces.out');
plot(y(1:50.0007:end,4),x)
xlabel('z coordinate(A)')
ylabel('Number of water molecules in membrane')
```

work_coor.m

```
load smdforces.out;
ftemp = smdforces(:,7)/69.479;
fsum = 0;
v = -1*0.0000100;
dt = 20;
for i = 1:length(smdforces)
   fsum(i+1) = fsum(i) + ftemp(i)*v*dt;
   w(i) = fsum(i);
end
plot(abs(smdforces(:,4)),w)
xlabel('z coordinate (A)')
ylabel('Work (kcal/mol)')
```

REFERENCES

1. Kong, K. F., L. Schneper, and K. Mathee, "Beta-Lactam Antibiotics: From Antibiosis to Resistance and Bacteriology", *Acta Pathologica, Microbiologica et Immunologica Scandinavica*, Vol. 118, No. 1, pp. 1-36, 2010.

2. Babic, M., A. M. Hujer, and R. A. Bonomo, "What's New in Antibiotic Resistance? Focus on Beta-Lactamases", *Drug Resistance Updates*, Vol. 9, No. 3, pp. 142-156, 2006.

3. Wilke, M. S., A. L. Lovering, and N. C. Strynadka, "Beta-Lactam Antibiotic Resistance: A Current Structural Perspective", *Current Opinion in Microbiology*, Vol. 8, No. 5, pp. 525-533, 2005.

4. Majiduddin, F. K., I. C. Materon, and T. G. Palzkill, "Molecular Analysis of Beta-Lactamase Structure and Function", *International Journal of Medical Microbiology*, Vol. 292, No. 2, pp. 127-137, 2002.

5. Ambler, R. P., "The Structure of Beta-Lactamases", *Philosophical Transactions of the Royal Society B: Biological Sciences*, Vol. 289, No. 1036, pp. 321-331, 1980.

6. Bush, K., G. A. Jacoby, and A. A. Medeiros, "A Functional Classification Scheme for Beta-Lactamases and Its Correlation with Molecular Structure", *Antimicrobial Agents and Chemotherapy*, Vol. 39, No. 6, pp. 1211-1233, 1995.

7. Page, M. G., "B-Lactamase Inhibitors", *Drug Resistance Updates*, Vol. 3, No. 2, pp. 109-125, 2000.

8. Rudgers, G. W., W. Huang, and T. Palzkill, "Binding Properties of a Peptide Derived from Beta-Lactamase Inhibitory Protein", *Antimicrobial Agents and Chemotherapy*, Vol. 45, No. 12, pp. 3279-3286, 2001.

9. Lim, D., H. U. Park, L. De Castro, S. G. Kang, H. S. Lee, S. Jensen, K. J. Lee, and N. C. Strynadka, "Crystal Structure and Kinetic Analysis of Beta-Lactamase Inhibitor Protein-II in Complex with TEM-1 Beta-Lactamase", *Nature Structural Biology*, Vol. 8, No. 10, pp. 848-852, 2001.

10. Yuan, J., D. C. Chow, W. Huang, and T. Palzkill, "Identification of a Beta-Lactamase Inhibitory Protein Variant That Is a Potent Inhibitor of Staphylococcus PC1 Beta-Lactamase", *Journal of Molecular Biology*, Vol. 406, No. 5, pp. 730-744, 2011.

11. Yuan, J., W. Huang, D. C. Chow, and T. Palzkill, "Fine Mapping of the Sequence Requirements for Binding of Beta-Lactamase Inhibitory Protein (BLIP) to TEM-1 Beta-Lactamase Using a Genetic Screen for Blip Function", *Journal of Molecular Biology*, Vol. 389, No. 2, pp. 401-412, 2009.

12. Reynolds, K. A., M. S. Hanes, J. M. Thomson, A. J. Antczak, J. M. Berger, R. A. Bonomo, J. F. Kirsch, and T. M. Handel, "Computational Redesign of the SHV-1 Beta-Lactamase/Beta-Lactamase Inhibitor Protein Interface", *Journal of Molecular Biology*, Vol. 382, No. 5, pp. 1265-1275, 2008.

13. Strynadka, N. C., S. E. Jensen, P. M. Alzari, and M. N. James, "A Potent New Mode of Beta-Lactamase Inhibition Revealed by the 1.7 Å X-Ray Crystallographic Structure of the TEM-1-BLIP Complex", *Nature Structural Biology*, Vol. 3, pp. 290-297, 1996.

14. Henriques, S. T., M. N. Melo, and M. A. Castanho, "Cell-Penetrating Peptides and Antimicrobial Peptides: How Different Are They?", *The Biochemical Journal*, Vol. 399, No. 1, pp. 1-7, 2006.

15. Heitz, F., M. C. Morris, and G. Divita, "Twenty Years of Cell-Penetrating Peptides: From Molecular Mechanism to Therapeutics", *British Journal of Pharmacology*, Vol. 157, pp. 195-206, 2009.

16. Eiriksdottir, E., K. Konate, U. Langel, G. Divita, and S. Deshayes, "Secondary Structure of Cell-Penetrating Peptides Controls Membrane Interaction and Insertion", *Biochimica Et Biophysica Acta-Biomembranes*, Vol. 1798, No. 6, pp. 1119-1128, 2010.

17. Elmquist, A., M. Hansen, and U. Langel, "Structure-Activity Relationship Study of the Cell-Penetrating Peptide pVEC", *Biochimica Et Biophysica Acta-Biomembranes*, Vol. 1758, No. 6, pp. 721-729, 2006.

18. Elmquist, A., M. Lindgren, T. Bartfai, and U. Langel, "Ve-Cadherin-Derived Cell-Penetrating Peptide, pVEC, with Carrier Functions", *Experimental Cell Research*, Vol. 269, No. 2, pp. 237-244, 2001.

19. Brasch, J., O. J. Harrison, G. Ahlsen, S. M. Carnally, R. M. Henderson, B. Honig, and L. Shapiro, "Structure and Binding Mechanism of Vascular Endothelial Cadherin: A Divergent Classical Cadherin", *Journal of Molecular Biology*, Vol. 408, No. 1, pp. 57-73, 2011.

20. Babakhani, A., A. A. Gorfe, J. Gullingsrud, J. E. Kim, and J. Andrew McCammon, "Peptide Insertion, Positioning, and Stabilization in a Membrane: Insight from an All-Atom Molecular Dynamics Simulation", *Biopolymers*, Vol. 85, No. 5-6, pp. 490-497, 2007.

21. Dunkin, C. M., A. Pokorny, P. F. Almeida, and H. S. Lee, "Molecular Dynamics Studies of Transportan 10 (Tp10) Interacting with a POPC Lipid Bilayer", *Journal of Physical Chemistry B*, Vol. 115, No. 5, pp. 1188-1198, 2011.

22. Herce, H. D. and A. E. Garcia, "Molecular Dynamics Simulations Suggest a Mechanism for Translocation of the HIV-1 TAT Peptide across Lipid Membranes", *Proceedings of the National Academy of Sciences of the United States of America*, Vol. 104, No. 52, pp. 20805-20810, 2007.

23. Lorenzo, A. C. and P. M. Bisch, "Analyzing Different Parameters of Steered Molecular Dynamics for Small Membrane Interacting Molecules", *Journal of Molecular Graphics and Modelling*, Vol. 24, No. 1, pp. 59-71, 2005.

24. Mager, I., E. Eiriksdottir, K. Langel, S. El Andaloussi, and U. Langel, "Assessing the Uptake Kinetics and Internalization Mechanisms of Cell-Penetrating Peptides Using a Quenched Fluorescence Assay", *Biochimica Et Biophysica Acta-Biomembranes*, Vol. 1798, No. 3, pp. 338-343, 2010.

25. Tsai, C. W., N. Y. Hsu, C. H. Wang, C. Y. Lu, Y. Chang, H. H. G. Tsai, and R. C. Ruaan, "Coupling Molecular Dynamics Simulations with Experiments for the Rational Design of Indolicidin-Analogous Antimicrobial Peptides", *Journal of Molecular Biology*, Vol. 392, No. 3, pp. 837-854, 2009.

26. Allen, M. P., "Introduction to Molecular Dynamics Simulation", *Computational Soft Matter: From Synthetic Polymers to Proteins*, Vol. 23, pp. 1-28, 2004.

27. Karplus, M. and J. A. McCammon, "Molecular Dynamcis Simulations of Biomolecules", *Nature Structural Biology*, Vol. 9, No. 9, pp. 646-652, 2002.

28. Foloppe, N. and A. D. MacKerell, "All-Atom Empirical Force Field for Nucleic Acids: I. Parameter Optimization Based on Small Molecule and Condensed Phase Macromolecular Target Data", *Journal of Computational Chemistry*, Vol. 21, No. 2, pp. 86-104, 2000.

29. Phillips, J. C., R. Braun, W. Wang, J. Gumbart, E. Tajkhorshid, E. Villa, C. Chipot, R. D. Skeel, L. Kale, and K. Schulten, "Scalable Molecular Dynamics with

NAMD", *Journal of Computational Chemistry*, Vol. 26, No. 16, pp. 1781-1802, 2005.

30. Humphrey, W., A. Dalke, and K. Schulten, "VMD: Visual Molecular Dynamics", *Journal of Molecular Graphics*, Vol. 14, No. 1, pp. 33-38, 1996.

31. Akdağ, İ. Ö., *Bacterial Uptake Mechanism of Peptides Investigated by Steered Molecular Dynamics Simulations,* M.S. Thesis, Boğaziçi University, 2011.

32. Joanne, P., C. Galanth, N. Goasdoue, P. Nicolas, S. Sagan, S. Lavielle, G. Chassaing, C. El Amri, and I. D. Alves, "Lipid Reorganization Induced by Membrane-Active Peptides Probed Using Differential Scanning Calorimetry", *Biochimica Et Biophysica Acta-Biomembranes*, Vol. 1788, No. 9, pp. 1772-1781, 2009.

33. Kale, L., R. Skeel, M. Bhandarkar, R. Brunner, A. Gursoy, N. Krawetz, J. Phillips, A. Shinozaki, K. Varadarajan, and K. Schulten, "NAMD2: Greater Scalability for Parallel Molecular Dynamics", *Journal of Computational Physics*, Vol. 151, No. 1, pp. 283-312, 1999.

34. Huang, W., Z. Beharry, Z. Zhang, and T. Palzkill, "A Broad-Spectrum Peptide Inhibitor of Beta-Lactamase Identified Using Phage Display and Peptide Arrays", *Protein Engineering*, Vol. 16, No. 11, pp. 853-860, 2003.